INFLUENCE OF ENCLOSURE GEOMETRIES AND INTERNAL INSTALLATIONS ON THE EXPLOSION PRESSURE OF HYDROGEN-AIR MIXTURES

A THESIS SUBMITTED IN PARTIAL FULFILLMENT OF THE REQUIREMENTS

FOR THE DEGREE OF MASTER OF SCIENCE IN RENEWABLE ENERGY

OF

THE UNIVERSITY OF NAMIBIA

BY

NDAMONONGHENDA NAOPANDILI UUNONA

201716708

OCTOBER 2025

SUPERVISOR: Assoc. Prof. Zivayi Chiguvare, University of Namibia

CO-SUPERVISOR: Dr.-Ing. Tim Krause, Physikalisch-Technische Bundesanstalt

CO-SUPERVISOR: Mr. Mohsen Shekoohian, Physikalisch-Technische Bundesanstalt

ABSTRACT

The use of green hydrogen gas as a clean energy carrier solution is gaining global momentum and Namibia is on track to being one of the major producers of green hydrogen. The growing emphasis on green hydrogen has elevated the importance of safety in its value chain. This thesis investigates the influence of enclosure geometries and internal installations on the explosion pressure of hydrogen-air mixtures within flameproof enclosures. The aim of this work is to investigate two critical aspects: the impact that different flameproof enclosure geometries have on the explosion pressure, and the role that internal installations play in exacerbating or mitigating the phenomenon of pressure piling.

Experimental tests were conducted in the metrological laboratories of Physikalisch-Technische Bundesanstalt, an Institute in the Federal Republic of Germany in compliance with the international standards, such as IEC 60079-1, in order to adhere to the safety guidelines which are vital for preserving structural integrity during hydrogen explosions. These experiments were conducted using specific enclosure geometries – spherical, cylindrical and multi-chambered enclosures. Different orifice sizes and welded internal installations were used to replicate the real-world industrial conditions of pressure piling.

The results demonstrated that enclosures with complex geometric design and internal installations were more susceptible to pressure piling effects due to localised pressure compression and uneven pressure distribution. Additionally, this work highlighted the importance of the proper design of the enclosure, emphasizing the need for optimized internal configurations to minimize risks.

The findings from these experiments contribute to enhancing and improving the design of flameproof enclosures, potentially informing future regulatory updates, promoting safer practices in hydrogen production plants, and ultimately, bridging the existing knowledge gaps in hydrogen explosion protection.

Keywords: Flameproof enclosure, explosion pressure, pressure piling, hydrogen-air mixture, internal installations.

LIST OF CONFERENCE PROCEEDINGS

N. N. Uunona, Z. Chiguvare, T. Krause & M. Shekoohian. Influence of enclosure geometries and internal installations on the explosion pressure of hydrogen-air mixtures. Hydrogen Safety Symposium, Hochschule RheinMain. Rüsselsheim, Germany. 26 July 2024. (Poster presentation).

TABLE OF CONTENTS

LIST OF TABLES

<u>LIST OF FIGURES</u>

LIST OF SYMBOLS, ABBREVIATIONS AND ACCRONYMS

BASF	Badische Anilin- und Sodafabrik
CSV	Comma-separated values
Ex d	Flameproof enclosures
DC	Direct current
DIN EN	German implementation of the European standard
HPP II	Harambee Prosperity Plan II
IEC	International Electrochemical Commission
ISO	International Organization for Standardization
ISO/TR	International Organization for Standardization/Technical Report
LEL	Lower explosive limit
NFPA	National Fire Protection Association
NSI	Namibia Standards Institute
OSHA	Occupational Safety and Health Administrations
PTB	Physikalisch-Technische Bundesanstalt
RTV	Room-temperature-vulcanizing
UEL	Upper explosive limit
vol.	Volume
WGSR	Water Gas Shift Reaction

ACKNOWLEDGEMENTS

Firstly, I would like to extend my heartfelt gratitude to my supervisors, Assoc. Prof. Zivayi Chiguvare and Dr.-Ing. Tim Krause, for their unwavering support, motivation, and dedication in ensuring the smooth completion of this work.

I would also like acknowledge and to express my sincerest appreciation to Mr. Mohsen Shekoohian (B.Eng.) for his immense assistance, patience and commitment to helping me understand every detail throughout the experiments.

A special thank you goes to Mr. Moritz Ackermann, the wonderful PTB International team, PTB Department 3.54, and the entire PTB family. Your support and collaboration were integral to the success of this research.

To my beloved Mama, *Mee* Olivia Kunamwene, your strength, love, and unwavering belief in me have carried me through this journey. I stand here today because of the inspiration and resilience I draw from you.

Lastly, to my nephew and godson, Desi, you kept me grounded and gave me purpose, even from far away. Your smile became my greatest source of motivation to push forward. I hope I’ve made you proud my baby.

Thank you all from the depths of my heart.

DEDICATIONS

Tate, Paulus Uunona Jekonia (+03 June 2023).

This work is dedicated to my father.

You left too soon to celebrate this milestone with me, but I held on strong to make you proud.

This is for you Pa, continue resting in peace.

DECLARATION

I, Ndamononghenda N. Uunona, hereby declare that this study is my own work and is a true reflection of my research and that this work, or any part thereof has not been submitted for a degree at any other institution.

No part of this thesis/dissertation may be reproduced, stored in any retrieval system, or transmitted in any form, or by means (e.g. electronic, mechanical, photocopying, recording or otherwise) without the prior permission of the author, or The University of Namibia in that behalf.

I, Ndamononghenda N. Uunona, grant The University of Namibia the right to reproduce this thesis in whole or in part, in any manner or format, which The University of Namibia may deem fit.

Ndamononghenda Naopandili Uunona		October 2025
Name of Student	**Signature**	**Date**

CHAPTER 1. INTRODUCTION

1.1. Background of the Study

The production of green hydrogen will be an essential tool for the global shift towards sustainable, zero-carbon emission technologies, driven by the increasing worldwide demand for clean energy. Hydrogen, an abundant natural gas, stands at the forefront of this clean energy paradigm, serving both as a fuel and an energy carrier [1]. However, the inherent explosive nature of hydrogen, particularly in the presence of an oxidizer such as air, and an ignition source can lead to an exothermic reaction (Figure 1) which is not particularly predictable.

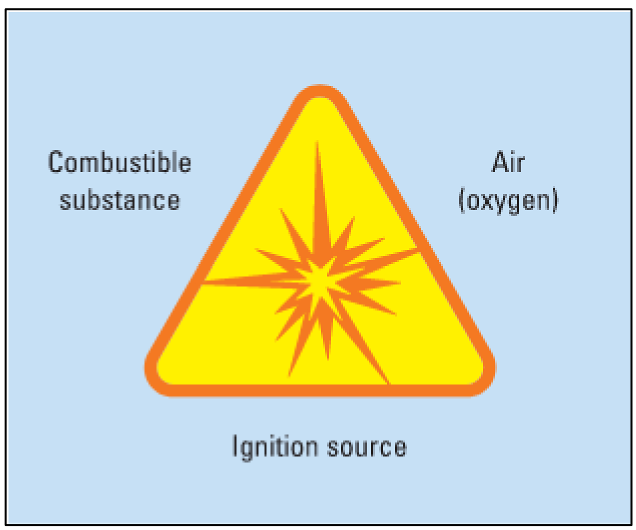

Figure 1: Three factors of explosion [2]

This behavior necessitates a thorough understanding of technical and organizational measures for hydrogen explosion protection prompting numerous experimental studies [3–6] in order to suggest appropriate safety precautions, and various protection principles. One of the safety protection precautions used, in this regard, is the type of protection called "flameproof enclosures" also referred to as "Ex d" [7]. These devices are characterized by the fact that, when there is an ignition within, they can withstand the explosion pressure safely such that the explosion cannot penetrate to the outside and ignite an explosive atmosphere outside of the enclosure.

Explosion pressure refers to the high pressure generated when a combustible gas, such as hydrogen, ignites and burns rapidly inside an enclosure or confined space [8]. This pressure is a critical factor in the design of safety measures, as it determines the ability of the enclosure to contain the explosion without rapturing. The determination of explosion pressure is essential for qualifying flameproof enclosures, ensuring they can safely withstand the forces generated during an explosion.

A related phenomenon, known as pressure piling, can further complicate explosion dynamics within enclosures. Pressure piling occurs when an initial explosion or ignition in one part of a confined space increases the pressure in another part of the enclosure, leading to a more severe secondary explosion [9]. This effect is often exacerbated by complex enclosure geometries and the presence of internal installations, such as baffles or partitions, which can cause uneven pressure distribution and localized pressure compression points.

Understanding both explosion pressure and pressure pile effects is crucial to developing effective explosion protection strategies. This understanding underpins the international standards for flameproof enclosures, which have evolved since the early studies by Beyling in 1906 [10]. The International Electrotechnical Commission (IEC) [9] created the first international standard for flameproof enclosures in 1957, and this standard has undergone numerous revisions to improve safety measures in response to ongoing research and technological advancements. One of the central tests in these standards is the determination of explosion pressure, which remains a cornerstone of enclosure qualification.

1.2. Statement of the Problem

The potential danger of hydrogen-air mixtures in enclosed spaces poses safety concerns that are not fully understood [11], particularly regarding how the shape of the enclosure and internal components impact explosion dynamics [12]. While current safety standards for flameproof enclosures offer a level of protection, they lack guidance on how these variables affect explosion pressures and pressure piling when dealing with hydrogen-air mixtures. This knowledge gap creates risks in the expanding hydrogen industry where secure storage and handling are paramount.

1.3. Aim and Objectives of the Study

This study aims to contribute to the improvement of the design and safety measures of flameproof enclosures by experimentally investigating how different enclosure geometries and internal installations influence the explosion pressure of hydrogen-air mixtures.

The objectives of this research are.

1. To quantify the explosion pressure in spherical, cylindrical, and multi-compartment enclosures filled with hydrogen-air mixtures.
2. To investigate the role of internal installations in influencing pressure piling and overall pressure distribution within these enclosures.
3. To analyze the pressure dynamics of hydrogen-air explosions, including pressure build-up and distribution, in relation to enclosure geometry.

Based on these objectives, this study addresses the following research questions:

1. How do different enclosure geometries (spherical, cylindrical and multi-compartment) influence the explosion pressure and rate of pressure rise for hydrogen-air mixtures?
2. What effect do internal installations have on pressure piling and pressure distribution in hydrogen-air explosion tests?
3. How do pressure dynamics, specifically pressure build-up of hydrogen-air mixture vary with enclosure geometry?

1.4. Significance of the Study

The importance of this research is that it tackles safety issues, particularly in the field of explosion protection, related to the use of hydrogen gas, especially given the increasing global focus on green hydrogen as a clean energy option. By delving into how the shape of enclosures and internal setups impact explosion pressure and pressure piling, this study will contribute to the understanding and better application of enclosures in the realm of explosion protection. These findings will improve safety protocols for storing and handling hydrogen, thus decreasing the likelihood of industrial mishaps. Moreover, the results of this research will influence updates to safety guidelines, promoting safer and more widespread integration of hydrogen technologies across various industries.

1.5. Limitations and Delimitations

To offer significant understanding regarding the impact of enclosure geometries and internal installations on explosion pressures, it would be crucial to recognize specific constraints that would affect the depth and breadth of the results obtained and to ensure a manageable scope.

1.5.1. Limitations

1. The study is limited by the scale and scope of the experiment and the simplification of setups, which might not fully capture the intricacies of real-world complex structures across all industries.
2. This research focuses primarily on hydrogen-air mixtures and may not account for the behavior of other gases or gas mixtures, which could exhibit different explosion characteristics.

1.5.2. Delimitations

1. This study is deliberately confined to the examination of hydrogen-air mixtures within flameproof enclosures and has excluded other types of explosion protection methods or gases.
2. This research specifically investigates the impact of enclosure geometry and internal installations without delving into other factors such as temperature variations and or external environmental conditions.
3. This work aligns its experimental approach with existing international standards for flameproof enclosures, ensuring relevance but also limiting exploration outside these established frameworks.
4. The explosions considered in this work are exclusively deflagrative in nature. Detonations are not relevant due to the test setups and parameters used.

CHAPTER 2. LITERATURE REVIEW

2.1. Introduction

This literature review discusses the dynamics of hydrogen-air explosions and how they are influenced by enclosure geometries and internal installations. Risks coupled with the properties of enclosure geometrics and internal installations that influence explosion pressures in hydrogen production plants are assessed. These risks substantiate the ongoing academic discourse about the persistent risks of explosions that have plugged industries that have in recent years embarked on energy production, and in this case, hydrogen gas is studied. It has been widely reported in the literature that significant risks are associated with the production of hydrogen gas [13–17]. While a plethora of literature has focused on the risks by listing and describing them, this study seeks to focus on the experimental properties of hydrogen gas explosion pressure has on flameproof enclosures, including spherical, cylindrical, and multi-chambered designs. It also focuses on the pressure piling effects and how this phenomenon influences the behavior of gas explosions within multi chamber enclosures.

2.2. The Genealogy and Politics of Hydrogen Gas Production

The discovery that was made in 1923 that hydrogen could be produced by a mixture of natural gas with steam, in the presence of a catalyst [18], laid a foundation for large-scale production of hydrogen gas. The shift of interest in producing hydrogen gas using unsustainable raw materials, such as natural gas and crude oil, was motivated by the large-scale industrial use of hydrogen in the petroleum industry [19, 20]. Today, various methodologies, such as Water-Gas Shift Reaction (WGSR), pyrolysis, electrolysis, and others – either alone or in conjunction with water splitting – are extensively used in the industry for hydrogen production [21].

Driven by the growing demand for a clean energy ecosystem, hydrogen as an energy carrier now forms a dynamic part of the energy transition process. However, as the 21st century unfolds, energy transitions get influenced by global power geopolitics [22]. The Namibian Green hydrogen strategy [23], a key part of the Harambee Prosperity Plan II (HPP II), aims to position Namibia as a leader in green hydrogen production by harnessing its vast renewable energy resources. On the other side of the globe, the Federal Republic of Germany has decided since 2020 to invest over 9 billion Euros in the import of green hydrogen gas and fund green hydrogen production projects across the globe, with Namibia being one of the key recipients of these investments [24].

2.3. Theoretical Background of Hydrogen Explosion Dynamics

Explosions in gas plants, particularly those involving hydrogen, present significant safety concerns due to the violent nature of these reactions. As noted in prior studies by Yu et al. [25] and Yang et al. [26], hydrogen is one of the most reactive and combustible gases, necessitating a detailed understanding of explosion dynamics to mitigate risks in industrial settings. The root cause of such an explosion lies in the rapid combustion or decomposition of a combustible gas and its mixing with an oxidant.

2.3.1. Hydrogen Combustion Reaction

The combustion reaction of hydrogen fuel used in this experiment is indicated by Equation (1), where two hydrogen molecules react with one oxygen molecule to form water vapor.

$$2H_2(g) + O_2(g) \rightarrow 2H_2O(g) \quad \text{Equation 1}$$

The chemical reaction mechanism is significantly complex than what equation 1 captures. Hydrogen combustion is a branched-chain reaction involving a series of intermediate steps with hydrogen (H), oxygen (O), and hydroxyl (OH) radicals acting as chain carriers[27, 28]. These radicals determine the overall rate of combustion by playing a critical role in propagating the reaction.

Reactions in the combustion system are therefore categorized into chain initiation reactions, chain branching reactions, chain propagating reactions, and chain termination reactions.

1. Initiation reactions – in order to start the chain reaction, chain initiation is required. This step is usually triggered by external energy such as heat or an electrical spark, providing the activation energy. This process involves the dissociation of a hydrogen molecule to reactive hydrogen radicals:

$$H_2(g) + M \rightarrow H(g) + H(g) + M \quad \text{Equation 1.1}$$

Where M represents a third body collider that provides (or removes) the energy necessary for breaking the chemical bond [28].

2. Chain branching – after initiation, the reaction proceeds through branching where a net radical production is achieved such that two radicals are formed from one atom or radical.

$$H(g) + O_2(g) \rightarrow OH(g) + O(g) \quad \text{Equation 1.2}$$

$$O(g) + H_2(g) \rightarrow OH(g) + H(g) \quad \text{Equation 1.3}$$

3. Chain propagating – the radicals formed sustain the chain reaction by reacting with hydrogen molecules to form water vapor and regenerate radicals:

$$OH(g) + H_2(g) \rightarrow H_2O(g) + H(g) \quad \text{Equation 1.4}$$

4. Chain termination reactions – this is stage represents the net destruction of radicals. It occurs when reactive radicals combine to form stable products, thereby reducing the radical concentration and ultimately slowing down the reaction.

$$H(g) + OH(g) \rightarrow H_2O(g) \quad \text{Equation 1.5}$$

$$H(g) + O(g) \rightarrow OH(g) \quad \text{Equation 1.6}$$

$$OH(g) + OH(g) \rightarrow H_2O(g) + O(g) \quad \text{Equation 1.7}$$

Understanding the significance of the reaction mechanism helps develop safety measures in mitigating explosion risks.

2.3.2. Explosive Limits and Most Ignitable Mixtures

The dynamics of hydrogen explosion pressure are rooted in several interrelated factors. For instance, the adiabatic combustion temperature plays a critical role in determining the explosion pressure, as governed by the ideal gas law [29]:

$$pV = nRT \quad \text{Equation 2}$$

Where p is pressure, V is volume, n is the number of moles of gas, R is the universal gas constant, and T is temperature in Kelvin. Equation (2) suggests that for a fixed volume enclosure (as is the case in flameproof enclosures), an increase in temperature from the combustion of hydrogen will directly result in a corresponding increase in pressure. In most cases, the explosion pressure (denoted as p_{ex}) represents the peak value attained during the explosion, and its magnitude depends on the enclosure's ability to withstand this pressure without failure. According to DIN EN 15967 [30], this is the highest pressure, determined under specific test conditions, that occurs in a closed container during an explosion of a specific mixture of explosive substances with air, or air and inert gases.

In practical industrial settings, the explosion pressure for a hydrogen-air mixture can reach up to 8.3 bar in enclosures such as spherical vessels due to symmetrical flame propagation [31]. For hydrogen gas to cause a combustible ignition (explosion), certain preconditions must be met with regards to the concentration, pressure and temperature. If the pressure and temperature of the hydrogen-air mixture are constant, the concentration that ignites with a minimum amount of energy is called the most ignitable mixture [2] (see Figure 2). This concentration varies for every gas and is limited by an explosion range of lower explosive limit (LEL) and upper explosive limit (UEL).

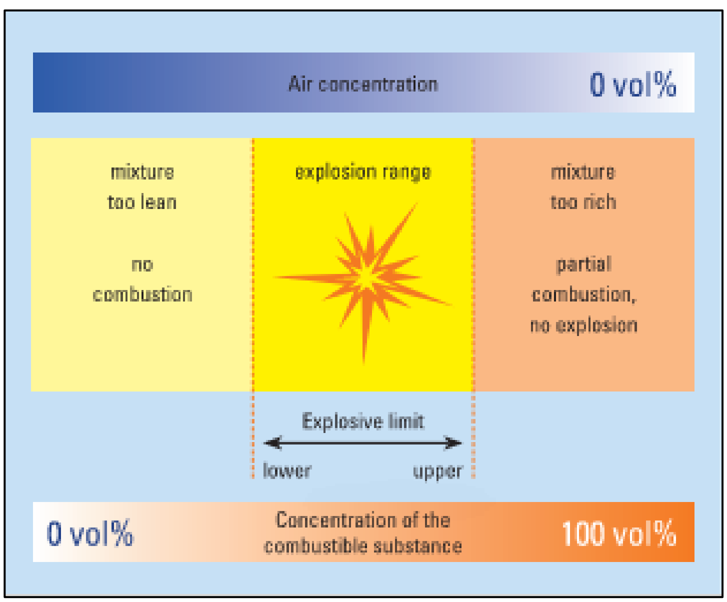

Figure 2: Explosive limits for any gas – air mixture [2]

Table 1 compares some of the common hydrocarbon gas properties with hydrogen gas. Explosion limits refer to the pressure-temperature boundaries for a specific fuel/oxidizer mixture that separates the region of slow and fast reactions [32] .The explosion range for hydrogen-air mixture is 4-75/vol-% with the most ignitable mixture ranging from 14-34/vol-% and its Stoichiometric Fuel-air mixture is 31/Vol-% [7].

Table 1: Comparison of explosion properties of hydrocarbons with hydrogen gas.

Gas	Stoichiometric Fuel-Air Mixture/Vol.-% [7]	Explosion Pressure p_{ex} $in\ bar$ According to [31] and Eq.3	Explosion Range / Vol.-% [31, 33]
Hydrogen - H_2	31	8,3	4 – 75
Methane - CH_4	9,8	9,03	5 – 15
Acetylene - C_2H_2	14	11,23	2,5 – 100
Ethylene - C_2H_4	8	10,01	2,7 – 36
Propane - C_3H_8	4,6	9,72	2,1 – 9,5

In the field of explosion protection, the explosion pressure, denoted as p_{ex}, is defined as the highest value of the pressure as shown in Table 1. The comparison of the explosion pressures can be calculated using Equation (3) [12] which was also verified by ChemSAFE [31]. On the other hand, the explosive limits and the most ignitable limits were verified with sources such as CHRYSALIS gas reference information [33] as well as ChemSAFE [31].

2.3.3. Pressure Development in Explosions

In a closed vessel, combustion results in an instantaneous release of energy, which increases the temperature of the gas mixture [34] and maximum explosion pressure, p_{ex}, attained during this process [12] is given by Equation (3) as:

$$p_{ex} = p_0 \frac{n_1 T_{ad}}{n_0 T_0} \qquad \text{Equation 3}$$

Here, p_0 describes the initial pressure of the fuel-air mixture before ignition, n_0 the number of moles, and T_0 the temperature before combustion, n_1 the number of moles after combustion, T_{ad} the adiabatic combustion temperature. Assuming that the conditions are adiabatic, the molar ratio $\frac{N_1}{N_0}$ is approximately 1 due to the minimal change in the number of moles. In ideal adiabatic conditions, the explosion pressure reaches its peak when the proportion of combustible material is optimal. However, real world conditions often deviate from these ideal assumptions due to factors such as heat loss to the enclosure walls or turbulences in the flame front [35].

2.3.4. Flame Propagation and Burning Velocity

Flame propagation plays a critical role in determining the severity of an explosion. In fuel-air mixtures, the flame front advances rapidly depending on the weight of the fuel, of which the case of a hydrogen-air mixture allows a quick diffusion of hydrogen molecules. The burning velocity is a crucial factor in determining the rate of pressure rise during an explosion. This signifies the rate at which the flame consumes unburnt gas.

Pressure and temperature are important factors affecting flame speed. Lewis and von Elbe have developed a pressure-temperature-burn velocity chart, illustrated in Figure 3, for an ozone-air mixture (40.06 %vol. ozone) in a spherical enclosure of radius = 15 cm [12].

This chart shows the relationship between pressure (p), the temperature of unburnt gas (T_u), temperature of burnt gas (T_b), the end temperature (T_e), and the radius of the enclosure.

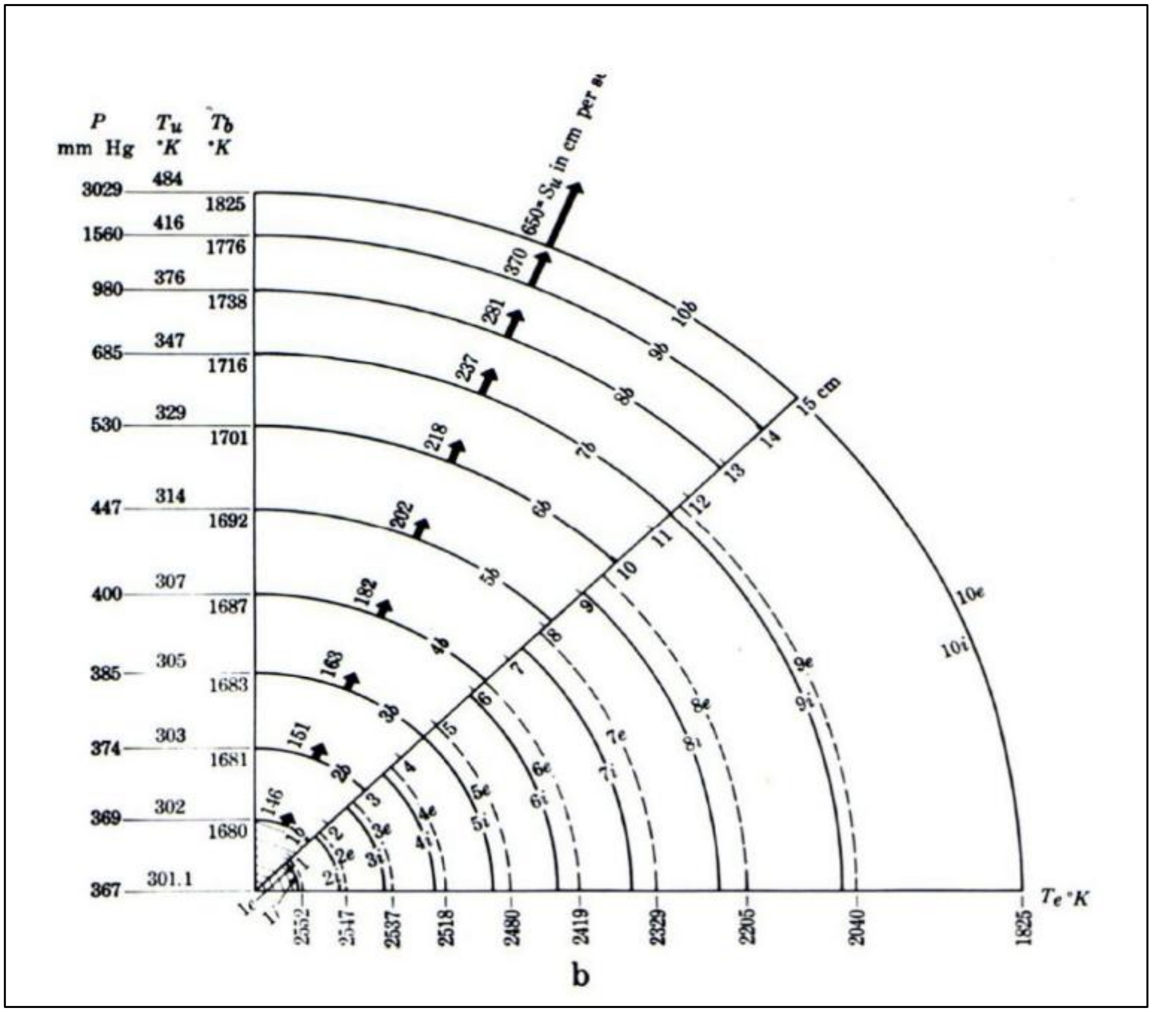

Figure 3: Pressure-temperature-burn velocity chart developed by Lewis and von Elbe for ozone-air mixture in a closed spherical enclosure [12]

As illustrated in Figure 3, the pressure, temperature and burning velocity are interconnected and influenced by the vessel's radius [12]. The study done by Razus et al [36], also showed that the burning velocity varies significantly based on the initial conditions and the geometry of the vessel. In smaller geometries, such as those with a smaller radius, the flame propagates much faster and the pressure rises more quickly, leading to a rapid explosion as compared to those with a larger radius and greater volume allowing for more heat dissipation before reaching enclosure walls. This relationship highlights why enclosure geometry is an important factor in determining the explosion severity.

2.3.5. Vessel Geometry and Explosion Dynamics

Due to the uniform nature of a sphere, the pressure buildup is faster and more intense and is governed by Equation (4) [37] where the flame radius r_b is given as a function of the pressure p inside the vessel.

$$r_b = r\left(\frac{\left({}^{p}/_{p_0}\right)\chi - 1}{\left({}^{p}/_{p_0}\right)\chi - \alpha}\right) \qquad \text{Equation 4}$$

Where r_b is the flame radius, r is the radius of the vessel, p is the final pressure inside the vessel, p_0 is the initial pressure, α is the ratio of the burnt to unburnt gas density and $\chi = 1/\gamma$, where γ is the ratio of specific heat of the unburnt gas.

The flame radius r_b expands as the pressure rises and the distance from the flame transfer point (ignition source) is calculated as

$$Z = r - r_b \ \ (p_z) \qquad \text{Equation 5}$$

Where p_z is the pressure in the enclosure just before ignition, or in the primary chamber, or just before ignition in the secondary chamber, in the case of multi-chamber vessels.

Based on other studies by Singh (1984, 1993) as referenced in Rogstadkjernet [38], an empirical relation of the flame transfer distance in cylindrical vessels is given by Equation

(6) and shows that the flame transfer distance Z is greatly influenced by the gas flow rate d_c

$$Z = {d_c}^{1.8} \qquad \text{Equation 6}$$

Although this equation is assumed to be geometry dependent and a poor representation of the actual flow characteristics, for the multi chamber enclosure with orifice division, it shows that time of flame transfer into the secondary chamber is dependent on the orifice opening.

2.3.6. Turbulence and Pressure Oscillations

During an explosion, the flame front is not always perfectly symmetrical [36, 39], particularly in industrial settings with compartmented design features and irregular geometries. As the flame propagates, it encounters obstacles and changes within the vessel's cross-sectional area, creating turbulence. Turbulence enhances the mixing of fuel and oxidizer, affecting the flame speed and ultimately influencing local pressure spikes, as the pressure reflects off the walls and internal installations of the enclosure.

In confined spaces the reflected pressure waves interact with each other, leading to pressure oscillations which further amplifies the overall pressure of the explosion [34]. The presence of multiple compartments or obstacles exacerbates these oscillations and ultimately creates localized areas of high pressure which can exceed the average explosion pressure [40].

2.3.7. The Role of Temperature in Hydrogen Explosions

Temperature plays a significant role in hydrogen-air mixture explosion dynamics [34, 41][41]. Hydrogen gas has a low ignition energy and a wide flammability rate [3], as shown in Table 1, meaning it can ignite at relatively low temperatures as compared to other fuels. The adiabatic temperature of hydrogen in air mixture is around 2500 K, which contributes to its high detonation potential [42].

In the context of explosion processes, a fundamental distinction is made between thermal ignition, thermal explosions and chain branching explosions, with the rate of reaction coefficient, k, being a key characteristic of the chemical reaction. This rate of reaction has a non-linear temperature dependence and is described by the Arrhenius equation (Equation (7)) [43].

$$k \sim A_0 e^{-\frac{E_a}{RT}} \qquad \text{Equation 7}$$

Where A_0 is a pre-exponential factor that has a temperature dependence that is often neglected. E_a is the activation energy, R the universal gas constant, and T the temperature of the system. Higher temperatures reduce the activation energy barrier, allowing the reaction to proceed more quickly, which increases the explosion severity.

While hydrogen holds immense potential to reduce carbon emissions across various industries, its highly explosive nature calls for strict safety precautions. When hydrogen is released and ignited, the resulting flame quickly propagates through a mixture of combustible gas and oxidant posing challenges [44] . Unlike traditional fuels, hydrogen's behavior in accident scenarios – characterized by rapid flame acceleration and a high detonation potential – requires specialized safety analysis and mitigation strategies [45] . One crucial safety measure involves using flameproof enclosures designed to contain explosions and vent them safely without letting the ignition spread externally. These enclosures play a role in preventing accidents in areas where hydrogen is used or stored. For that reason, flameproof enclosures are the main focus of this study.

2.4. Factors Influencing Explosion Pressure and its Measurements

It is important to understand the factors that impact explosion pressure when designing flameproof enclosures for industries where combustible gases like hydrogen are prevalent. Explosion pressure is influenced by various factors, ranging from fuel characteristics [40] to enclosure design [34, 40]. This section discusses some of the main factors and their influence on explosion pressure and measurement accuracy.

2.4.1. Fuel and Oxidizer Characteristics

The type and concentration of fuel plays a critical role in determining the explosion pressure. For hydrogen-air mixture scenarios, the ratio of hydrogen and air proportions influences explosion dynamics [31]. Due to the low ignition energy of hydrogen gas and its wide flammability range, this gas is volatile and as a result, it has a broad spectrum of potential explosion pressure as compared to other gases. It is therefore imperative to maintain the right and safe fuel-to-oxidizer ratio to optimize safety and control explosion pressure in practical industrial settings.

2.4.2. Initial Conditions: Temperature and Pressure

Initial conditions such as temperature and pressure have an impact on the explosion reaction and although it is not possible to have control over them in practical industrial settings, it is important to understand the severity of their influence [46]. Higher ambient temperatures can accelerate the chemical reaction thus increasing the rate of combustion and the corresponding explosion pressure [41]. Similarly, a high initial pressure within an enclosure amplifies the overall explosion severity by compressing the fuel-oxidizer mixture before ignition, concurrently exacerbating the explosion [47].

During experimental tests, it is imperative to have control over these parameters to ensure reliable results.

2.4.3. Enclosure Geometry

The physical characteristics of the enclosure, such as its shape and volumetric feature, significantly influence how pressure builds up and propagates during an explosion [34]. Enclosures, such as those of spherical geometry, have been used for experimentally studying the explosion pressure in fuel-air mixtures and have been set as the basis for comparison with other enclosure designs, to build on the understanding of pressure distribution during an explosion.

Further studies have been carried out with compartmentalized vessels [48] as well as, different types of volumetric geometries, such as interconnected tubes [37] or cylindrical and spherical, [47, 49, 50] that allow more heat dissipation and result in different explosion pressures. This paper delves deeply into investigating the influence that various geometries of enclosure have on the explosion pressure, particularly in hydrogen-air mixtures. A comprehensive discussion therefore accompanies the experimental results obtained.

2.4.4. Internal Installations and Obstructions

Internal installations such as orifices, partitions and baffles influence the explosion pressure by altering the flow of pressure waves and flame fronts [50]. These installations can either exacerbate or reduce explosion severity. In compartmentalized designs, exacerbation of explosion is experienced due to localized pre-compression of explosion pressure, this is also due to the partitions that reflect pressure waves leading to localized pressure spikes[48].

Experiments conducted by Krause et al [51] demonstrated that internal installations significantly impact the static and dynamic stress within flameproof enclosures. They further went on to demonstrate that the positioning of obstructions, combined with the location of the ignition source, plays a key role in the overall pressure buildup and must be carefully considered at design.

2.4.5. Pressure Piling

Pressure piling is a phenomenon observed in enclosures with multiple compartmented designs or setups with internal installations that lead to localized pre-compression during an explosion [37]. According to the IEC standard [9], pressure piling is a result of ignition, in a compartment or subdivision of an enclosure, of a pre-compressed gas mixture, for example, due to a primary ignition in another compartment or subdivision. It is not just the confined space or rapid energy release that causes pressure piling but rather the way the pressure waves interact within the enclosure.

The IEC6079-1 standards have stated the conditions that under which pressure piling can occur [7]:

1. During a series of explosion tests with the same configuration, the pressure values deviate by more than 1.5 times
2. or the pressure rise time is less than 5 ms.

In a scenario involving pressure piling as illustrated in Figure 4, when the explosion in the primary chamber compresses unburnt gas in a connected chamber, the pressure in the secondary chamber before ignition (p_1) becomes higher than the atmospheric pressure, leading to an even greater final pressure (p_k).

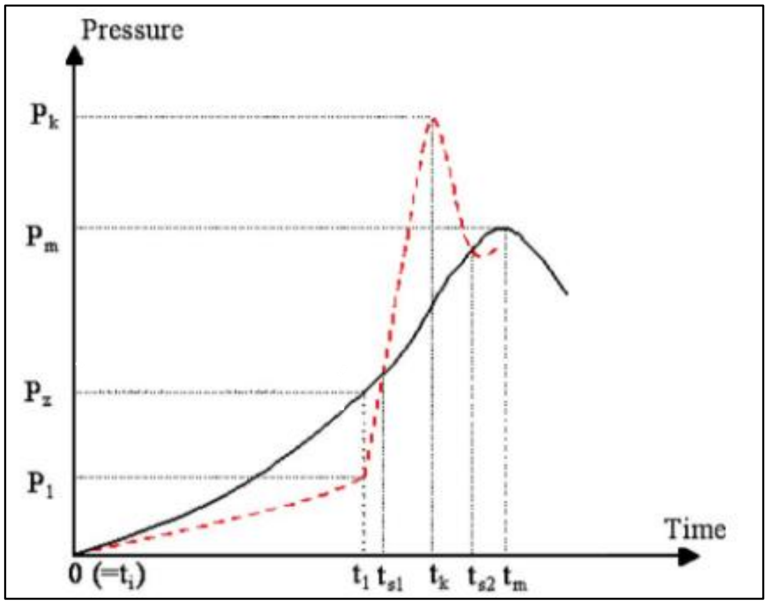

Figure 4: Pressure history in primary chamber (−) and secondary chamber (---) [52].

Studies have been done on cylindrical vessels interconnected by a duct filled by a propane–air or a methane–air stoichiometric mixture at initial atmospheric temperature and pressure [40]. This duct is separated by orifices of different sizes in order to show the effect of pressure piling due to duct opening. The results highlight the importance of managing internal installations to prevent extreme pressure piling that could exceed the enclosure's design limit.

2.4.6. Measurement Accuracy and Challenges

Accurate measurements in explosion pressure experiments are important such that they help in evaluating risks and ensuring that the experimental samples meet the set safety standards. Factors such as geometric complexity, heat dissipation and turbulent flow can have a profound effect on the measurement accuracy, as they can introduce discrepancies between predicted calculated results and experimental results.

Heat dissipation along with turbulences within the enclosure can lead to deviations between the result measurements [36]. Experimental equipment such as measuring devices that are typically used to capture data in real time must be routinely calibrated in order to minimize errors due to factors such as thermal shock, internal wear, temperature fluctuations etc. [12]. Regular calibration of measuring devices ensures accuracy and reliability of test results by aligning the device's output with known reference standards [53].

2.5. Theory of Pressure Piling and its Effects

Pressure piling is a vital phenomenon in the field of explosion protection, especially in flameproof enclosures designed for housing devices that result in complex geometries and partitions. This phenomenon occurs when the pressure from the initial explosion in the primary compartment compresses the unburnt gas in an adjacent secondary compartment, which consequently leads to a severe explosion in the secondary compartment [12]. This phenomenon poses severe risks in industrial settings where combustible gases such as hydrogen gases are present as it significantly amplifies the overall explosion pressure.

2.5.1. Mechanisms of Pressure Piling

The propagation of pressure waves within the interconnected compartments of an enclosure is the driving force behind the mechanism that is responsible for pressure piling on an enclosure. When an explosion is executed in the primary compartment, the explosion flame front rapidly consumes the fuel-air mixture and consequently generate high-pressure waves [52]. These waves travel through the openings between these compartments ultimately compressing the unburnt fuel mixture in adjacent compartments. When the compressed gas ignites, a secondary explosion is experienced which produces a violent explosion that is significantly higher than that observed in the primary compartment [52].

Section 2.3. above stated that the ideal gas law governs the relationship between pressure, volume, and temperature [29]. Thus, in the context of pressure piling, a significant increase in temperature due to the combustion process causes a corresponding increase in pressure. However, in complex enclosure designs, such as those with multiple chambers, the compressed fuel mixture in the secondary compartments leads to an even greater final pressure [48], deviating from the ideal assumptions in single-chamber explosions with evenly distributed flame propagation.

2.5.2. Mathematical Representation of Pressure Piling

Expanding further on Equation (3), and applying the assumption of an adiabatic process, the relationship between the initial and final pressures and temperatures can be described as:

$$\frac{p_1}{p_0} = \frac{T_1}{T_0} \qquad \text{Equation 8}$$

Where p_1 and p_0 are the final and initial pressures, respectively, and T_1 and T_0 are the final and initial temperatures, respectively.

Due to the amplification of the explosion pressure because of the pre-compression of the unburnt fuel-mixture in the secondary compartment, this relationship does not hold true because of the effect of pressure piling.

A deflagrative index K_G is introduced, which quantifies the rate of pressure rise in a gas explosion and can be used to assess the severity of pressure piling effects [54].

$$K_G = V^{1/3}\left(\frac{dp}{dt}\right)_{max} \qquad \text{Equation 9}$$

Where V is the volume of the enclosure and $\left(\frac{dp}{dt}\right)_{max}$ is the maximum rate of pressure rise.

The maximum rate of pressure rise is given by

$$\left(\frac{dp}{dt}\right)_{max} = \frac{3(P_{ex} - P_0)}{R_{vessel}}\left(\frac{P_{ex}}{P_0}\right)^{\frac{1}{\gamma}} S_L$$

Where S_L is the laminar flame velocity and R_{vessel} is the radius of the enclosure.

The relationship between the deflagrative index in the secondary chamber and that of the primary chamber is then given by η which is the amplification factor due to the pre-compression of the fuel mixture in the secondary chamber.

$$K_{G_2} = \eta K_{G_1} \qquad \text{Equation 10}$$

This amplification is what then causes the localized pressure spikes that exceed the designed pressure limits of enclosures and ultimately lead to catastrophic failure when inappropriately managed.

2.5.3. Experimental Observations of Pressure Piling

Experimental studies, including those performed by Krause et al. [12], and Li et al [40], have demonstrated the impact internal installations and complex designed enclosures significantly have on pressure piling using flammable fuel mixtures such as methane-air and/or acetylene-air mixtures.

The experimental work conducted for this research paper initially conducted a comprehensive theoretical analysis of pressure piling by employing fundamental equations and studying previous experimental studies. Subsequently, two experimental settings were prepared – an enclosure installed with a metallic plate with different orifice size openings as well as an enclosure with internal installation made from welded steel plates and blocks replicating electrical devices.

The purpose of these configurations is to replicate the circumstances observed in real-world industrial applications. The experimental research confirmed the validity of the theoretical analysis and demonstrated that the relevant requirements in the standard were met.

2.6. Safety Regulations and Standards in Hydrogen Production Plants

Hydrogen, which is known for its vigorously violent explosive nature, demands thorough safety measures when it comes to the handling of it in large quantities in large scale industrial settings. To mitigate the risks associated with hydrogen explosions, various international bodies, such as the IEC [9], have come up with safety standards and regulations that establish guidelines to help ensure that facilities comply with the best practices for explosion protection, environmental safeguarding and safety processes.

2.6.1. Overview of Key International Standards

Hydrogen production and handling is governed by safety regulations that have been developed by international standard bodies such as the International Electrochemical Commission (IEC) [9], the National Fire Protection Association (NFPA) [55], and the International Organization for Standardization (ISO) [56]. These organizations provide comprehensive frameworks that industries must adhere to for the safe operation of hydrogen systems.

- **IEC 60079-1** [9], is one of the most relevant standards that focuses on explosion protection by flameproof enclosures (Ex'd). This standard outline the equipment for flameproof enclosures that can contain explosive gases and mitigate the ignition of explosive atmosphere outside the enclosure. This standard furthermore details the design specifics, testing procedures and certification process of enclosures used in flammable gas production facilities like those of hydrogen gas. Specific tests, particularly related to the tests performed for this thesis' experiment, include assessing the enclosure's ability to withstand internal explosions and evaluating whether explosion pressure can penetrate enclosure walls to ignite the explosive atmosphere outside.
- **NFPA 2** (Hydrogen Technologies Code) [55], sets forth guidelines for the production, storage, and use of hydrogen across various industries. The NFPA standards also include provisions for hazard analysis, equipment selection, and installation practices for safe handling of hydrogen gas. On the other hand, **NFPA 55** [57], compliments these efforts by addressing safety protocols of hydrogen systems as compressed gases and cryogenic fluids.

- **ISO/TR 15916** [56], provides basic considerations for hydrogen safety systems. These standards cover risk assessment, hazard identification and mitigation strategies for the handling and storage, and use of hydrogen gas. It emphasizes the importance of safety considerations in designs in order to reduce the risks of explosions and the critical role that engineering control plays in minimizing human exposure to hazardous conditions.

2.6.2. Importance of Hazard Assessment

Identifying potential explosion risks, understanding the conditions under which hydrogen becomes explosive, and implementing the necessary safety precautions are the fundamentals of hydrogen safety management. Hazard assessment is essential to ensuring that hydrogen facilities operate safely and key elements in this process include:

- **Explosion Prevention** – measures such as controlling ignition sources, maintaining a safe fuel-air mixture concentration are just some of the measures employed to prevent explosions. NFPA 2 [55], specifies that hydrogen plants must be designed with adequate ventilation systems to prevent the accumulation of hydrogen gas which could potentially lead to an explosion.
- **Explosive containment** – As mentioned in IEC 60079-1 [9], flameproof enclosures play a pivotal role in containing explosions and preventing their propagation to the surrounding atmosphere outside the enclosure. The enclosures are designed to withstand the pressure generated during an internal explosion and dissipate energy safely within the container ensuring no damage to the exterior surroundings.

- **Emergency venting systems** – during an explosion, emergency venting systems is required in order to safely relieve the pressure and consequently reducing the damage. The use of emergency venting systems are requirements from various standards, including ISO/TR 15961 [56] and NFPA 55 [57]. These standards ensure the design of these systems to direct explosive gases away from critical equipment and personnel areas, thus ensuring minimal potential damage.

2.6.3. Role of Inherent Safety Design

One of the most fundamental ways of ensuring the safety in the green hydrogen value chain is through inherent safety designs [58], a philosophy aimed at eliminating or significantly reducing hazards rather than relying on protective measures. This approach relies on the following strategies:

- **Minimizing hydrogen storage volumes** – facilities can reduce the risks of large-scale explosions by reducing the amount of stored hydrogen on site [17]. This strategy is important especially in cases where it is possible to allow more real time use of the hydrogen gas instead of storing it.
- **Limiting explosive atmospheres** – maintaining the hydrogen-air mixture in the lean and rich mixture regions, such that the mixture concentration is below the Lower Explosive Limit (LEL) (4%-volume in air) and above the Upper Explosive Limit (UEL) (75%-volume in air), is a key part in reducing explosion risks [59, 60][61]. This will inherently reduce the potential for an explosion as there will be insufficient oxygen to support combustion.
- **Passive safety design considerations** – incorporating passive safety features into hydrogen systems is one of the inherently safety design aspects that is employed

to mitigate the risk of explosions. For example, using materials that are designed to have high thermal stability or low flammability in order to prevent the escalation of an explosion in the event of hydrogen leakage [11].

2.6.4. Regulatory Compliance and Audits

To maintain safety in hydrogen production plans and the overall value chain, it is imperative to comply with regulatory measures and safety audits. International authorities such as the Occupational Safety and Health Administration (OSHA) [61], and local authorities such as the Namibia Standards Institute (NSI) [62], often require production facilities to conduct regular safety audits and inspections that typically involve risk assessments, compliance checks, and documenting and reporting incidents on site.

2.6.5. Safety Innovations and Technological Advancements

Recent technological advancements have been developed to contribute to safety enhancement in gas production plants with the aim of monitoring, detecting and mitigating risks associated with explosions. Some of the notable advancements include:

- **Gas leakage detection systems** – modern gas production facilities employ the use of gas leakage detection technologies that continuously monitor the gas levels in real-time, concurrently triggering alarms, and initiating shutdown procedures before concentration reaches dangerous levels.
- **Explosion suppression systems** – in small, enclosed spaces where gas leaks could potentially lead to a confined explosion, explosion suppression systems can be installed in order to detect explosions at inception stages and release suppressant agents in order to quench the flames and prevent further propagation.

- **Condition monitoring and preventive maintenance** – this is a proactive approach that can be employed in facilities to prevent incidents caused by equipment malfunctioning or degradation [11]. This approach monitors equipment health, and schedule maintenance before incidents occur.

2.6.6. Lessons Learnt from Past Explosion Events

Ever since the global shift towards clean energy transition, hydrogen use has gained attention. Hydrogen incidents all over the world have been reported and they provide valuable lessons that shape current safety standards and regulations [63]. Some of the notable incidents include, but are not limited to:

- **The 2019 Hydrogen Tank explosion in South Korea** [64] – in May 2019, a devastating incident happened in Gangneung South Korea, where a hydrogen tank exploded due to a hydrogen gas leak, however the source of ignition inside the hydrogen tank has not been proven. This incident highlights the importance of real-time leak monitoring and rigorous safety inspections.
- **Hydrogen explosion incident in BASF Germany** [65] – in July 2024, an explosion occurred at the BASF chemical plant in Ludwigshafen, Germany. This incident was caused by a brief ignition of hydrogen gas that leaked and ultimately injured 15 people on site. This incident emphasizes the importance of stringent safety measures and the importance of employing monitoring systems, particularly for leakage detection in large scale industrial settings.
- **Hydrogen fuelling station explosion in Germany** [66] – in June 2024, a fire broke out following an explosion at a hydrogen fuelling station that was newly opened in Augsburg, Germany. According to the investigations done, the

explosion was attributed to a failure in the safety valve mechanism which resulted in the hydrogen leaking and igniting. This incident highlights the importance of regular maintenance to prevent such occurrences in fuelling infrastructures.

CHAPTER 3. RESEARCH METHODS

3.1. Research Instruments

The basic equipment used for this experiment can be categorized into four types: test sample enclosures, ignition system, gas mixing and filling system, and measuring and logging system.

3.1.1. Test Sample Enclosures

A total of five enclosures were used for this research (see Figures 5 to 7), which for better clarity will be referred to as follows:

- **Sphere** – consisting of a 10L volume stainless steel flameproof spherical enclosure
- **Short Tube** – consisting of a 250mm length cylindrical stainless-steel tube, with a diameter of 161.5mm
- **Long Tube** – consisting of a 500mm length cylindrical stainless-steel tube, with a diameter of 161.5mm
- **Twin Tube** – consist of the combination of 250mm and 500mm cylindrical stainless-steel tubes of same diameter.
- **Complex housing** – This is a replicated design of a flameproof enclosure that is currently of industrial-use as an electrical system housing enclosure.

1. Sphere

Figure 5 shows the spherical test sample that was equipped with four pressure sensors, namely p_1, p_2, p_3 and p_4, installed on the cover flush against the wall at 45° angle. The ignition for this test was a centrally located tip-ignition electrode within the enclosure.

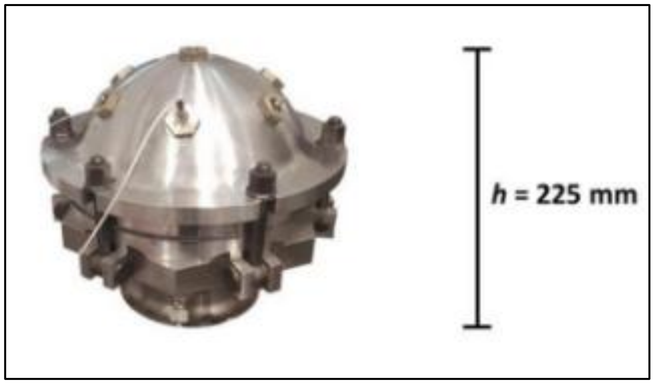

Figure 5: The sphere test sample.

2. Short and Long Tube

Both cylindrical enclosures (Figure 6) were configured in a similar manner, such that the gas inlet pipe was located at one end of the tube and the gas outlet was positioned at the other end. The ignition for this setup is provided by a spark plug installed near the gas inlet side of the tube. The setup included two pressure sensors of the same model, Kistler 601CAA: Sensor 1, measuring pressure 1 (p_1), was positioned on the gas inlet side of the tube, while Sensor 2, measuring pressure 2 (p_2), was located on the gas outlet side.

3. Combined tube

The same procedure was applied to the combined tube setup. However, because the setup is such that there had to be an orifice placed between the tubes to separate it into two chambers, the gas inlet side is considered the primary chamber, while the gas outlet side is considered the secondary chamber. This setup is sometimes referred to as the twin-tube setup as the two cylindrical enclosures replicate a twin setup and therefore the term is used interchangeably with the combined tube setup.

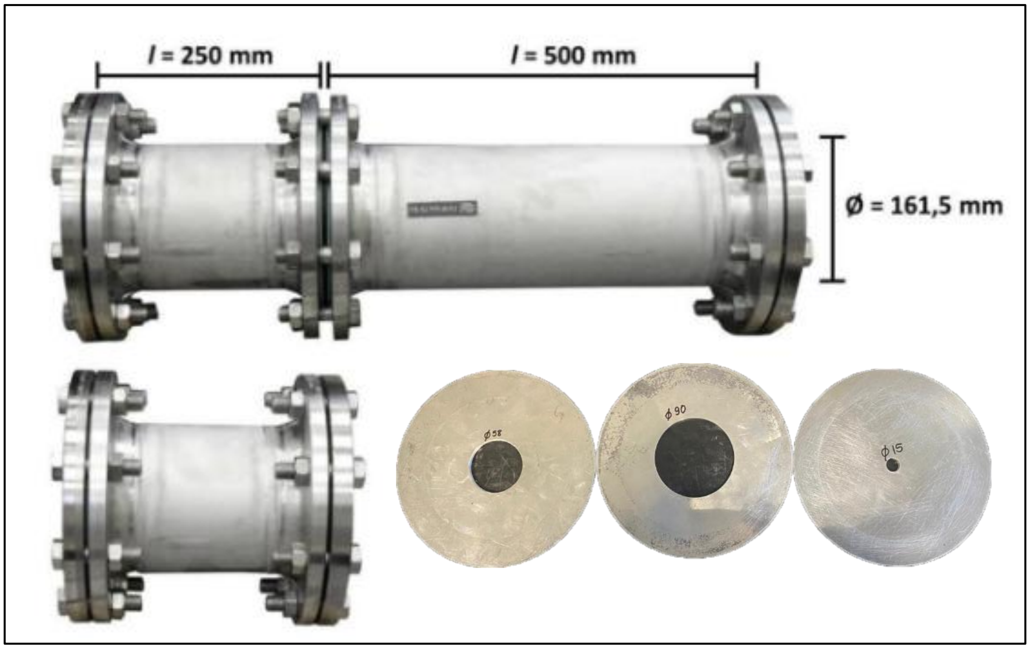

Figure 6: Cylindrical test samples and the orifice plates used to separate the chambers.

4. <u>Complex housing</u>

Besides the basic symmetrical geometry test samples, this experiment also utilized a replica of a real industrial flameproof enclosure. This enclosure is designed with multiple chambers with the primary intention of housing electrical devices, as shown in Figure 7. For the test, the sample was equipped with six sensors strategically installed on various faces of the enclosure.

Ignition in these tests was initiated using a spark plug system, which was affixed to the wall on the gas inlet side of the enclosure. To establish a baseline for explosion pressure, the initial test was conducted in an empty multi-chamber enclosure. Subsequent tests were then performed with internal installations, where electrical components were replicated using steel plates and welded steel blocks, allowing for the evaluation of how these installations affect explosion pressure within the enclosure.

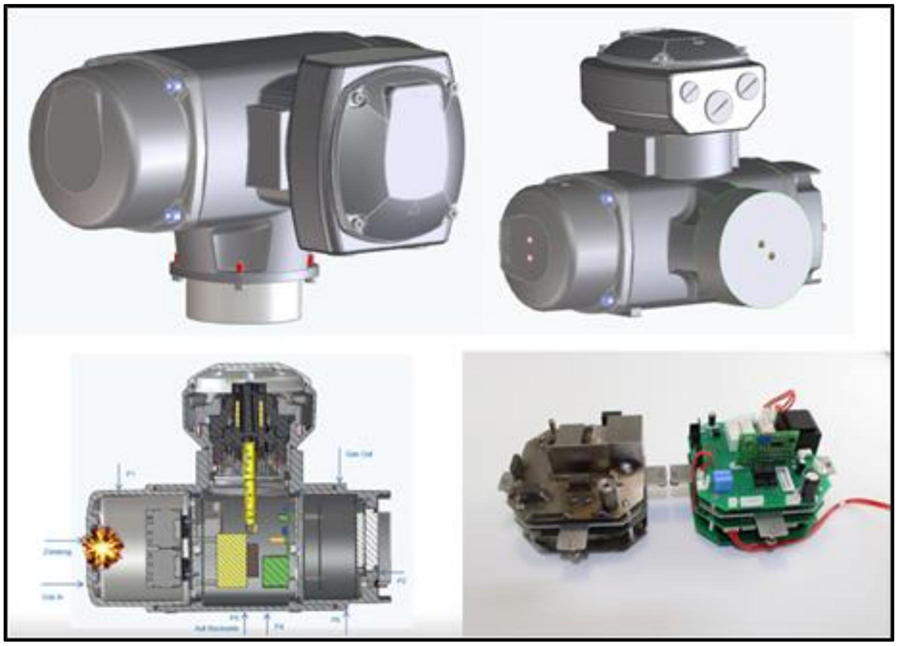

Figure 7: Multi-chamber enclosure.

3.1.2. Ignition System

Depending on the specific experimental configuration, either spark plugs affixed to the wall of the test sample or tip electrodes for central ignition were employed to ignite the corresponding fuel-air mixture. Figure 8 illustrates the two ignition systems used.

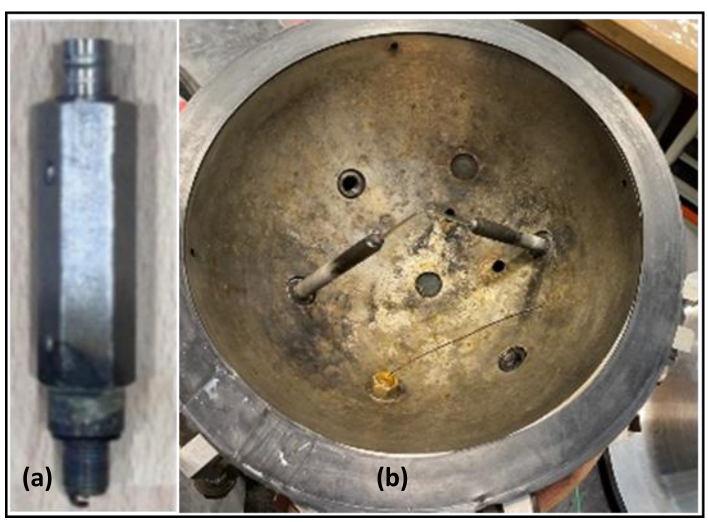

Figure 8: Explosion ignition systems; (a) spark plug, (b) tip electrodes.

3.1.3. Gas Mixing and Filling System

1. Oxygen analyzer

The oxygen analyzer used for the tests is the SEEVOMEX model 2210 as shown in Figure 9. This device allows the user to determine the percentage of gaseous fuel in the enclosure to achieve the right stoichiometric ratio for optimal explosion pressure. Calibration of the oxygen analyzer is necessary at the beginning of every test, as detailed in the SEEVOMEX manual [67].

Figure 9: Oxygen analyzer.

2. Control program

The desired gas composition, the ignition, and the valves were controlled via the test bench control program in a control room computer on site as shown in Figure 10. Data such as temperature, humidity and oxygen level/content are also shown.

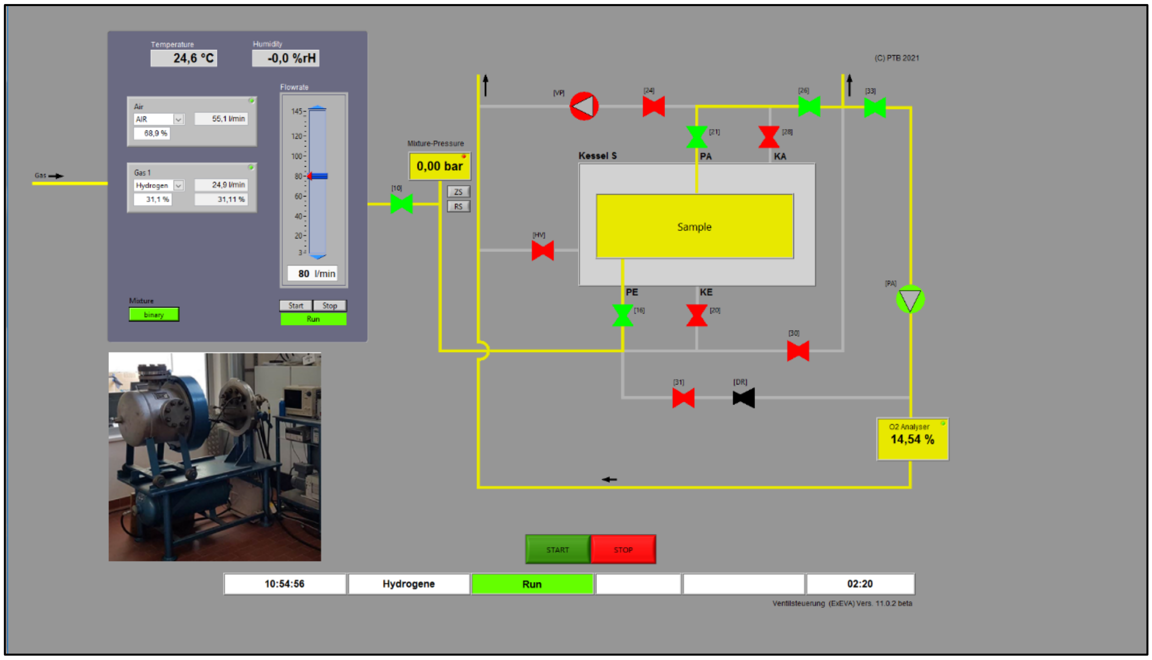

Figure 10: Gas mixing and filling system.

3.1.4. Measuring And Logging Systems

1. Pressure sensors

The experiments used Kistler's piezoelectric sensors for taking pressure measurements. The key parameters of these sensors are provided in Table 2.

Kistler 601CAA model sensors were purposely chosen for this experiment due to their advantage in low overload limit of 300 bar and a high sensitivity in the natural frequency as compared to other Kistler sensor models.

Table 2: Technical specifications for the Kistler piezoelectric sensors.

Type	Sensitivity 0-50 bar
601CAA + 1mm RTV	-36.84 pC/bar
601CAA + 1mm RTV	-36.90 pC/bar

601CAA + 1mm RTV	-37.57 pC/bar
601CAA + 1mm RTV	-36.71 pC/bar
601CAA + 1mm RTV	-36.70 pC/bar
601CAA + 1mm RTV	-36.71 pC/bar
601CAA + 1mm RTV	-36.86 pC/bar

A series of tests performed by Krause [68] have shown that thermal shock is a significant factor influencing measurement results when determining explosion pressure. To prevent thermal shock generated by the explosion and to avoid it from affecting the results obtained, a 1mm thick layer of room-temperature-vulcanizing (RTV) silicon was recommended to be applied to the sensor tip as shown in Figure 11.

Figure 11: Kistler 601CAA pressure sensors with 1mm RTV silicone.

2. <u>Sensor Data Capturing</u>

Kistler LabAmp web interface (Figure 12) in conjunction with the control program is used for capturing sensor data and recording their measurements during the test. Data such as the sensor serial number, sensitivity settings and low-pass filter frequency are preset and captured for the control program to be able to communicate with each sensor and record live signals. This web interface gets the signals from the amplifier.

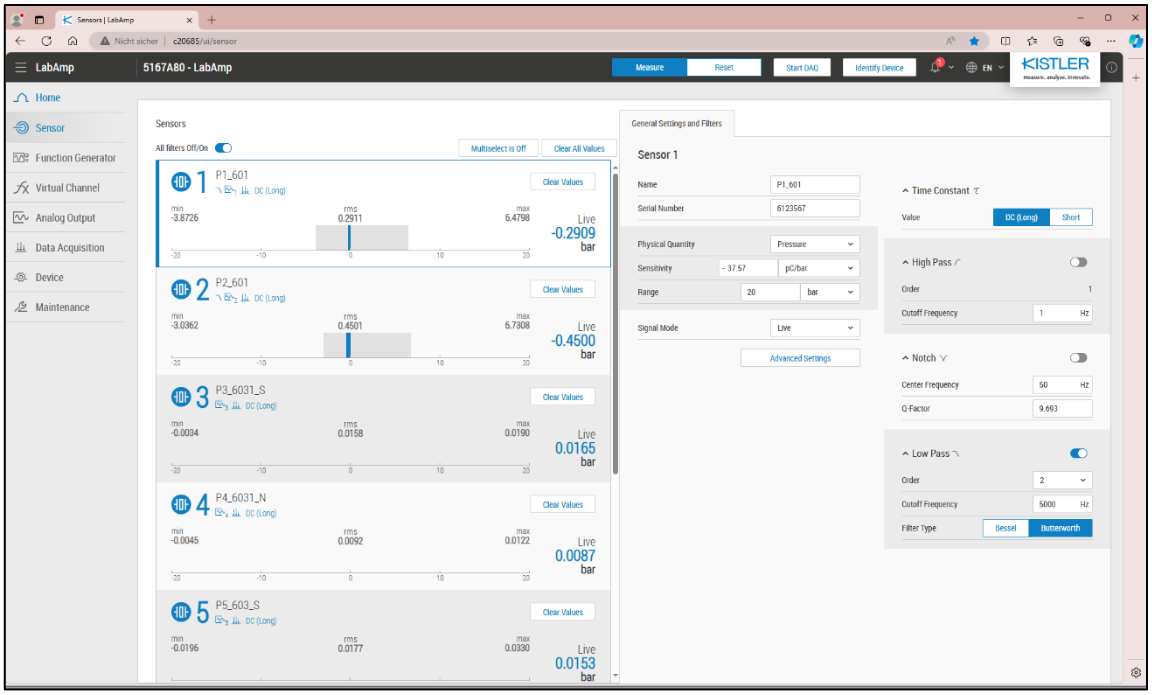

Figure 12: Kistler LabAmp web interface.

3. <u>Charge Amplifier</u>

The Kistler LabAmp 5167 charge amplifier (Figure 13) was used for receiving and amplifying the explosion pressure signal from the sensors. The charge amplifier operates by receiving signals from the piezoelectric pressure sensors and transforming the charge present at the sensor output into a measurable voltage. The amplifier is controlled via the LabAmp web interface by providing means to configure the sensitivity, measuring range, and frequency for filtering the measured values obtained from the pressure sensors.

Adjustments to the frequencies of the high and low pass filters can be made manually. To conduct these tests, a constant frequency of 5kHz was employed for filtering.

Figure 13: Kistler LabAmp 5167 charge amplifier.

4. <u>Oscilloscope</u>

The voltage signal produced by the amplifier is transmitted to an oscilloscope, specifically the Yokogawa model DL850, as shown in Figure 14. From there, the measurements are examined in real time and stored as comma-separated values (CSV) files for subsequent analysis. The use of low-pass filters with a cutoff frequency of 5 kHz is necessary for recording pressure signals [53].

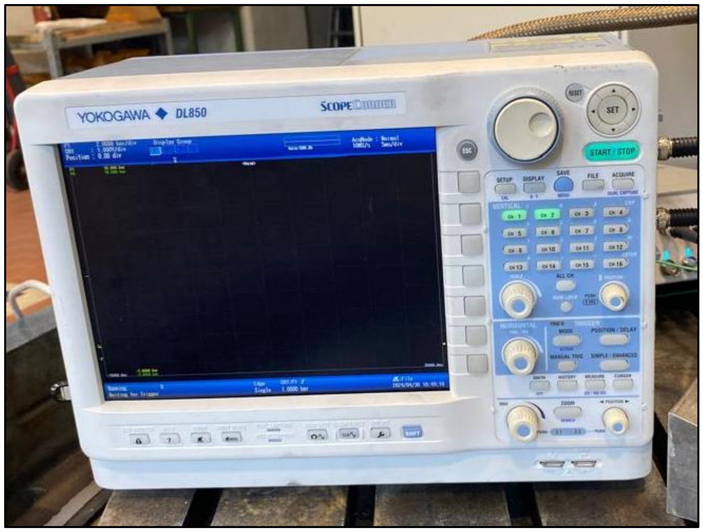

Figure 14: Yokogawa DL850 Oscilloscope.

To ensure adequate resolution of the measurement results, it is recommended to use a sampling rate that is at least ten times the highest signal frequency. This means that a sampling rate of at least 50 ksps should be selected for signals up to 5 kHz.

3.2. Experimental Setup

Figure 15 depicts the overarching model corresponding to the fundamental framework employed in the experiment.

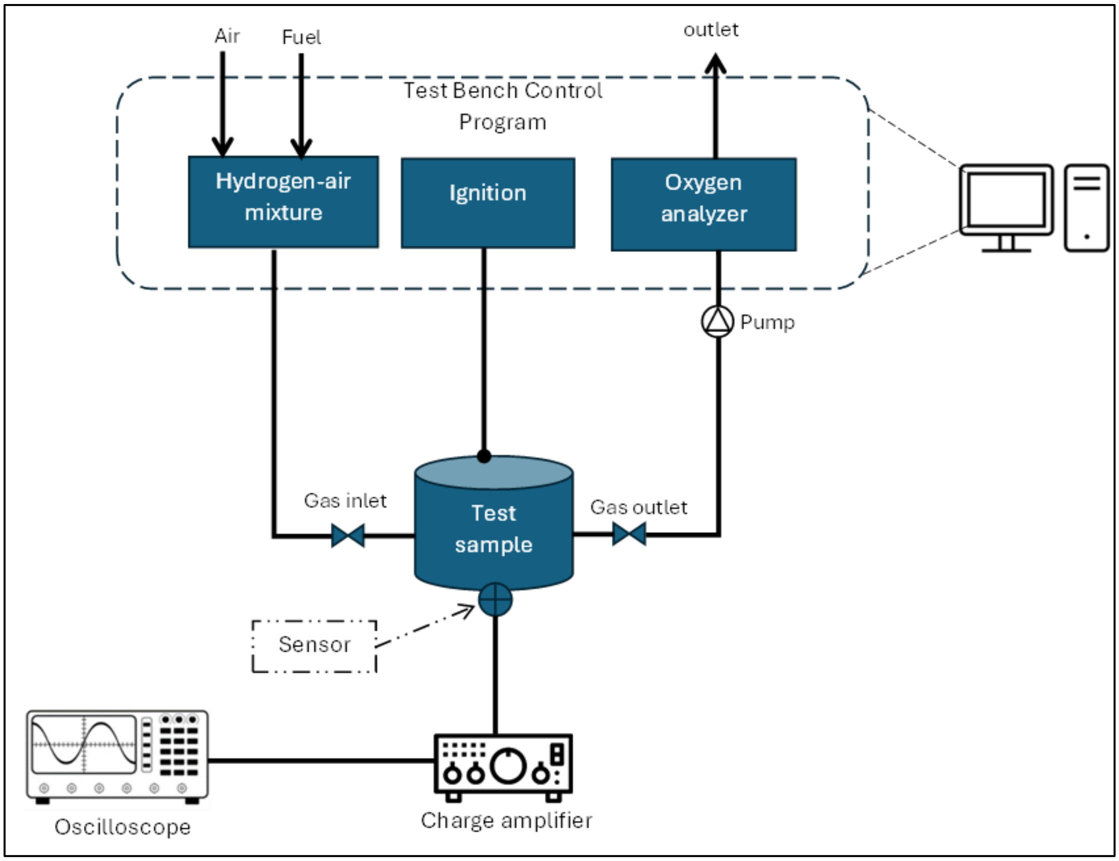

Figure 15: Schematic layout of the experiment setup.

The geometric characteristics of the test sample, together with the quantity and placement of the pressure sensors, gas pipes, and the ignition, are merely illustrative.

The electronic components of the experimental configuration, outlined in section 3.1, were calibrated using several methods and according to their individual user manual recommendations to showcase their metrological characteristics. All the tests performed in this experiment were conducted at room temperature and ambient air pressure.

The experimental configuration utilized hydrogen gas supplied from compressed gas cylinders that were commercially produced and supplied. Prior to every test, the enclosures were initially purged with nitrogen gas – during the air cleaning process. The hydrogen-air mixture is then injected into the test sample using a mass flow controller through the test bench control system. The mass flows are controlled based on predetermined setpoint values, with flow rates ranging from 50L/min to 80L/min, depending on the volume of the test sample.

Each piezoelectric pressure sensor used for the test is affixed to the walls of the test samples and effectively secured with a torque of 4 Nm. An electrical link is established between the sensors and the charge amplifier using highly insulated connecting cables.

Subsequently, the sensor output signals are captured and saved using an oscilloscope equipped with a recording feature through the analog outputs of the charge amplifier. The triggering device in an ignition system is attached to the wall of the test sample. In order to enable simultaneous initiation of the logging system, the ignition system was linked to the test bench control system (Figure 16).

Both signal acquisition and signal processing are integral components of the measurement chain. Signal acquisition is conducted using an oscilloscope equipped with a recording element positioned behind the charge amplifier. The sampling frequency typically operates at 5 kHz. A direct current (DC) coupling is chosen for the input modules to capture the complete signal without any suppressed DC components. The subsequent signal processing for filtering and display is performed using the Python programming language.

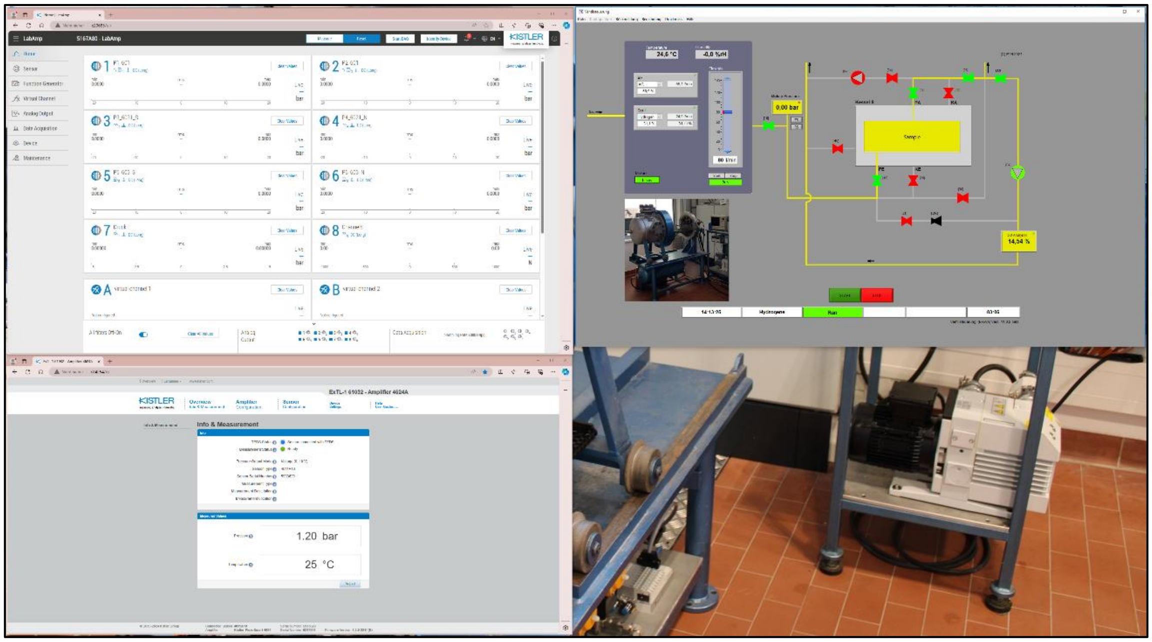

Figure 16: A screenshot overview of the computer screen for test bench control program.

This experiment examined the phenomena of pressure piling using two different methodologies: Firstly, three distinct plates with different orifice openings are positioned between the two cylindrical chambers to form primary and secondary explosion chambers.

The second part employs an intricately crafted enclosure with several chambers and internal installations that replicate electrical devices.

3.3. Experimental Procedures

The procedures for the experiment followed the steps as shown in Figure 17 as a flowchart. Before conducting each experiment, the oxygen analyzer had to undergo calibration as specified in the supplied manual, in order to ensure accurate measurements of oxygen levels during the tests.

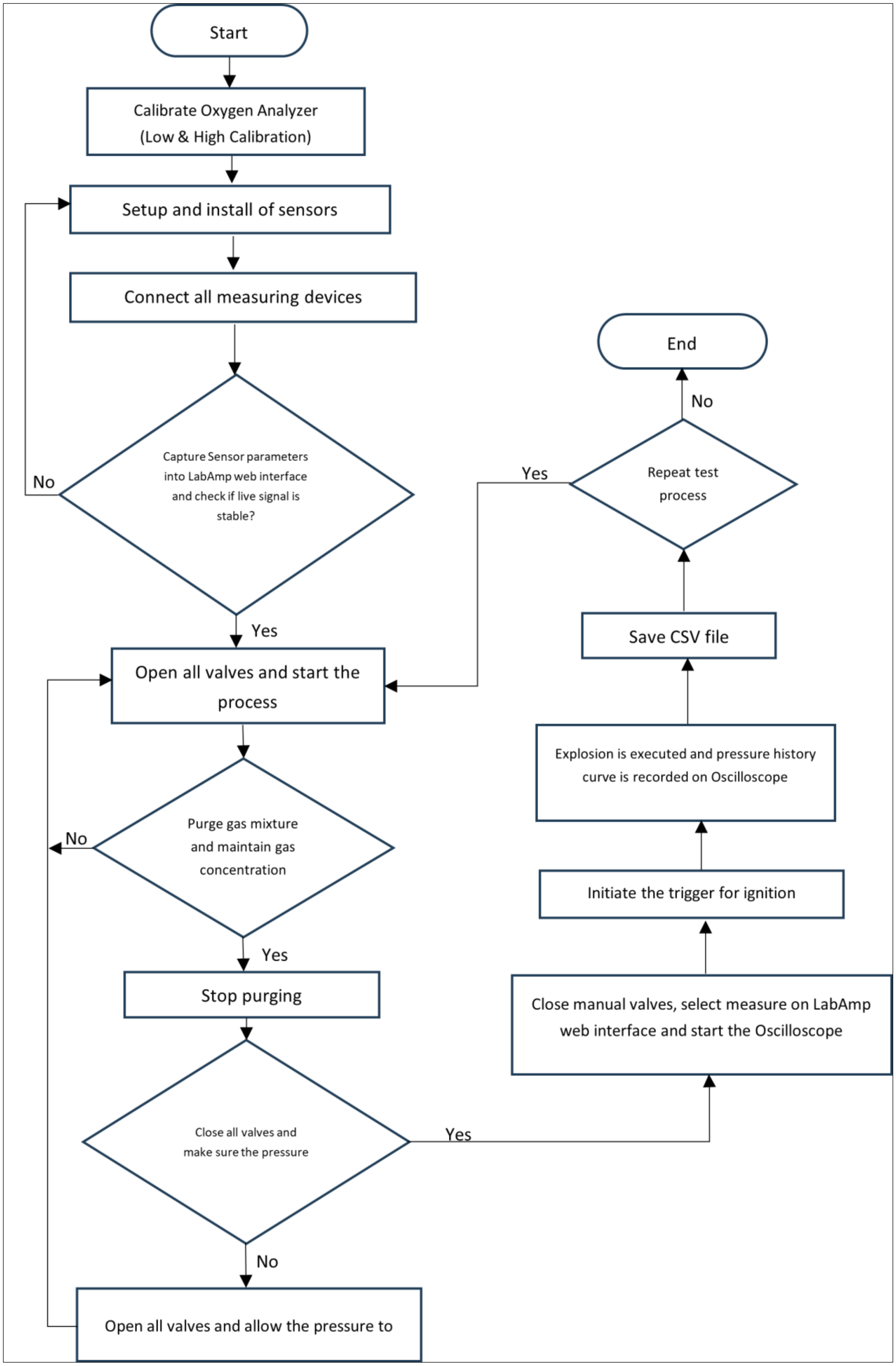

Figure 17: Flowchart for the experimental procedures.

The calibration was performed using two separate procedures.

1. **Low calibration procedure -** the low calibration was conducted by injecting 100% pure Nitrogen gas (N_2) into the test samples to purge any residual oxygen or air from the housing. This step is essential to eliminate any contamination and create a baseline with a zero concentration of oxygen gas. Following this, the calibration is carried out by adjusting the oxygen concentration to 0% to establish the baseline reading.
2. **High calibration procedure** - The second phase is the high calibration which involves flushing the housing with ambient air. This procedure adjusted the oxygen content to a standard atmospheric level of 20.95%, which was then maintained consistently throughout the testing phase. During the process, the test bench valve control program provided real-time oxygen content readings obtained from the oxygen analyzer to ensure that the calibration was accurate.

Once the oxygen analyzer calibration was completed, the experiments proceeded with the following steps:

1. Gas mixing preparation - both manual (hand valves) and automated valves were opened to enable the hydrogen-air mixture to freely enter the enclosure. The concentration of hydrogen-air mixture for each test series is initially established in the test bench's control system. In accordance with the IEC 60079-1 standard [9], the designated hydrogen fuel ratio for each test was set at 31 ± 1%. This ratio was particularly chosen to replicate real-world conditions where the hydrogen-air mixtures are within the explosive limits. To achieve a quiescence and uniformity,

the hydrogen-air mixture was filled into the test sample for approximately three minutes.

2. As soon as the required hydrogen-air ratio is established, the oxygen analyzer located at the outflow continuously measures the oxygen concentration in the housing. Real-time monitoring was crucial to verify that the mixture was properly prepared. The filling process was then halted once the oxygen analyzer reached a consistent reading of 14.54%. Both the hand valves and automated valves coupled to the oxygen analyzer were then closed in order to isolate the test enclosure and prevent any backflow or leakage of the fuel-air mixture.
3. The test control program governs the operation of the ignition process and the data logging system. Once the test sample was securely isolated, the ignition system was then triggered. Following the initiation of the trigger, an explosion is executed within the enclosure. During this moment, the control system monitors the ignition and the resulting combustion parameters in real time.
4. The measured variables were passed through the charge amplifier that employed a low-pass filter with a designated cutoff frequency of 5 kHz, as outlined in the IEC60079-1 standard requirements [9], to capture the explosion dynamics accurately. Thereafter, the filtered data was transmitted to the oscilloscope, where the pressure-time histories were recorded and stored as a CSV file for future analysis.
5. For each configuration, 5-10 repetitions of explosion tests were conducted, in order to ensure results' repeatability and reliability. The data for maximum attained pressure, from each sensor, from each test was recorded on an Excel sheet, which facilitated subsequent analysis. Descriptive statistics, such as mean values,

and standard deviations were calculated and used to observe result uncertainties to validate the experimental findings. Further detailed information of the excel recorded data is provided in **Appendix 2** of this thesis report.

6. In preparation for the next test, the test sample was air-cleaned, by filling it with normal air to remove any residual gas mixture, until the oxygen level reached 20.95%. This process was important to prevent contamination or carryover effects between successive tests. The test sample was therefore replenished with a fresh mixture to guarantee complete purging of the test sample before proceeding to the next test.

This rigorous approach contributed to the validity and reliability of the result findings obtained from the experiments.

CHAPTER 4. RESULTS AND DISCUSSION

4.1. Explosion Pressure Test Results and Discussions

A series of tests were performed on basic geometric enclosures: Spherical, short and long cylindrical tubes. The aim for these tests was to establish a basis for understanding how the geometry of an enclosure influences the pressure dynamics of a hydrogen-air mixture during a deflagration explosion.

4.1.1. Spherical Enclosure

Figure 18 gives a graphical representation of the pressure history curve for the spherical enclosure. The curves indicated on this graph are for all the four sensors used to measure the explosion pressure within the spherical enclosure.

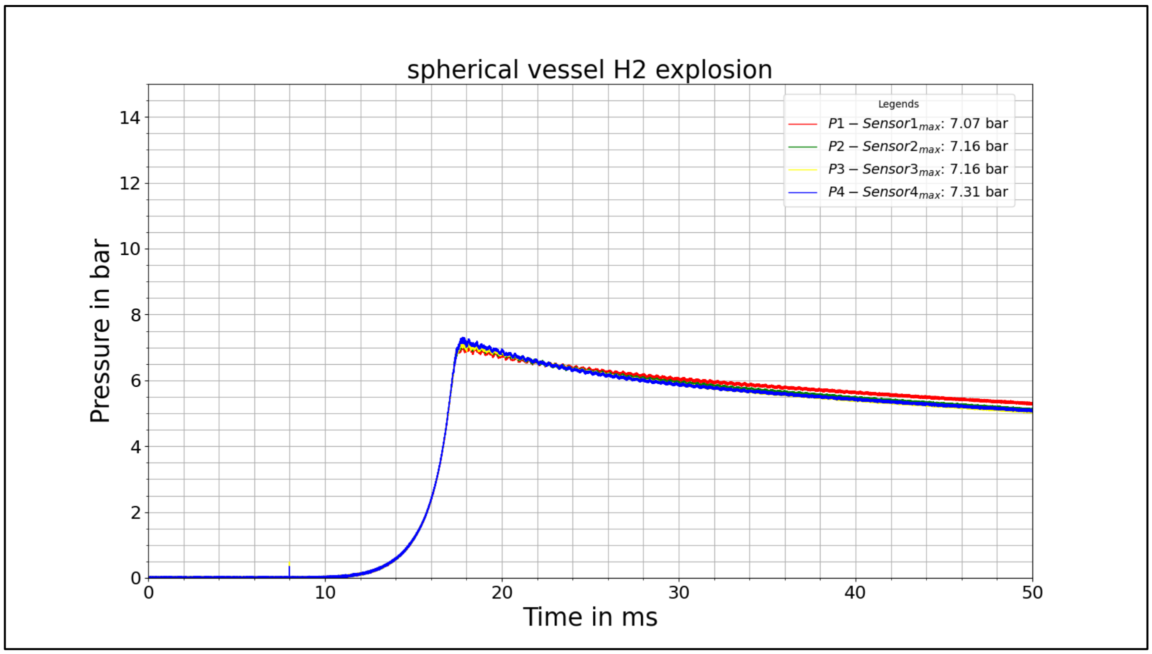

Figure 18: Pressure history curves for the spherical enclosures.

The curves indicate a rapid and steep rise in pressure following the ignition, reaching a peak value of 7.31 bar, which was recorded by pressure sensor P_4. This sharp increase aligns with theoretical expectations for spherical enclosures, as this type of enclosure tends to distribute pressure evenly and symmetrically, resulting in minimum heat dissipation during combustion. The symmetrical design of a spherical enclosure ensures nearly uniform flame propagation.

The literature reviewed in Chapter 2 has shown that spherical enclosures typically demonstrated higher peak pressure due to reduced surface area for heat dissipation, which was confirmed in the experiments by Krause and Markus [51]. Moreover, small to no disturbances were observed in the spherically propagating flame front and there was a low presence of turbulence due to geometric uniformity and this contributed to retaining the high-pressure readings.

Uncertainty plots have been generated for the pressure measurements of each sensor to provide insight into the variability of the measurements obtained. Figure 19 shows the results of uncertainty for the spherical enclosure. The graph utilizes the standard deviation data for the four sensors, and they range between 0.04 to 0.06 bar. This degree of variation reflects the relatively stable conditions within the enclosure, where the geometry reduces inconsistencies within the flame propagation and pressure developed. However, due to unavoidable minor human errors such as sensor misalignments, calibration limitations and sometimes minor inhomogeneities in the gas-air mixtures, minor deviations are prone to be picked up and contribute to the uncertainty level.

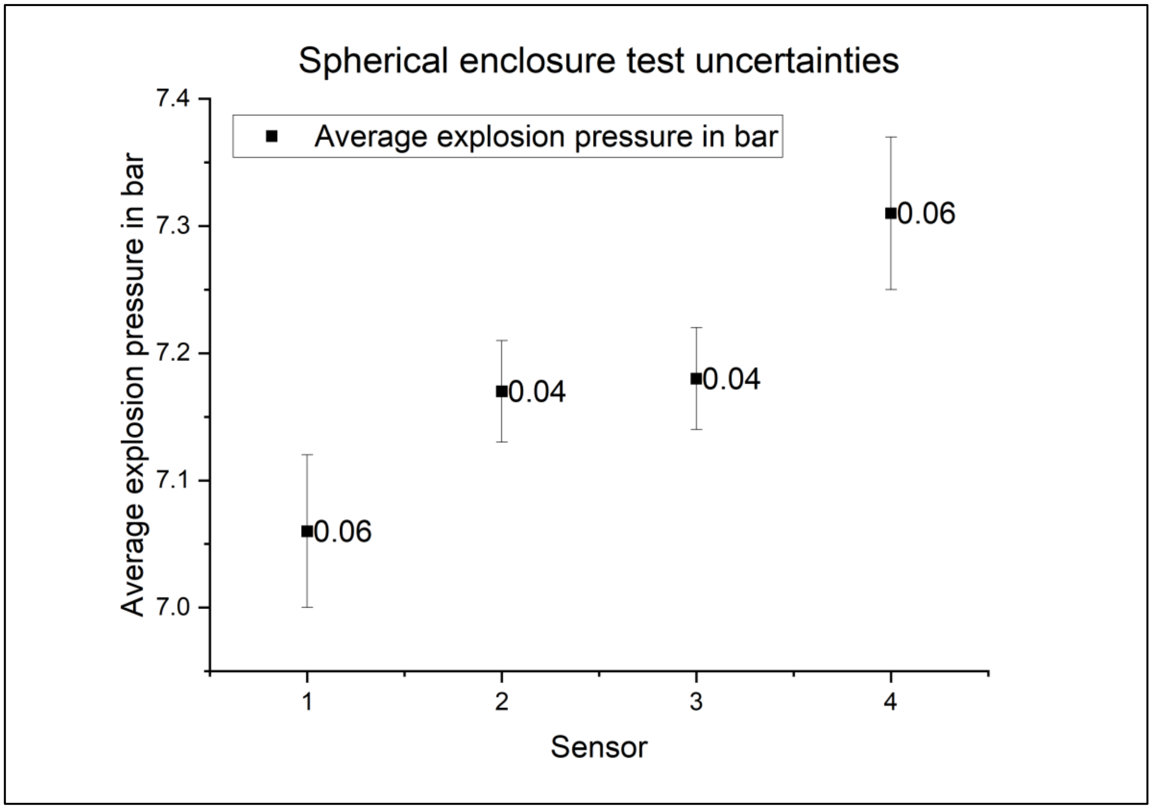

Figure 19: Spherical enclosure pressure sensor results uncertainties.

4.1.2. Cylindrical Enclosures – Short and Long Tube

The explosion pressure in the short tube reaches a maximum of 6.75 bar, while the long tube is 6.65 bar, as shown in Figure 20 and Figure 21, respectively. The cylindrical tubes have shown slightly lower maximum explosion pressure compared to the spherical enclosure (Figure 18), and this can be attributed to the longer shape of the cylinder, which allows for more surface area for heat dissipation. These results support the findings of Li and Hao (2020), which suggested that elongated geometries promote greater heat dissipation due to their geometric advantage of increased surface area[49].

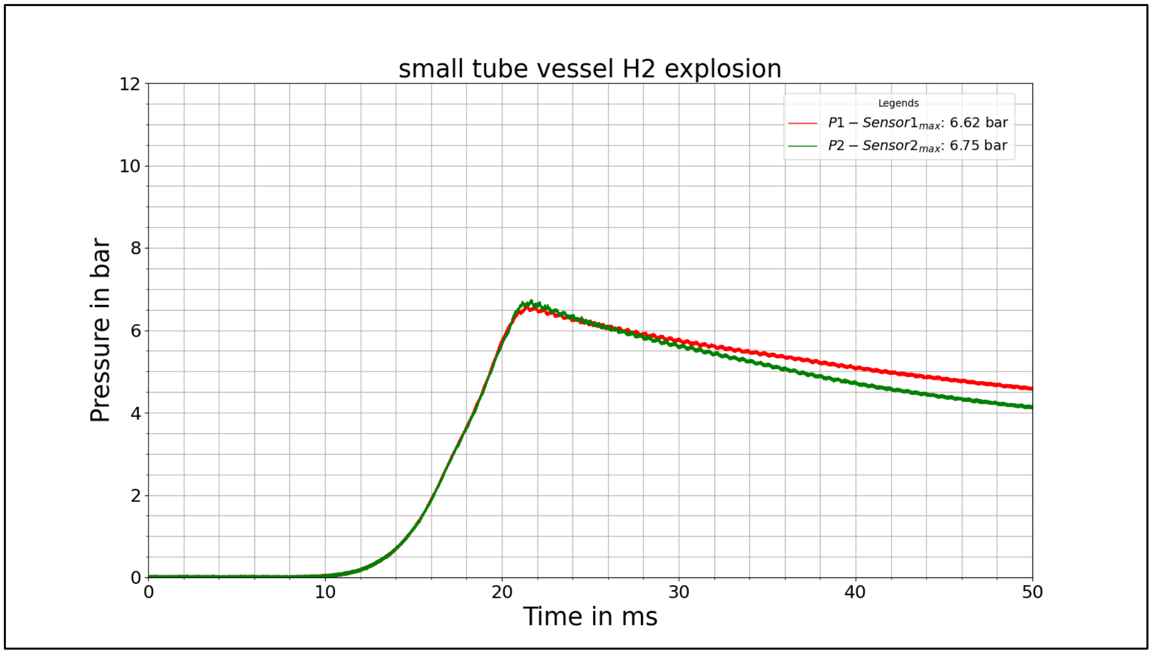

Figure 20: Pressure history curves for the short cylindrical enclosure.

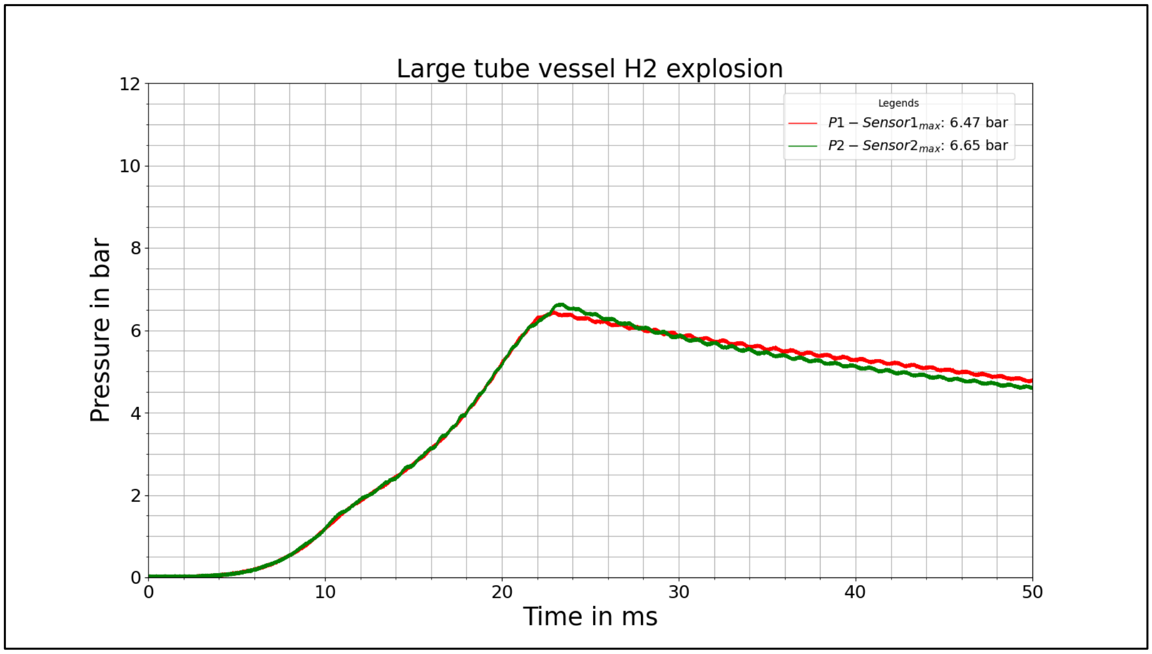

Figure 21: Pressure history curves for the long cylindrical enclosure.

Furthermore, the short and long tubes differ slightly in the maximum pressure recorded. The long tube demonstrated a rise in pressure that was slower and more gradual as compared to that of the short tube which is much steeper and faster. The long tube geometrically has a larger surface area as compared to the short tube. Therefore, during the explosion, the increased surface area facilitates the heat dissipation, reducing the energy available for sustaining high pressures. In contrast, the short tube, with its small surface area experiences less heat dissipation and thus records higher peak pressures. These findings reinforce existing studies which highlighted the effect of internal surface area and flame propagation distance on explosion pressures [51].

The uncertainties in the results reading from the sensors in both the short and long cylindrical enclosures are represented in Figure 22 and Figure 23, respectively.

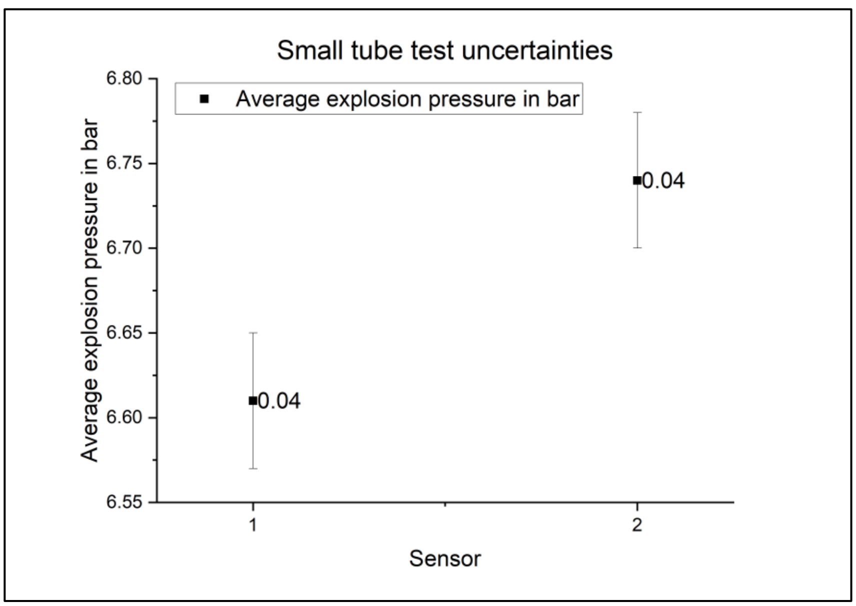

Figure 22: Small cylindrical enclosure pressure sensor results uncertainties.

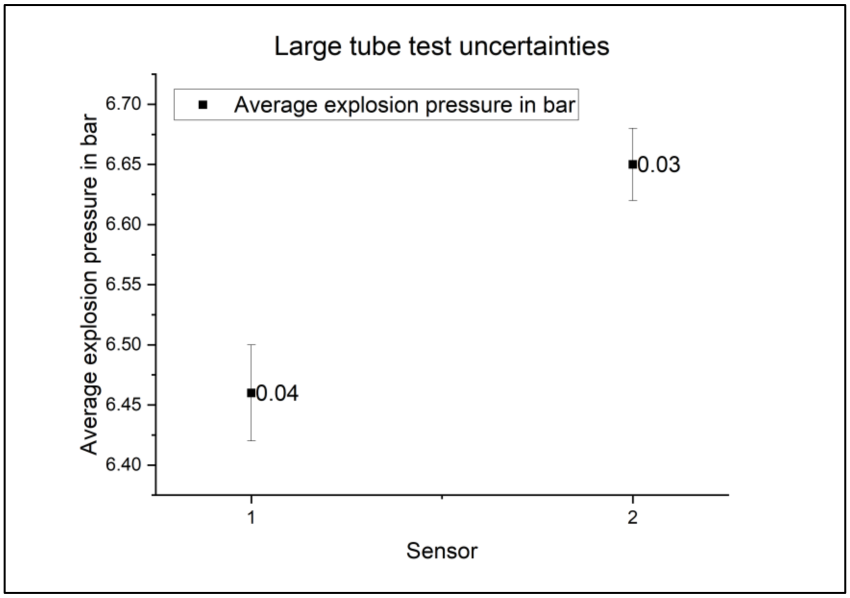

Figure 23: Large cylindrical enclosure pressure sensor results uncertainties.

The standard deviation between the readings is also in the range of 0.03 to 0.04 bar, similarly to that of a spherical enclosure. The slightly lower deviation values of the results can be attributed to the reliability of the sensors used and trusted calibration.

Figure 24 of the close comparison plot highlights the differences observed in pressure history profiles between the three basic geometries. The plot shows that the spherical geometry displayed the highest and most sustained maximum pressure, while the two cylindrical geometries declined faster after reaching their peak pressure values. The relatively low peak pressure results from the cylindrical enclosures are attributed to the high heat dissipation due to the design structure of the enclosure. In contrast, the spherical enclosure benefits from a central ignition point which allows for a more even distribution of pressure within the enclosure and consequently reduces localized heat dissipation.

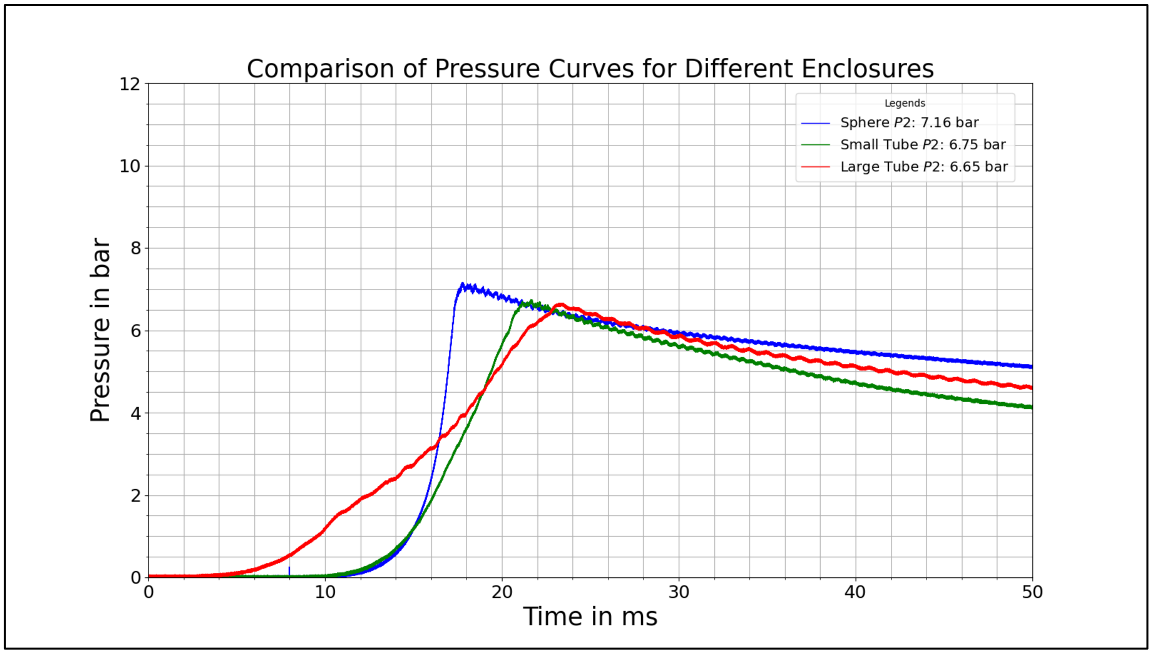

Figure 24: Comparison of the highest pressure recorded for the basic geometries.

In addition, the large cylindrical enclosure experienced a slow rise in pressure after the trigger. This could be attributed to the elongated length of the enclosure and the large cross-sectional area for the flame to propagate as compared to the spherical and short cylindrical enclosures. The comparative analysis displayed in Figure 24 confirms that the spherical enclosure provides a more confined environment with less thermal losses and consequently leads to higher peak pressures compared to cylindrical configurations.

The results discussed above for the basic geometric enclosures demonstrate the significant influence of enclosure geometry on the explosion pressure dynamics for hydrogen air mixtures. The discrepancies observed between the experimentally obtained values and those from ChemSAFE in Table 1 can be attributed to the practical absence of adiabatic conditions as an assumption. In the actual experiment, the thermal energy is released through the wall of the enclosure. Moreover, following a brief travel distance, disturbances arise in the initially spherically symmetrical flame front, leading to an increase in turbulence and the corresponding cooling of the heated combustion gases. In essence, every experimental measurement is inherently affected by measurement uncertainties stemming from a range of systematic and statistical factors throughout the entire measurement process, resulting in additional deviations.

4.2. Pressure Piling Observation Results and Discussions

4.2.1. Combined Tube Setup

The second part of the experimental work utilized cylindrical enclosures that were connected to replicate a tube with two compartments. This was done by separating the two enclosures with a steel plate with an orifice opening of 15mm, 58mm and 90mm diameters. Note that the words chamber and compartment are used interchangeably, both essentially referring to a section of the enclosure often separated by a partition or barrier to influence the flow of explosion pressure and dynamics within the system. The purpose of incorporating an orifice opening is to demonstrate the pressure piling effect for each size and here are the key observations displayed in graphical plots in Figure 25, Figure 26, and Figure 27, for 15, 58 and 90 mm orifice, respectively.

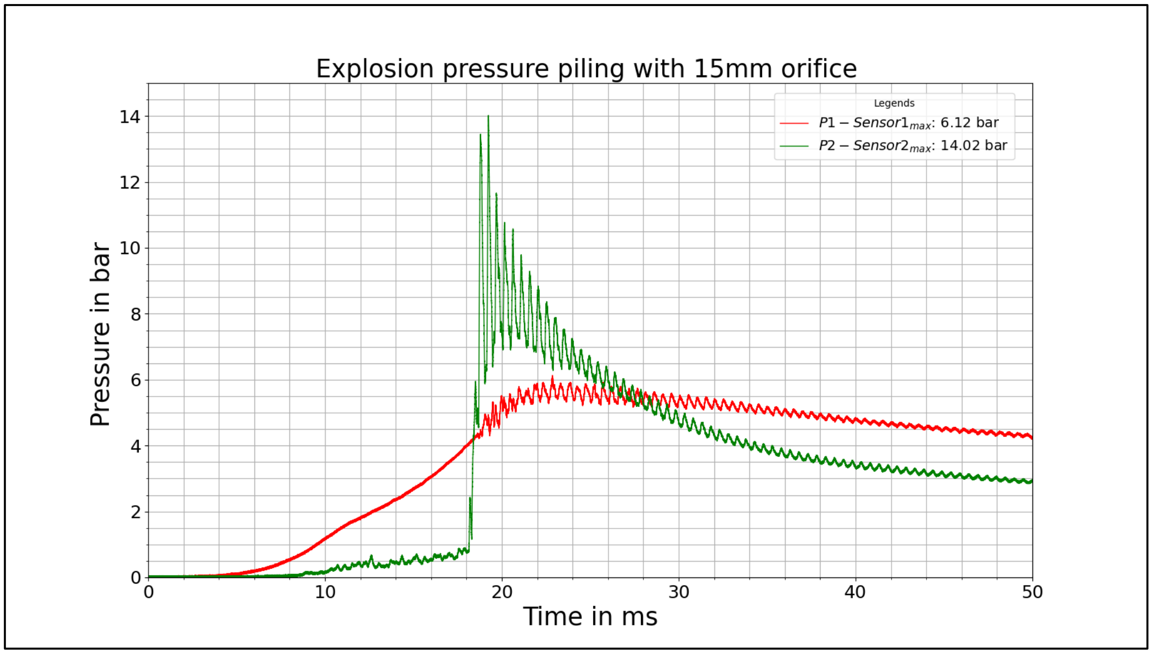

Figure 25: Explosion pressure profile for combined tubes with 15 mm orifice.

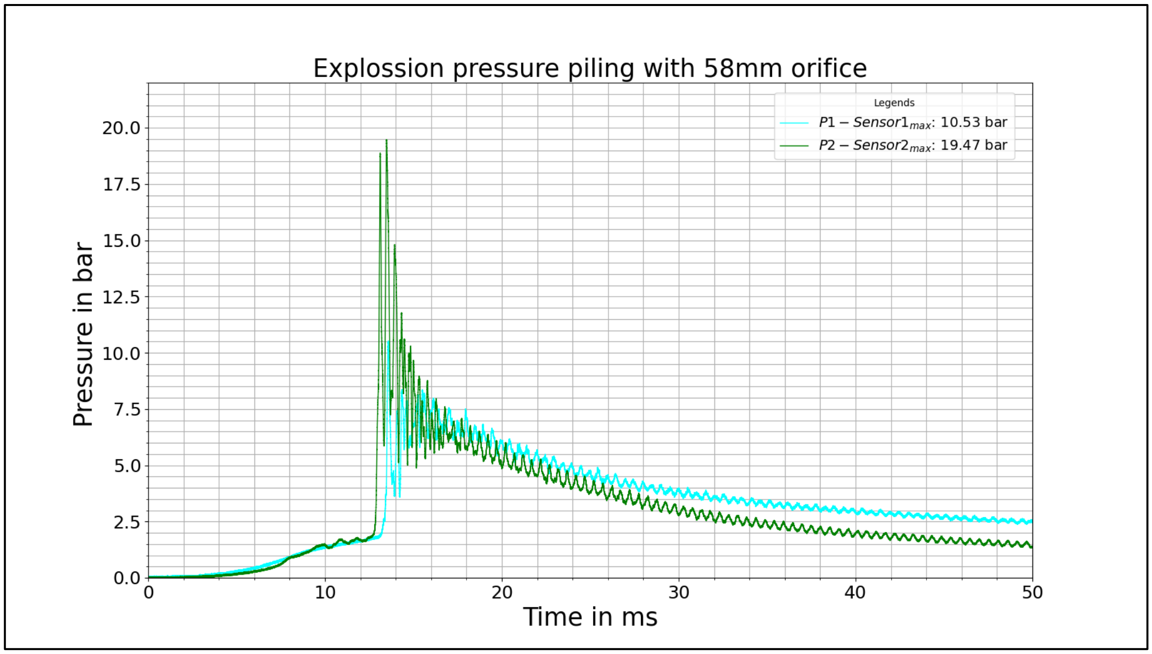

Figure 26: Explosion pressure profile for combined tubes with 58 mm orifice.

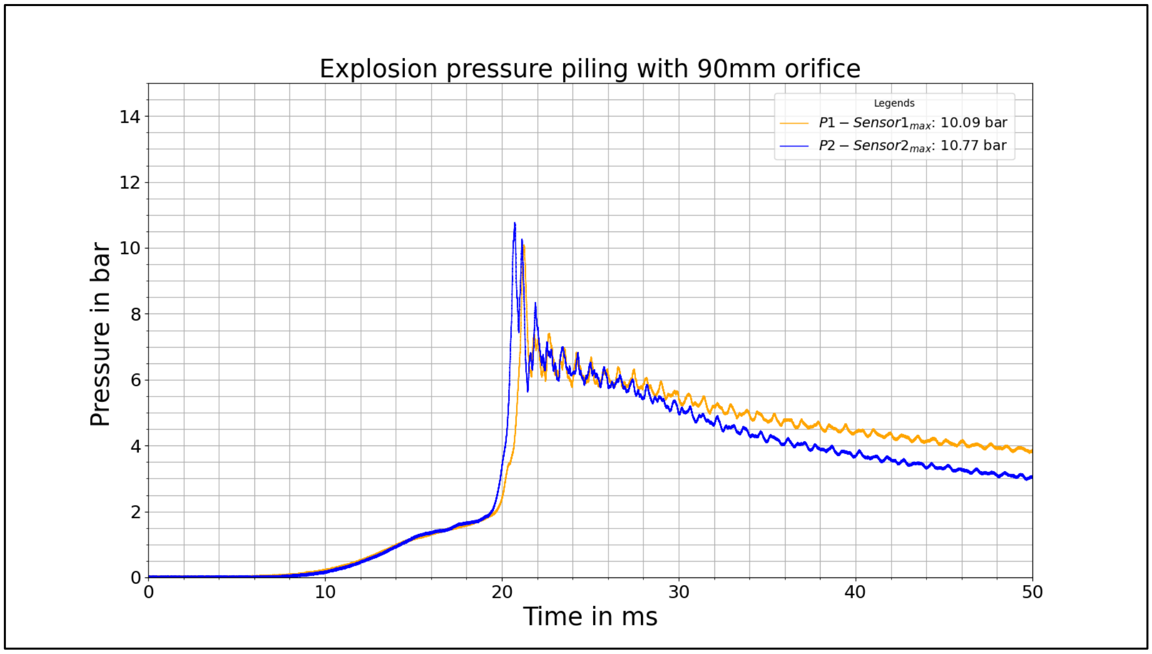

Figure 27:Explosion pressure profile for combined tubes with 90 mm orifice.

- **15mm orifice (Figure 25)**

The results in Figure 25 reveal a stark difference between the peak pressure observed in the primary chamber and that observed in the secondary chamber. The maximum pressure in the primary chamber observed was 6.12 bar while in the secondary chamber it was significantly higher, peaking at 14.02 bar. The results show a rise in pressure of $\cong 130\%$. This strong disparity between the results in the two chambers indicates a strong pressure piling effect.

The pressure rise in the primary chamber was observed to be slow and controlled as compared to that in the secondary chamber. The slow and controlled pressure rise in the primary chamber is an indication that the orifice restricts the flow of the explosion flame between the compartments. The delay in pressure build-up by P_2, in the secondary chamber, indicates the presence of pressure piling, where the pre-compression led to a more intense secondary explosion.

- **58 mm orifice (Figure 26)**

The primary chamber of this configuration observed a peak pressure of 10.53 bar, while the pressure in the secondary chamber reaches 19.47 bar, basically an increase in pressure of $\cong 85\%$. The pressure rise in the primary chamber is notably steeper and reaches a higher peak as compared to that of the 15 mm orifice, reflecting a more rapid combustion due to the larger orifice allowing for faster gas flow between the compartments.

Despite the large orifice size, there was still substantial pressure piling, though the effect is less pronounced compared to the 15 mm orifice, indicated by the peak pressure in the secondary chamber. The restricted gas flow between the chambers led to a high initial pressure build-up in the primary chamber, causing great energy transfer to the secondary chamber ultimately causing pressure piling peaks. However, for this orifice opening, the pressure piling effect was observed to be less severe as the larger opening facilitated a better gas flow and pressure distribution between the compartments.

- **90 mm orifice (Figure 27)**

In the case of the 90 mm orifice, the primary chamber observed a peak pressure of 10.09 bar, not far off from the peak pressure in the secondary chamber that was 10.77 bar, essentially a small increase of $\cong 6\%$. This change in the pressure reading is basically negligible as there is not much restriction observed in the flow of the combustible gas between the chambers and therefore indicates a minimal pressure piling effect. Like the 58 mm orifice, the pressure in the primary chamber is observed to rise quickly and reaches a similar peak. However, the rate of pressure rise appears to be more controlled. The pressure piling effect in this configuration is significantly reduced, as the pressure in the secondary chamber does not vastly exceed that of the primary chamber. The larger orifice in this configuration allows for better gas and pressure equalization between the chambers, leading to more balanced and safer pressure distribution.

The reduced severity of pressure piling in this configuration as observed aligns with observations from the literature [49], which emphasizes that large openings between compartments minimize the risk of pressure amplification by facilitating more uniform gas and pressure flow.

Figure 28 graph closely compares the explosion pressure-time histories for the different orifices, and how the pressure piling effect is observed due to the differences in the orifice sizes.

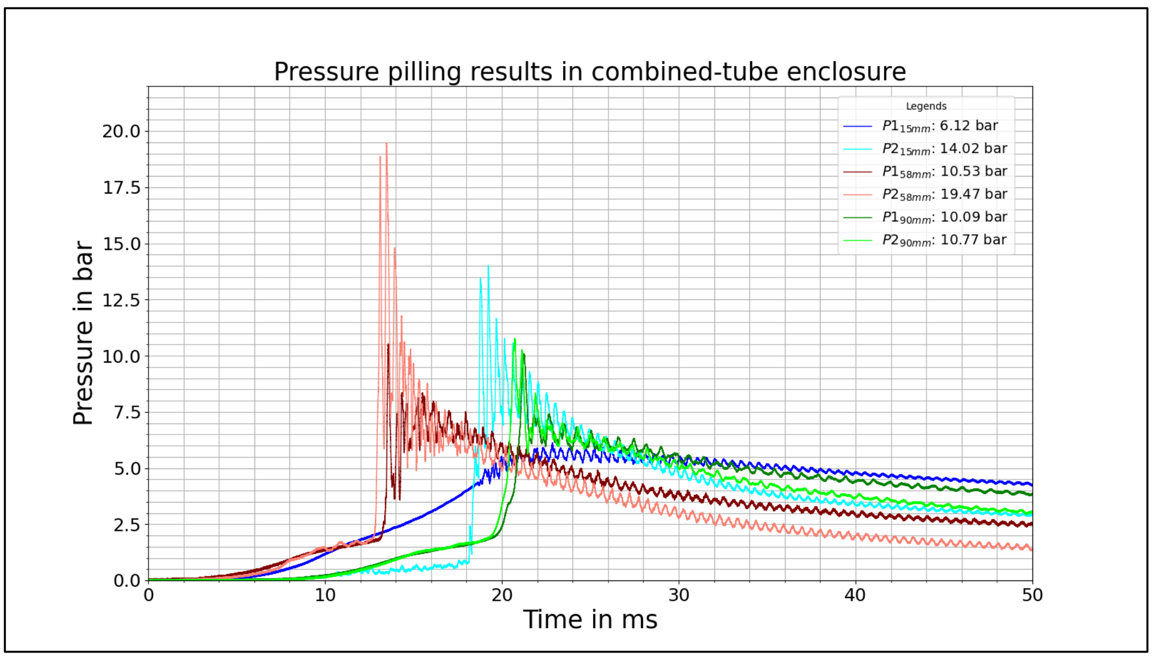

Figure 28: Pressure piling effect due to various orifice sizes.

The results clearly demonstrate that the size of the orifice plays a critical role in controlling the severity of pressure piling, hence translating in to how the separation of compartments, whether it being a building or piping, affects the flow of explosion pressure and results in pressure piling effects. The orifice between the compartments restricted the free flow of the combustion gas, hence resulting in a delay in pressure transfer. This delay therefore causes a pre-compression of the unburnt gas in the secondary chamber ultimately resulting in an intense explosion upon ignition. This is depicted on the graph in Figure 28, where a close comparison is made for all the results from the three orifices. The secondary chamber results are a steep increase in pressure highlighting the accumulation of energy due to pressure piling.

The steel plate with variable orifice sizes creates an obstruction that delays the flow of pressure between the two compartments. This setup replicates real-world scenarios where internal installations, such as partitions, piping, or valves, may influence the dynamics of pressure buildup in explosion-prone environments.

Various research works also showed that the shape of the secondary compartment and the way the jet was directed into it greatly influenced the explosion violence or rate of pressure rise [44]. The interaction between the flame front and the compartmentalized structure is key to understanding how pressure piling can amplify explosion pressures beyond what would be expected in a single, open enclosure.

This finding is critical for designing safer industrial installations where explosive gases might accumulate, as it suggests that minimizing internal obstructions can reduce the risk of severe pressure piling up.

The results of this experiment support the objective of investigating the role of internal installations in pressure piling. It further suggests that careful consideration must be given to the design of interconnected enclosures or compartments to prevent extreme pressure piling, which could lead to catastrophic failure in industrial settings. By controlling the size of openings and minimizing obstructions, it is possible to manage and mitigate the risks associated with pressure piling in explosions.

The findings from these tests underscore the importance of careful consideration of partitioning designs between various structures in industrial settings. Structures or systems designed with internal partitions or valves that create restrictive orifices between compartments can lead to pressure piling effects and ultimately increase the risk of catastrophic explosions. Therefore, by optimizing the size and configuration of these partitions or valves, it is possible to alter the pressure differentials and improve safety in interconnected compartments.

4.2.2. Multi Chambers System

The explosion pressure recorded in the empty enclosure, shown in Figure 29, is comparable to that recorded in the cylindrical enclosure from earlier experiments. The maximum explosion pressure recorded was 6.7 bar, with the remaining sensors detecting pressures in a range of 6.34 bar to 6.63 bar. Figure 30 displays the uncertainties observed between sensor readings. This consistency across the sensor readings indicates a relatively uniform pressure distribution in an empty enclosure with minimal to no obstructions. The readings deviated in a small range between 0.05 bar to 0.07 bar.

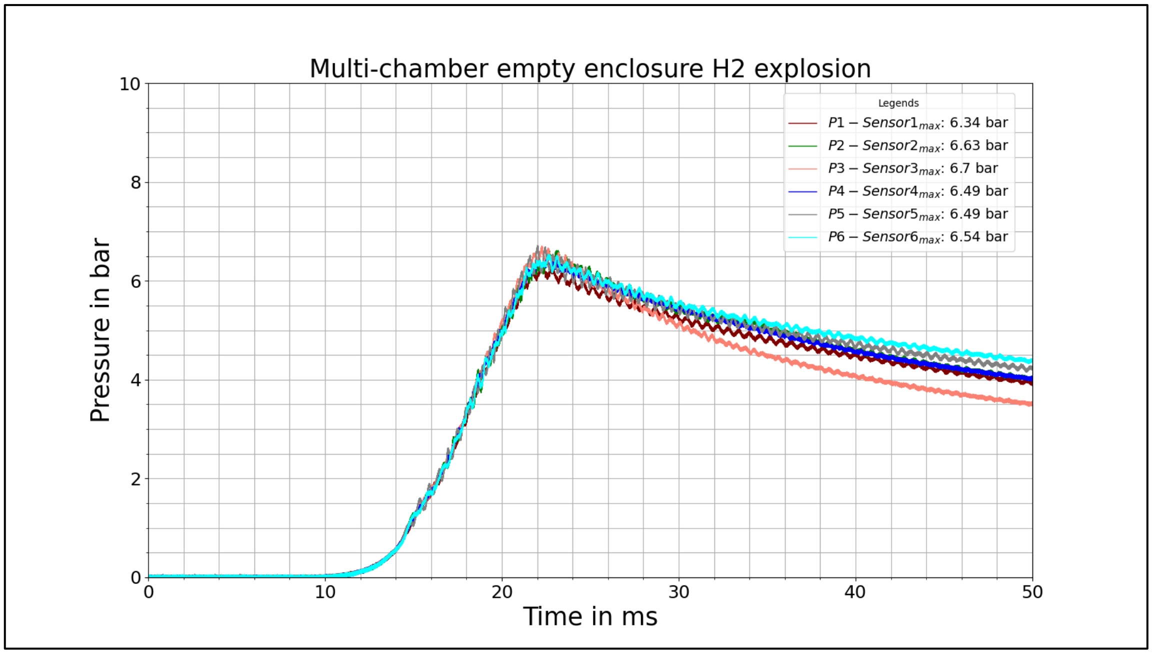

Figure 29: Empty multi chamber enclosure test results.

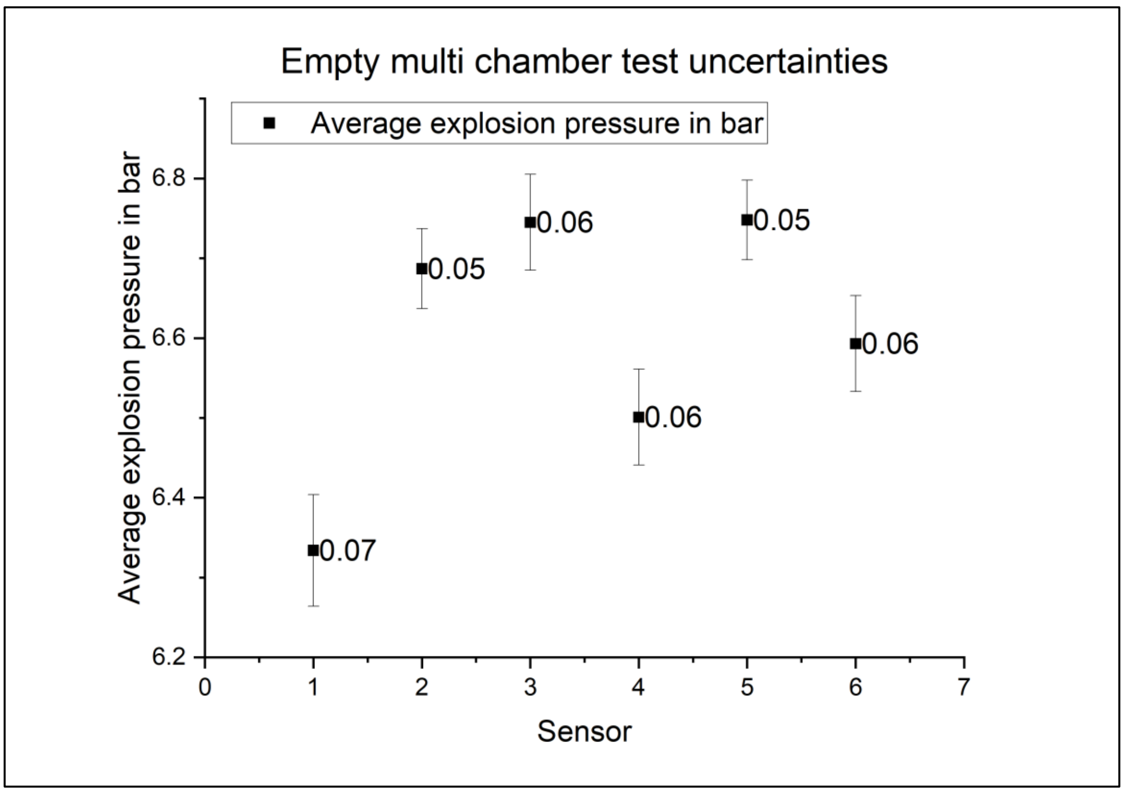

Figure 30: Pressure sensor results reading uncertainties for empty multi-chamber enclosure.

The flame propagation in this configuration involved the flame front passing through multiple compartments; However, due to lack of significant internal installations, the flame transmission and pressure buildup was relatively controlled. Following igniting in the first compartment, the flame was transmitted through a narrow conduit to the second compartment, where exceptionally high rates of pressure increase were recorded. The second compartment had a minor connection to a third compartment, which was then linked to an additional compartment, and so forth. This configuration is not precisely analogous to the twin-tube enclosure design, as the pressure buildup in compartment two was released into a third compartment.

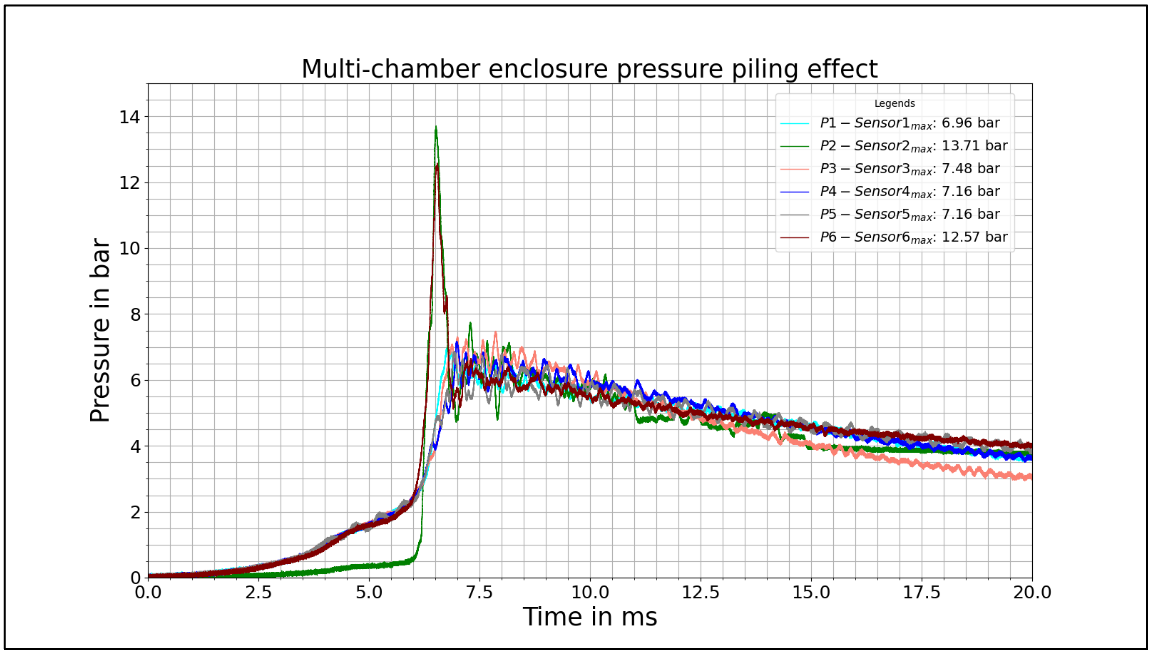

Figure 31: Pressure piling results of multi-chamber enclosure.

The results in Figure 31 show the observations from the explosion test with the configuration containing internal installations and how they can have a profound effect on the explosion pressure dynamics of the hydrogen-air mixture, especially in terms of pressure piling. When compared with the baseline test of the empty enclosure in Figure 30, the introduction of internal obstructions caused a significant pressure increase, validating the findings from previous experimental studies in the literature review. These findings confirm that pressure piling is not merely a function of the amount of energy released in an explosion but is also heavily influenced by how the internal structure of the enclosure shapes the pressure waves and flame propagation.

Even though not all peak pressures in the experiment can be classified as pressure piling, the results from sensors P_2 and P_6, 13.71 bar and 12.57 bar respectively, clearly meet the conditions for typical pressure-piling behavior (Figure 31). This is due to the localized pre-compression of gases in the most confined spaces of the enclosure compartments, which aligns with the pressure dynamics characteristic of pressure piling.

In these regions, the internal installations acted as barriers, delaying the transfer of pressure waves between chambers. As a result, flame propagation was confined and accelerated in these areas, leading to a rapid pressure buildup that fulfills the criteria for pressure piling, such as the sharp rise in pressure and significant amplification.

The peak pressure readings from sensors P_2 and P_6 clearly indicate that pressure piling occurred according to standard criteria of IEC60079-1, where the pre-compression of gases and delayed ignition caused a substantial increase in local pressures. The configuration of internal components and the complex geometry of the enclosure created conditions that facilitated pressure amplification, thus mimicking and fulfilling the true conditions of pressure piling. This suggests that, under certain configurations, internal installations within enclosures can create high-pressure peaks, amplifying local overpressures and posing risks consistent with those seen in fully developed pressure-piling scenarios.

In addition, the uncertainty plot analysis in Figure 32, for the multi chamber enclosure with internal installations reveals greater variability in pressure readings. For example, the reading of pressure sensor P_2 shows a standard deviation of 0.92 bar, indicating more pronounced fluctuations in pressure readings. This could be attributed to the complex pressure dynamics introduced by internal obstructions which result in disruption of the uniform propagation of pressure waves and ultimately leading to localized pressure spikes.

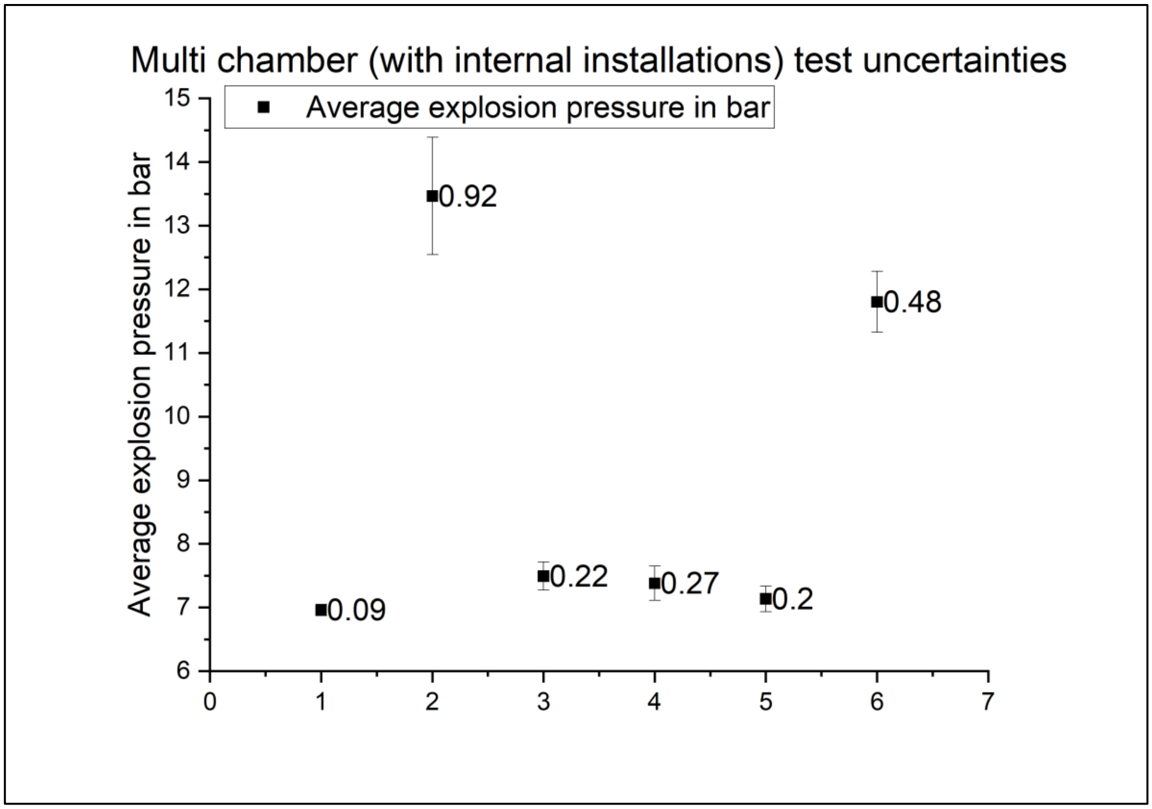

Figure 32: Pressure sensor results reading uncertainties for multi-chamber enclosure with internal installations.

The findings from these experiments have revealed that designs such as those of the multi-chamber enclosure with internal obstructions can have a profound effect on the pressure dynamics of hydrogen-air mixture explosions. These obstructions amplify local pressures and pose significant safety risks especially in industrial settings where multi-compartment enclosures and interconnected piping systems are common. Therefore, the application of flameproof enclosure housings for such installations can help mitigate the risks associated with pressure piling.

CHAPTER 5. CONCLUSION

The presented work explores the effect of enclosure geometries and internal installations on the dynamics of explosion pressure, specifically for hydrogen-air mixtures. This work quantified the impact of factors such as geometric features, compartmentalization and enclosure design obstacles, through a series of controlled experiments conducted in flameproof enclosures with compliance to the testing procedures provided by the International Electro-commission standards, IEC60079-1. The findings from these experiments provide valuable insights into the safety considerations necessary for the design of flameproof enclosures that are to be used in hydrogen production and handling facilities.

The experiments yielded significant observations:

1. **Geometric influence** – two basic enclosure designs were used to investigate the explosion pressure dynamics of hydrogen-air mixture, which were spherical, and cylindrical. The spherical enclosure recorded the highest peak pressure of 7.16 bar, whilst the cylindrical enclosures, both short and long designs, yielded lower pressures of 6.75 bar and 6.65 bar, respectively. The spherical enclosure pressure results were observed to be a smooth pressure curve and a sharp increase in peak pressure that aligned well with theoretical expectations.
2. **Orifice and pressure piling** – the combined tube enclosure configuration, two cylindrical enclosures were connected, with a steel plate with an orifice to separate them, to make a two-compartment cylindrical setup. This configuration reveals the relationship between pressure piling and how it is affected by structural compartment designs. The orifice with a small diameter (15 mm) led the most

significant pressure piling results, with difference of 7.9 bar between the primary and the secondary chamber. This pressure piling behavior was less pronounced in the orifice with a larger diameter (90 mm), underscoring the role of restricted openings in amplifying the effect of pressure piling.

3. **Multi chamber effect with internal installations** – the test with a multi chamber enclosure revealed that internal installations contribute significantly to the effect of pressure piling due to the localized pressure compression within the enclosure that ultimately influences the flame propagation and pressure buildup. A peak pressure of 13.71 bar and 12.57 bar in specific compartments was evidence that confirmed that the structure had localized pre-compressions, and as a result increased the risk of pressure piling.
4. **Sensor consistency and uncertainties** – explosion tests repeatability was significant in highlighting the importance of precise measurement calibrations and ensuring reliability in controlled experimental conditions. Analysis of repeatability has shown that pressure readings recorded across multiple tests were generally consistent, although high uncertainties were observed in multi-chamber configurations with internal installations.

What is desirable in real installations is an enclosure without obstructions and inner fittings, so that consistent pressure build up is allowed before explosion can rupture the vessel. In the case of the analyzed geometries, the cylindrical geometry results in a safer storage container.

CHAPTER 6. RECOMMENDATIONS FOR FUTURE WORK

Working on a flameproof enclosure to study the explosion pressure dynamics of hydrogen-air mixtures has many challenges, some of which have been discovered in the study done for this thesis. Building on the findings of this study, the following recommendations are proposed for future research:

1. Numerical simulations of pressure dynamics – complementary to the physical experiments, computational fluid dynamics (CFD) simulations would be good to allow for a more in-depth analysis of flame and pressure propagation, especially in complex geometries (which were not analyzed in the case of this thesis).
2. Consideration of enclosure material – investigating different enclosure materials and coatings could provide valuable data on how material properties influence heat dissipation, pressure piling, and resistance to explosion pressure.
3. Broader range of enclosure configurations and orifice sizes – expanding the study to include additional orifice sizes and shapes would offer more comprehensive insights into how various compartmental connections impact pressure piling.
4. Incorporation of real-world conditions – introducing factors such as varying hydrogen-air ratios, environmental conditions, and partial enclosure leaks could provide a more realistic basis for predicting explosion behavior in industrial applications.

CHAPTER 7. REFERENCES

[1] Capurso T, Stefanizzi M, Torresi M, et al., Perspective of the role of hydrogen in the 21st century energy transition. Energy Convers Manag 2022,; 251: 114898.

[2] R-Stahl. Essential Explosion Protection. Waldenburg, Germany, (Available at: https://rstahl.com), [accessed 1 July 2024], Waldenburg: R. STAHL Schaltgeräte GmbH, 2018.

[3] Essmann S, Dymke J, Höltkemeier-Horstmann J, et al., Ignition characteristics of hydrogen-enriched ammonia/air mixtures. *Applications in Energy and Combustion Science* 2024; 17: 100254.

[4] Jordan T, Askar E, Holtappels K, et al., Fuels – Introduction | Hydrogen safety. In: *Reference Module Chemistry, Molecular Sciences and Chemical Engineering.*, Amsterdam: Elsevier, 2024.

[5] Nan F, Luo Z, Cheng F, et al., Research progress and development trends of hydrogen explosion suppression materials and mechanisms. *Process Safety and Environmental Protection* 2024; 184: 1318–1331.

[6] Askar Enis, Holtappels Kai., Process- and Plant-Safety. Bundesanstalt für Materialforschung und -prüfung (BAM), 2020, (Available at: https://bam.de), [accessed 21 August 2024].

[7] International Electrotechnical Commission., *IEC 60079-1: Explosive atmospheres. Part 1, Equipment protection by flameproof enclosures 'd'.* 7th ed. Geneva, Switzerland: International Electrotectnical Commission (IEC), 2014.

[8] Neikov OD., Safety Engineering in the Production of Powders., *in: Handbook of Non-Ferrous Metal Powders: Technologies and Applications, 2nd edn,* Amsterdam: Elsevier, 2018, pp. 865–928

[9] International Electrotechnical Commission., IEC 60079-1. (Available at: https://webstore.iec.ch) [2014, accessed 2 Sep 2025,], Geneva: International Electrotechnical Commission (IEC).

[10] von Pidoll U., *Explosionsschutz in der CTR und Weiterführung der Aufgaben in ihren Nachfolgeorganisationen*., Braunschweig: Physikalisch-Technische Bundesanstalt (PTB), 2015.

[11] Hoseyni SM, Mesbah Mostafa MO, Cordiner J., Mitigating risks in hydrogen-powered transportation: A comprehensive risk assessment for hydrogen refuelling stations, vehicles, and garages. *Int J Hydrogen Energy* 2024; 91: 1025–1044.

[12] Krause T., *Dynamische Messung von Sicherheitstechnisch Relevanten Explosionsdrücken Dissertation*., Ilmenau: Technische Universität Ilmenau, 2023.

[13] Piria R, Honnen J, Pfluger B, et al., *Securing Hydrogen Imports for Germany: Import needs, risks and strategies on the way to climate neutrality*, (Available at: https://kopernikusprojekte.de), [accessed 23 August 2024]., Berlin: Kopernikus Project, 2022.

[14] Klingl S, Altgelt F, Österlein E., *Global Alliance Powerfuels, Renewable Hydrogen Project Risks*, (Available at: https://www.powerfuels.org), [accessed 23 August 2024]., Berlin: Deutsche Energie-Agentur GmbH (DENA), 2024.

[15] Sprenger T, Wild P, Pickert L., *Geopolitical Risks in Global Hydrogen Trade* (Available at: https://www.ewi.uni-koeln.de/en), [accessed 23 August 2024]., Cologne: Institute of Energy Economics (EWI), 2023.

[16] Min M, Yoon C, Yoo N, et al., Hydrogen Risk Assessment Studies: A Review Toward Environmental Sustainability. *Energies 2025,* 18: 229.

[17] Calabrese M, Portarapillo M, Di Nardo A, et al., Hydrogen Safety Challenges: A Comprehensive Review on Production, Storage, Transport, Utilization, and CFD-Based Consequence and Risk Assessment. *Energies (Basel)* 2024; 17: 1350.

[18] Kayfeci M, Keçebaş A, Bayat M., Chapter 3 - Hydrogen production. *Solar Hydrogen Production Processes : Systems and Technologies* 2019; 45–83., Amsterdam: Elsevier.

[19] Balat M, Balat M., Political, economic and environmental impacts of biomass-based hydrogen. *Int J Hydrogen Energy* 2009; 34: 3589–3603.

[20] Qazi UY. Future of Hydrogen as an Alternative Fuel for Next-Generation Industrial Applications; Challenges and Expected Opportunities. *Energies 2022,* 15: 4741.

[21] Anwar G, Abdullah NN., The impact of Human resource management practice on organizational performance. *International journal of Engineering, Business and Management (IJEBM)* 2021; 5: 2456–8678.

[22] Blondeel M, Bradshaw MJ, Bridge G, et al., The geopolitics of energy system transformation: A review. *Geogr Compass* 2021; 15: e12580.

[23] Ministry of Mines and Energy Namibia., *Republic of Namibia. Green Hydrogen and Derivatives Strategy II*. Windhoek, Namibia, November 2022.

[24] National Hydrogen Council., *Hydrogen Action Plan Germany 2021 - 2025*, (available at: https://www.fz-juelich.de/ptj), (accessed 23 August 2024)., Projektträger Jülich (PtJ), 2024.

[25] Yu X, Kong D, He X, et al., Risk Analysis of Fire and Explosion of Hydrogen-Gasoline Hybrid Refueling Station Based on Accident Risk Assessment Method for Industrial System. *Fire 2023,* 6: 181.

[26] Yang W, Zheng L, Wang C, et al., Effect of ignition position and inert gas on hydrogen/air explosions. *Int J Hydrogen Energy* 2021; 46: 8820–8833.

[27] Shimizu K, Hibi A, Koshi M, et al., Updated kinetic mechanism for high-pressure hydrogen combustion. *J Propuls Power* 2011; 27: 383–395.

[28] Sun W, Vasu S, Blais MS., Fundamentals. *Machinery and Energy Systems for the Hydrogen Economy*. Elsevier, 2022; 11–30.

[29] Eslinger MR, Lundell CE, Rodriguez RE., *A Calculated Bang: Explosive Predictions and the Ideal Gas Law*. Buffalo, NY: National Center for Case Study Teaching in Science, University at Buffalo, 2020.

[30] European Technical Committee CEN/TC 305., *DIN EN 15967: Determination of maximum explosion pressure and the maximum rate of pressure rise of gases and vapours*., Epub ahead of print March 2022. Berlin: DIN Media GmbH., DOI: 10.31030/3290404.

[31] Physikalisch-Technische Bundesanstalt (PTB); Federal Institute for Materials Research and Testing (BAM)., Chemsafe: Database for safety-related parameters in explosion protection. *https://www.chemsafe.ptb.de/*. [Accessed 25 August 2024] Braunschweig/Berlin: PTB and BAM.

[32] Glassman I, Yetter R A and Glumac N G., Explosive and general oxidative characteristics of fuels, in: Combustion, 5th edn, Amsterdam: Academic Press (Elsevier), 2014., ch. 3, p. 293

[33] Chrysalis Scientific Technologies., *Lower and Upper Explosive Limits for Flammable Gases and Vapors (LEL/UEL)*, (Available at: https://www.chrysalisscientific.com), [20 November 2013, accessed 25 August 2024]., Chrysalis Scientific Technologies Inc.

[34] Phillips H., Maximum explosion pressure in flameproof enclosures: The effects of the vessel and the ambient temperature. *Journal of Hazardous Materials - J HAZARD MATER* 1984; 8: 251–259.

[35] Padhiary A., *Analysis of Heat Loss during Flame Wall Interaction of Premixed Propagative Flames and Diffusive Spray Flames*. Doctorate, *National Higher School of Mechanics and Aerotechnics*., Poitiers: ISAE-ENSMA (École Nationale Supérieure de Mécanique et d'Aérotechnique), 2016.

[36] Razus D, Brinzea V, Mitu M, et al., Burning velocity of propane-air mixtures from pressure-time records during explosions in a closed spherical vessel. *Energy and Fuels* 2012; 26: 901–909.

[37] Singh J., Gas explosion in inter-connected vessels: pressure piling. *Institution of Chemical Engineers (IChemE), 2017.*

[38] Rogstadkjernet L., *Combustion of Gas in Closed, Interconnected Vessels: Pressure Piling*. Bergen: University of Bergen, 2004.

[39] Furlong AJ, Bond NK, Pegg MJ, et al. Evaluation of dust and gas explosion potential in chemical looping processes. *J Loss Prev Process Ind* 2024; 89: 105277.

[40] Li D, Dai S, Lin T. Evaluation of the explosion pressure parameters in flameproof enclosures under the pressure piling condition. *Energies (Basel)*; 14. Epub ahead of print 1 December 2021. DOI: 10.3390/en14238156.

[41] Kuznetsov M, Czerniak M, Grune J, et al., Effect of Temperature on Laminar Flame Velocity for Hydrogen-Air Mixtures at Reduced Pressures., in: *International Conference on Hydrogen Safety (ICHS)*. Karlsruhe Institute of Technology, 2013.

[42] The Engineering Toolbox., *Adiabatic Flame Temperatures*. (Available at: https://*www.engineeringtoolbox.com)*, [accessed 2 November 2024]., The Engineering Toolbox, 2024.

[43] McAllister S, Chen J Y and Fernandez-Pello A C, 2011, Chemical kinetics, in: Fundamentals of Combustion Processes, Mechanical Engineering Series, New York: Springer, pp. 49–73, https://doi.org/10.1007/978-1-4419-7943-8_3

[44] Duan Q, Xiao H, Gao W, et al., Experimental investigation of spontaneous ignition and flame propagation at pressurized hydrogen release through tubes with varying cross-section. *J Hazard Mater* 2016; 320: 18–26.

[45] Patel P, Garaniya V, Baalisampang T, et al., A technical review on quantitative risk analysis for hydrogen infrastructure. *J Loss Prev Process Ind* 2024; DOI: 10.1016/J.JLP.2024.105403.

[46] Cao W, Li W, Yu S, et al., Explosion venting hazards of temperature effects and pressure characteristics for premixed hydrogen-air mixtures in a spherical container. *Fuel* 2021; 290: 120034.

[47] Zhao Y, Wu J, Zhou R, et al., Effects of the length and pressure relief conditions on propagation characteristics of natural gas explosion in utility tunnels. *J Loss Prev Process Ind*; 75. Epub ahead of print 1 February 2022. DOI: 10.1016/J.JLP.2021.104679.

[48] Li D, Dai S., Numerical simulation of the effect of diaphragm orifice diameter in a flameproof enclosure with an interconnected structure during pressure piling. *Thermal Science* 2022; 27: 137.

[49] Li J, Hao H., Numerical and analytical prediction of pressure and impulse from vented gas explosion in large cylindrical tanks. *Process Safety and Environmental Protection* 2019; 127: 226–244.

[50] Ogungbemide D., A CFD study of the effects of pipe bending angle on pressure piling in coal dust explosions in interconnected vessels. *Fire Saf J* 2022; 128: 103540.

[51] Krause T, Bewersdorff J, Markus D., Investigations of static and dynamic stresses of flameproof enclosures. *J Loss Prev Process Ind* 2017; 49: 775–784.

[52] Di Benedetto A, Salzano E, Russo G., Predicting pressure piling by semi-empirical correlations. *Fire Saf J* 2005; 40: 282–298.

[53] Krause T, Kanbur H, Springer N, et al., Acceleration sensitivity of piezoelectric pressure sensors and the influence on the measurement of explosion pressures. *J Loss Prev Process Ind* 2023; 82: 104999.

[54] Zhang P, Wang J, Liang J, et al., Explosions of gasoline vapor/air mixture in closed vessels with different shapes and sizes. *J Loss Prev Process Ind* 2019; 57: 327–334.

[55] National Fire Protection Association (NFPA)., NFPA 2: Hydrogen Technologies Code, [accessed 29 August 2024]., Quincy, MA: NFPA, 2020.

[56] Hydrogen Tools., ISO/TR 15916 - *Basic Considerations for the Safety of Hydrogen Systems*, (Available at: https://h2tools.org), [accessed 29 August 2024]., Geneva: International Organization for Standardization (ISO), 2024.

[57] Hydrogen Tools., NFPA 55 Compressed Gases and Cryogenic Fluids Code Chapter 10: Gas Hydrogen Systems, (Available at: https://h2tools.org), [accessed 29 August 2024]., Quincy, MA: National Fire Protection Association (NFPA), 2024.

[58] Noordende H, Xiao C., *Green Hydrogen Inherent Safety Practices on Large Industrial Scale*. (Available at: https://ispt.eu), [accessed 4 November 2024]., Amersfoort: Institute for Sustainable Process Technology (ISPT), 2023.

[59] Keçebaş A, Kayfeci M., Hydrogen properties. *Solar Hydrogen Production: Processes, Systems and Technologies*, Amsterdam: Elsevier, 2019; 3–29.

[60] Silla E, Arnau A, Tuñón I, et al., Fundamental principles governing solvents use. *Handbook of Solvents: Second Edition* 2014; 1: 11–72., Amsterdam: Elsevier.

[61] Occupational Safety and Health Administration., *Oil and Gas Extraction - Overview* (Available at: https://www.osha.gov/oil-and-gas-extraction), [accessed 4 November 2024]., Washington DC: U.S. Department of Labor, 2024.

[62] Namibian Standard Institution., *Creating peace of mind*., (Available at: https://www.nsi.com.na), [accessed 4 November 2024]., Windhoek: Namibian Standard Institution, 2024.

[63] Wen JX, Marono M, Moretto P, et al., Statistics, lessons learned and recommendations from analysis of HIAD 2.0 database. *Int J Hydrogen Energy* 2022; 47: 17082–17096.

[64] Kim S, Kim Y., Review: Hydrogen Tank Explosion in Gangneung, South Korea (Available at: https://proceedings.aiche.org), [accessed 4 November 2024]., American Institute of Chemical Engineers (AIChE), 2019.

[65] BASF., *Final report: Explosion and Subsequent Fire*, (Available at: https://www.basf.com) [accessed 4 November 2024]., Ludwigshafen: Badische Anilin- und Sodafabrik (BASF), 2024.

[66] Hydrogen Tools., Fire at Hydrogen Fueling Station, (Available at: https://h2tools.org), [2024, accessed 4 November 2024]., H2tools Org.

[67] SEEVOMEX., Installation Manual: SERVOTOUGH OxyExact 2210, 2015., Crowborough: Servomex Group Ltd.

[68] Krause T, Markus D., Herausforderungen bei der dynamischen Messung von Explosionsdrücken. *tm - Technisches Messen*; 84. Epub ahead of print 11 January 2017. DOI: 10.1515/teme-2016-0051.

APPENDIX 1 – ETHICAL CLEARANCE

RESEARCH ETHICS CLEARANCE CERTIFICATE

Reference Number: SoS-0258

Date: 26 November 2024

Dear Miss Ndamononghenda Uunona

This is to inform you that your application for research ethics approval has been approved for the duration of your studies. **You are required to apply for permission to conduct research from the relevant ministry/institution, if applicable, in addition to this ethical clearance**. You may contact the Ethics office (ethics@unam.na) for additional information.

Project title: Influence of enclosure geometries and internal installations on the explosion pressure of hydrogen-air mixture
Student number: 201716708
Level of degree: Postgraduate
Name of degree: Master of Science in Renewable Energy
Email address: **uunonann@gmail.com**
Supervisor(s): Dr. Zivayi Chiguvare & Dr. Tim Krause

Please note the following standard requirements for approval:
This ethical approval is issued by the University of Namibia's Research Ethics Committee following the University of Namibia's Research Ethics Policy and Guidelines. Ethical approval is given in respect of undertakings contained in the research ethics guidelines outlined below:

1. Any significant changes in the conditions or undertakings outlined in the approved Proposal must be communicated to the ethics committee. An application to make amendments may be necessary.
2. Any breaches of ethical undertakings or practices that have an impact on the ethical conduct of the research must be reported to the ethics committee.
3. The Principal Researcher must report issues of ethical compliance to the ethics committee (through the Chairperson) at the end of the Project or as may be requested by the ethics committee.
4. The ethics committee retains the right to:

i) Withdraw or amend this Ethical Clearance if any unethical practices (as outlined in the Research Ethics Policy) have been detected or suspected.

ii) Request for an ethical compliance report at any point during the research.

The ethics committee wishes you the best in your research.

Yours sincerely

Prof. Ezikeil G Kwembeya (Chairperson of School of Science (SoS) Decentralized Ethics Committee)

Prof. Davis Mumbengegwi (Head of MRS, Centre for Research Services)

University of Namibia, Centre for Research Services
Office of the Pro-Vice Chancellor: Research Innovation and Development
Private Bag, 13301 Windhoek, Namibia
340 Mandume Ndemufayo Avenue, Pioneers Park,
+264-61-2064624; ethics@unam.na, Fax+264-61-206 4624

APPENDIX 2 – RESEARCH PERMISSION LETTER

CENTRE FOR RESEARCH SERVICES
Office of the Pro-Vice Chancellor: Research, Innovation & Development
University of Namibia, Private Bag 13301, Windhoek, Namibia
340 Mandume Ndemufayo Avenue, Pioneers Park, Office F223 - Fblock, Second Floor
☎ +264 61 206 4673; E-mail:kmbulu@unam.na; URL.: http//www.unam.edu.na

UNAM
UNIVERSITY OF NAMIBIA

RESEARCH PERMISSION LETTER

Date: 16/01/2025

Student Name: Ndamononghenda Uunona

Student Number: 201716708

Programme: Master of Science in Renewable Energy

Approved Research Title: Influence of enclosure geometries and internal installations on the explosion pressure of hydrogen-air mixture

TO WHOM IT MAY CONCERN:

I hereby confirm that the above-mentioned student is registered at the University of Namibia for the programme indicated. The proposed study met all the requirements as stipulated in the University guidelines and has been approved by the relevant committees.

The proposal adheres to ethical principles as per attached Ethical Clearance Certificate. Permission is hereby granted to carry out the research as described in the approved proposal.

Best Regards

Dr. AEE Shikongo
Head: Postgraduate Research Support Services
Tel: +264 61 206 3129
E-mail: aeshikongo@unam.na

CENTRE FOR RESEARCH SERVICES
Office of the Director
2025 -01- 16
University of Namibia
UNAM

APPENDIX 3 - DRAWINGS

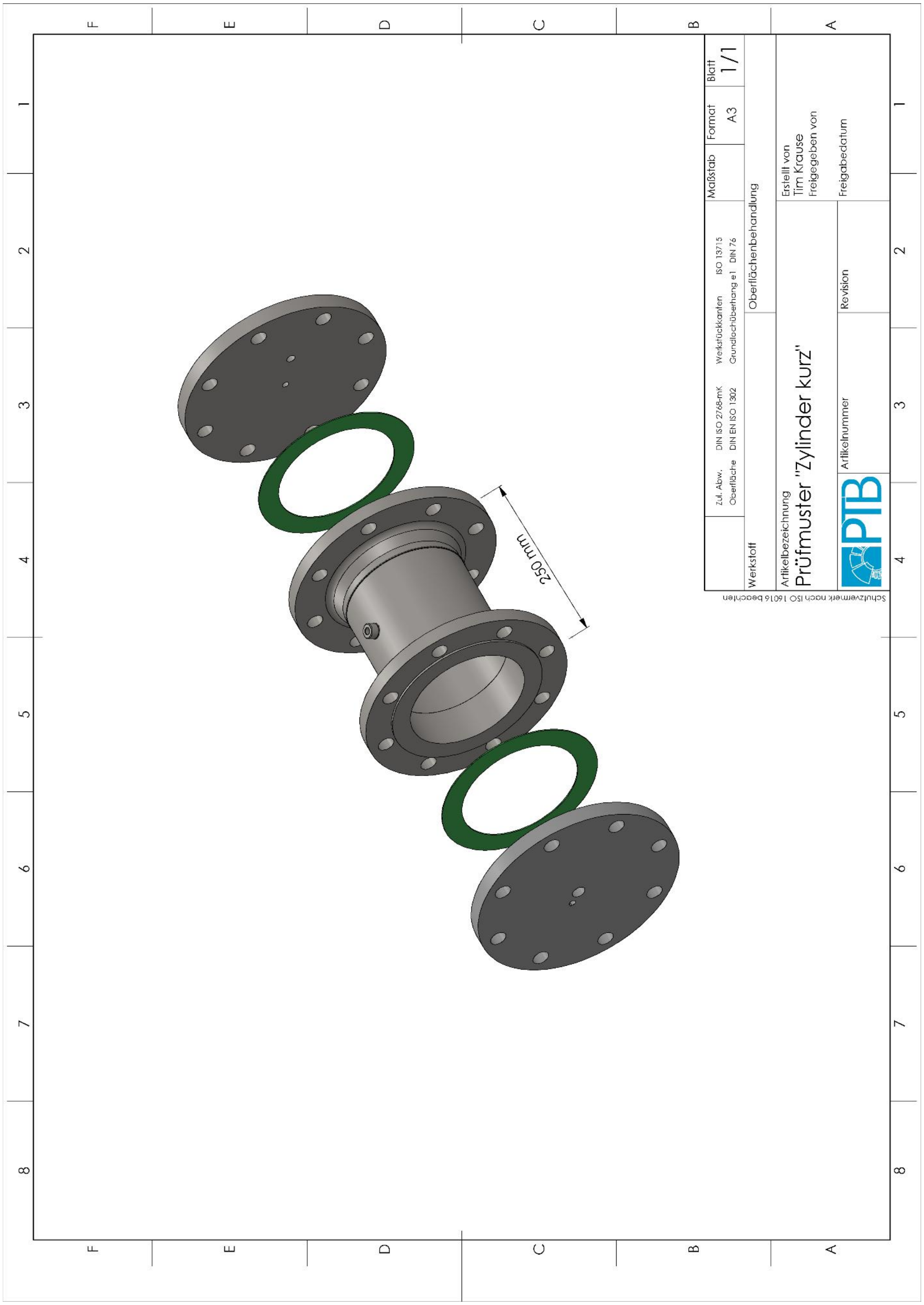

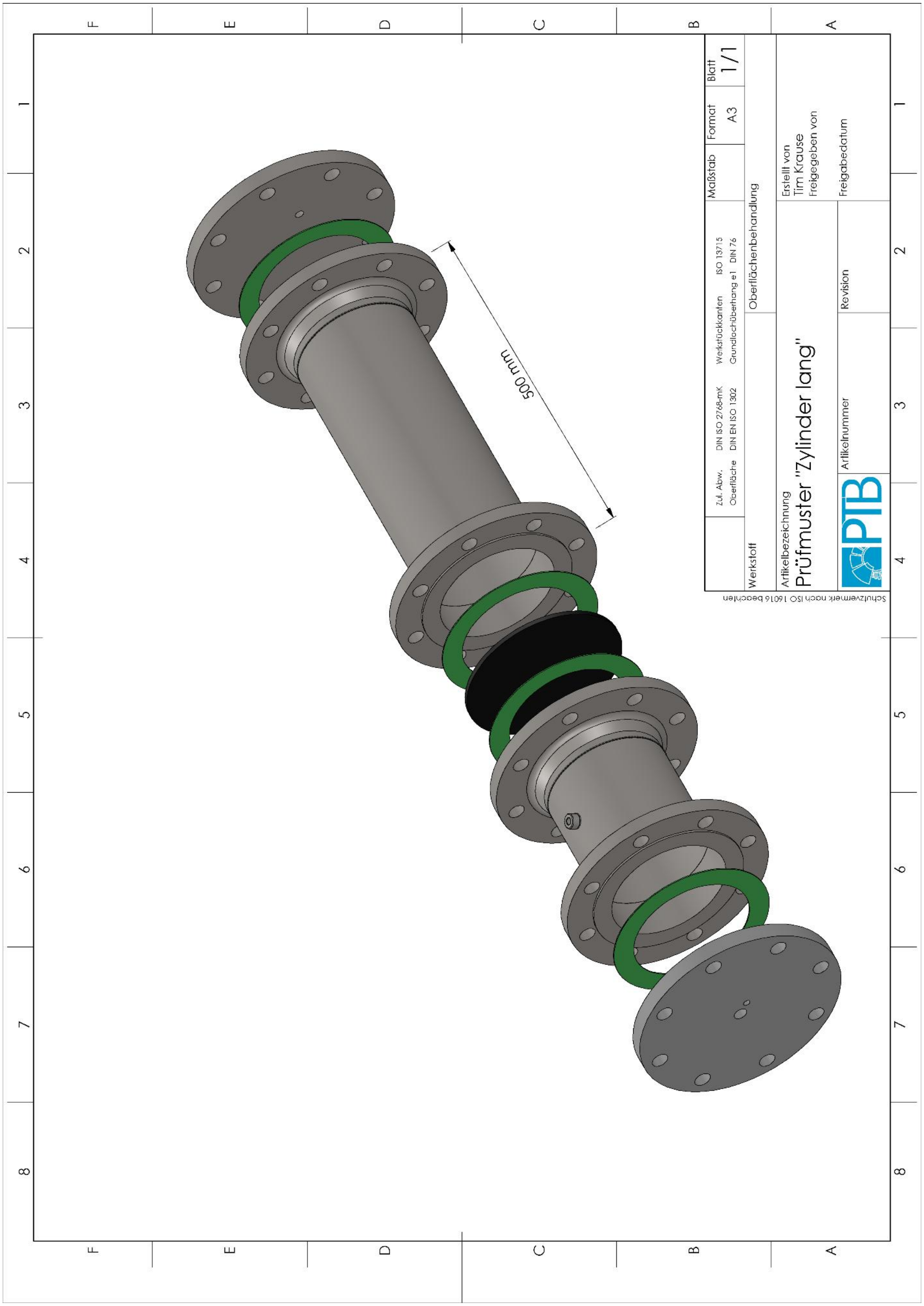
500 mm
Zul. Abw. DIN ISO 2768-mK
Oberfläche DIN EN ISO 1302
Werkstückkanten ISO 13715
Grundlochüberhang e1 DIN 76
Maßstab
Format
A3
Blatt
1/1
Werkstoff
Oberflächenbehandlung
Artikelbezeichnung
Prüfmuster "Zylinder lang"
Erstellt von
Tim Krause
Freigegeben von
Freigabedatum
Revision
Artikelnummer
PTB
Schutzvermerk nach ISO 16016 beachten

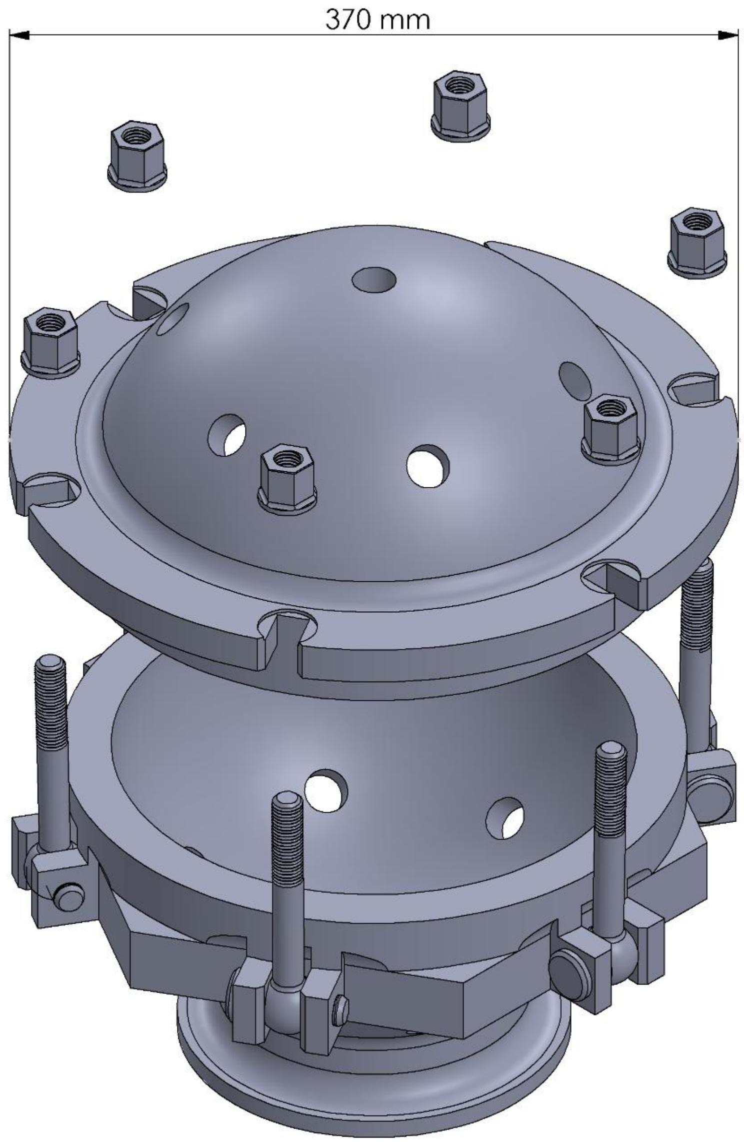

	Zul. Abw. DIN ISO 2768-mK Oberfläche DIN EN ISO 1302	Werkstückkanten ISO 13715 Grundlochüberhang e1 DIN 76	Maßstab	Format A4	Blatt 1/1

Werkstoff	Oberflächenbehandlung

Artikelbezeichnung

Prüfmuster "Kugel"

Erstellt von
Tim Krause
Freigegeben von

Freigabedatum

PTB

Artikelnummer

Revision

Schutzvermerk nach ISO 16016 beachten

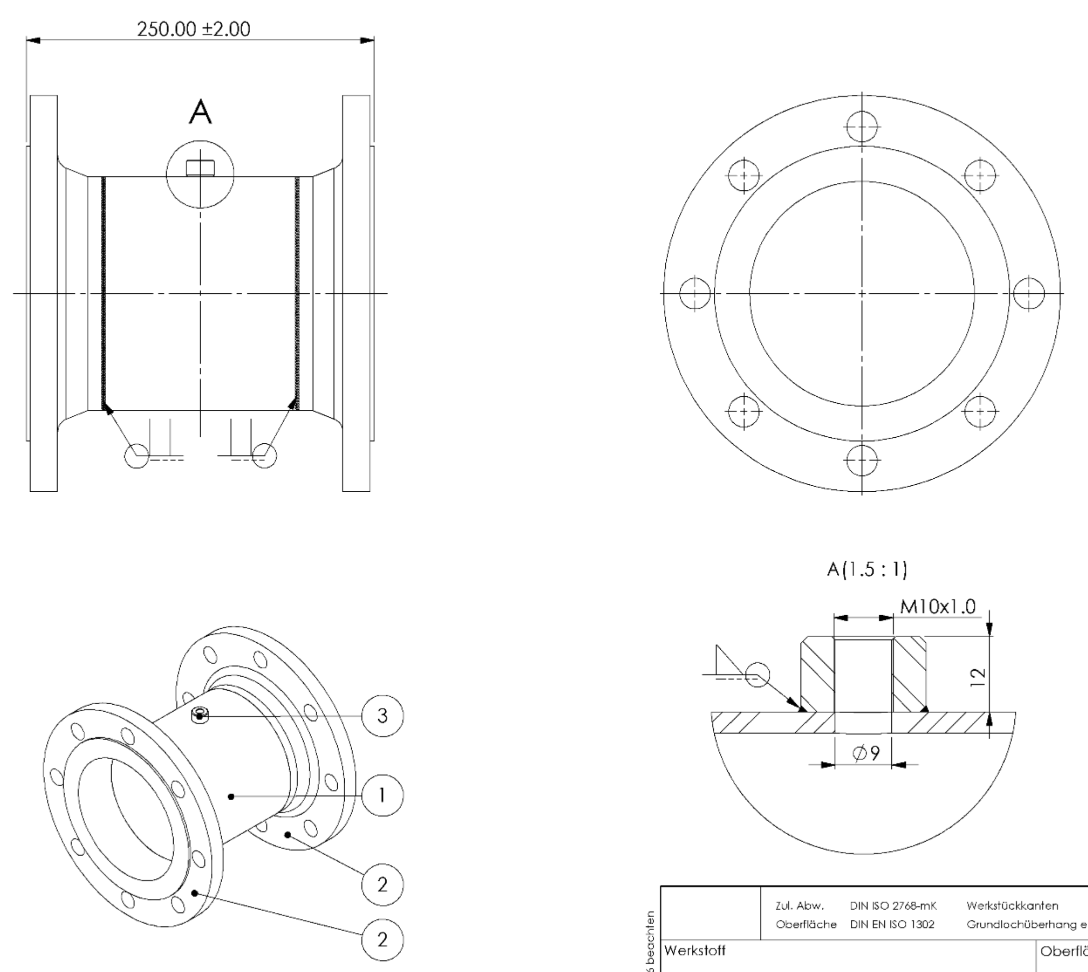

POS-NR.	MENGE	BENENNUNG	MATERIAL	STANDARD
1	1	ROHR	TP304L	ASTM A 312
2	2	V-FLANSCH	F304L	EN 1092-1/11/B1, PN16 DN150
3	1	ANSCHLUSS GAS	S30467	ASTM A 887

Schutzvermerk nach ISO 16016 beachten

Zul. Abw. DIN ISO 2768-mK Oberfläche DIN EN ISO 1302	Werkstückkanten ISO 13715 Grundlochüberhang e1 DIN 76	Maßstab 1:3	Format A3	Blatt 1/1
Werkstoff	Oberflächenbehandlung			
Artikelbezeichnung Kammer A		Erstellt von Tim Krause Freigegeben von		
PTB	Artikelnummer	Revision	Freigabedatum	

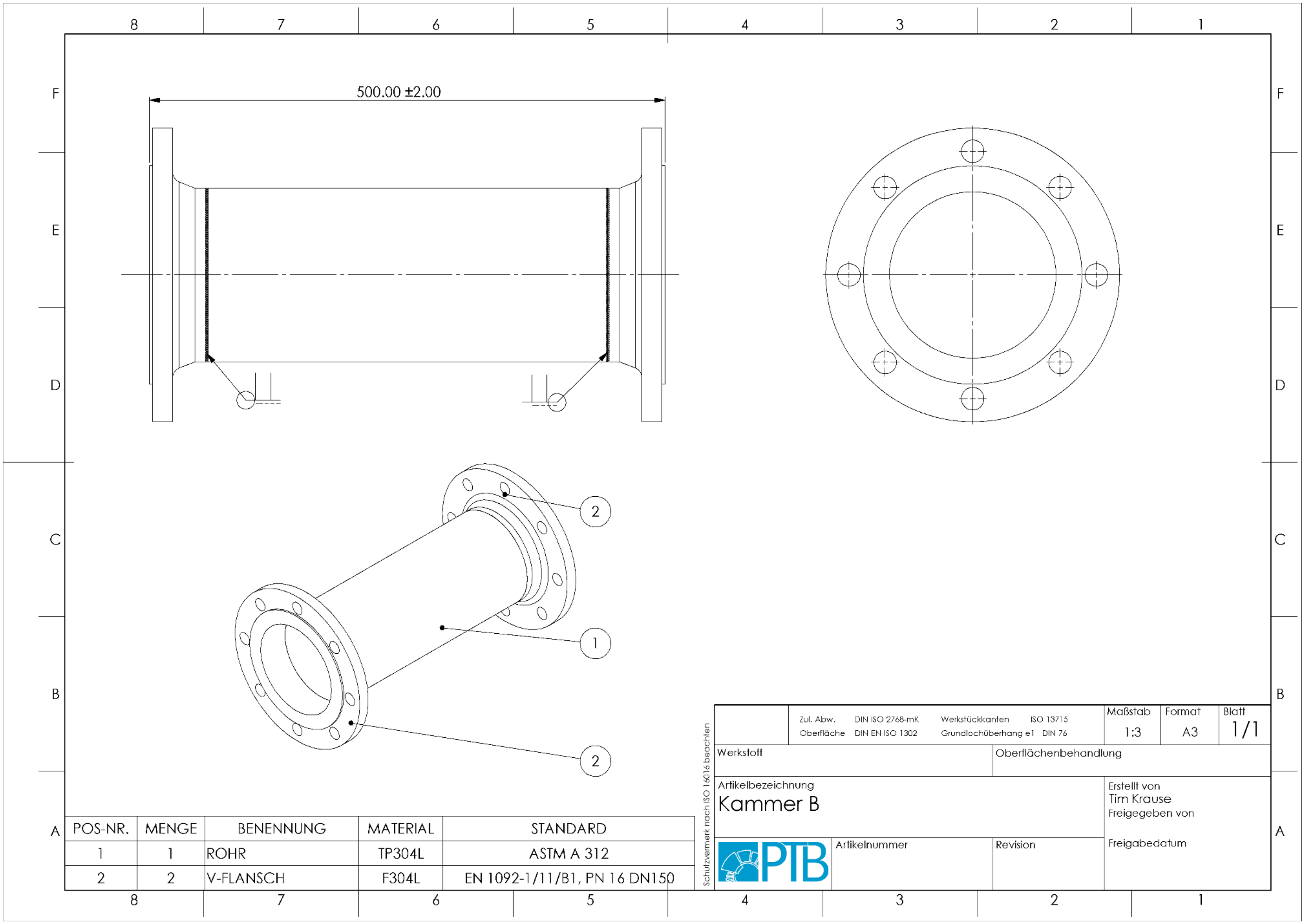
500.00 ±2.00
1
2
2
POS-NR. | MENGE | BENENNUNG | MATERIAL | STANDARD
1 | 1 | ROHR | TP304L | ASTM A 312
2 | 2 | V-FLANSCH | F304L | EN 1092-1/11/B1, PN 16 DN150
Schutzvermerk nach ISO 16016 beachten
Zul. Abw. DIN ISO 2768-mK
Oberfläche DIN EN ISO 1302
Werkstückkanten ISO 13715
Grundlochüberhang e1 DIN 76
Maßstab 1:3
Format A3
Blatt 1/1
Werkstoff
Oberflächenbehandlung
Artikelbezeichnung
Kammer B
Erstellt von
Tim Krause
Freigegeben von
Artikelnummer
Revision
Freigabedatum

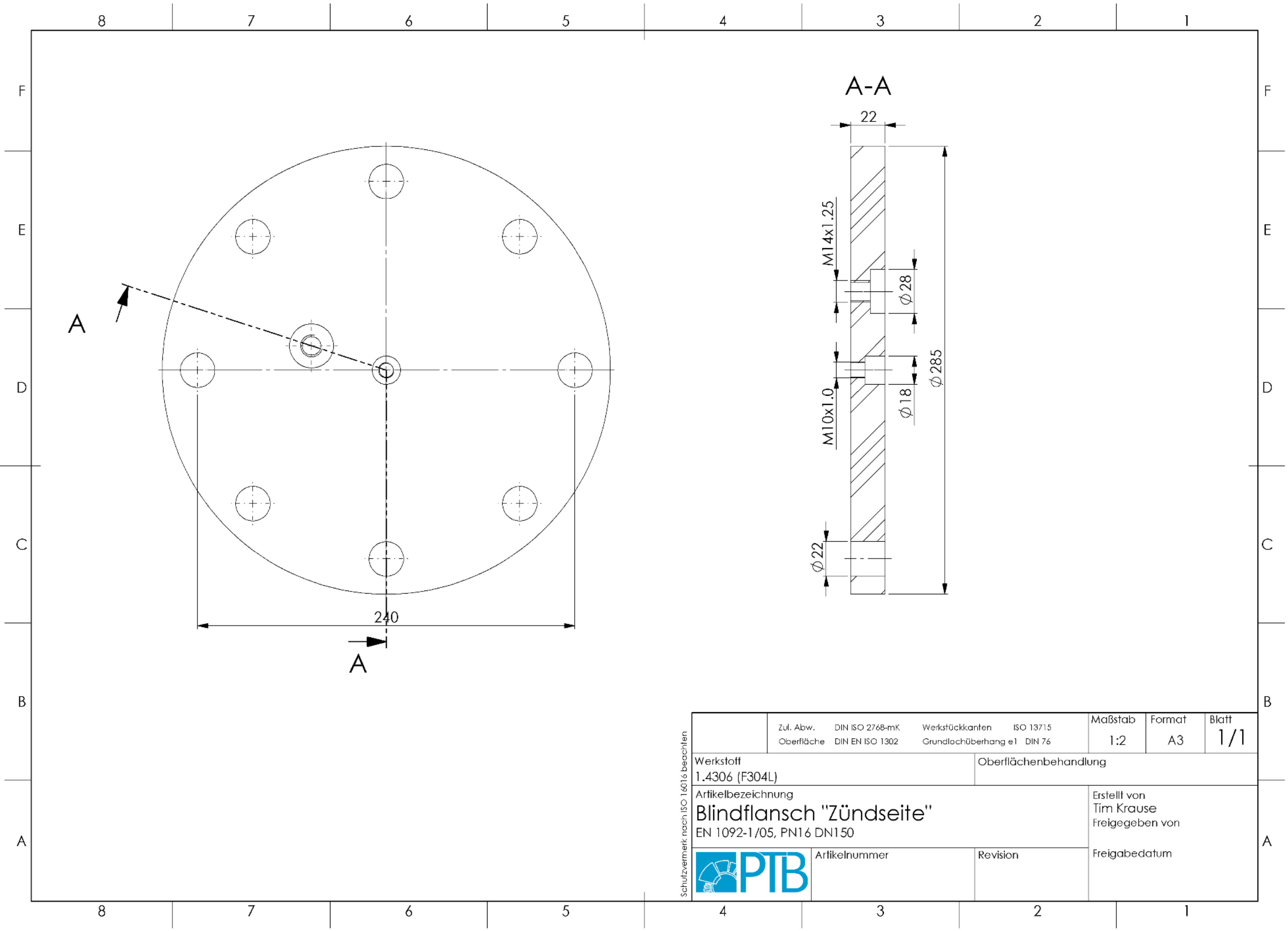
A-A
22
M14x1.25
M10x1.0
⌀28
⌀18
⌀285
⌀22
240
A
A
Zul. Abw. DIN ISO 2768-mK
Oberfläche DIN EN ISO 1302
Werkstückkanten ISO 13715
Grundlochüberhang e1 DIN 76
Maßstab 1:2
Format A3
Blatt 1/1
Werkstoff
1.4306 (F304L)
Oberflächenbehandlung
Artikelbezeichnung
Blindflansch "Zündseite"
EN 1092-1/05, PN16 DN150
Erstellt von
Tim Krause
Freigegeben von
Artikelnummer
Revision
Freigabedatum
PTB
Schutzvermerk nach ISO 16016 beachten

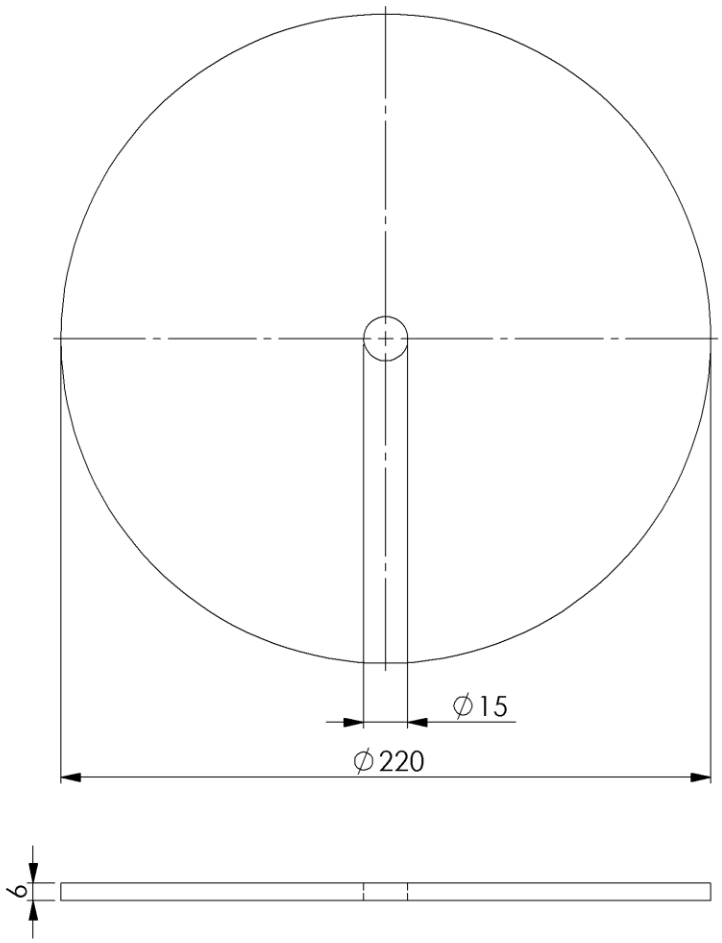

Zul. Abw.	DIN ISO 2768-mK	Werkstückkanten	ISO 13715	
Oberfläche	DIN EN ISO 1302	Grundlochüberhang e1	DIN 76	

Maßstab 1:2 | Format A4 | Blatt 1/1

Werkstoff
3.1645 (EN AW-2007)

Oberflächenbehandlung

Artikelbezeichnung
Lochblende

Erstellt von
Tim Krause
Freigegeben von

Freigabedatum

PTB

Artikelnummer

Revision

Schutzvermerk nach ISO 16016 beachten

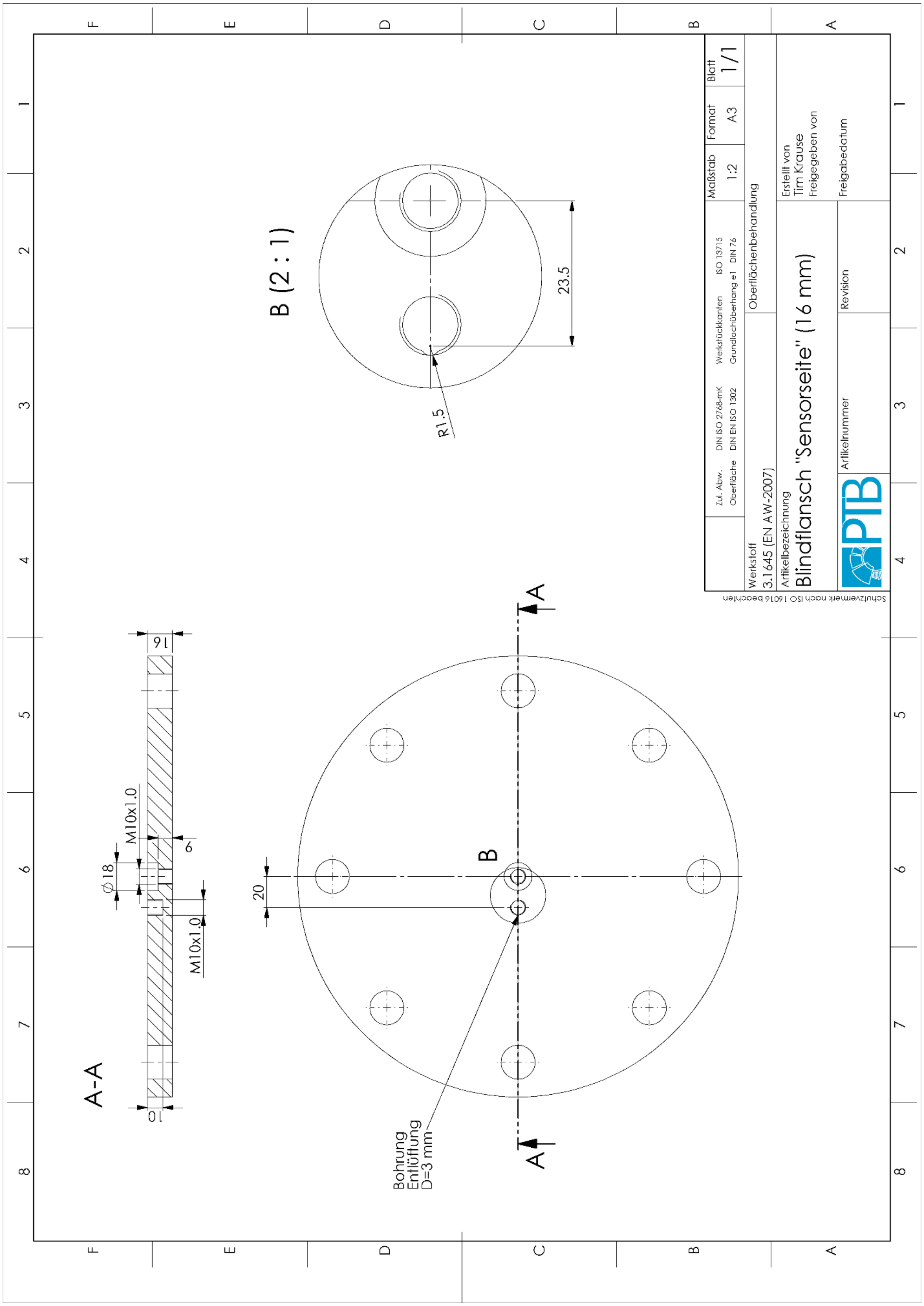

A-A
B (2 : 1)
B
A
16
10
6
∅18
M10x1.0
M10x1.0
20
23.5
R1.5
Bohrung
Entlüftung
D=3 mm
Zul. Abw. DIN ISO 2768-mK
Oberfläche DIN EN ISO 1302
Werkstückkanten ISO 13715
Grundlochüberhang e1 DIN 76
Maßstab 1:2
Format A3
Blatt 1/1
Oberflächenbehandlung
Werkstoff
3.1645 (EN AW-2007)
Artikelbezeichnung
Blindflansch "Sensorseite" (16 mm)
Erstellt von
Tim Krause
Freigegeben von
Freigabedatum
Revision
Artikelnummer
PTB
Schutzvermerk nach ISO 16016 beachten

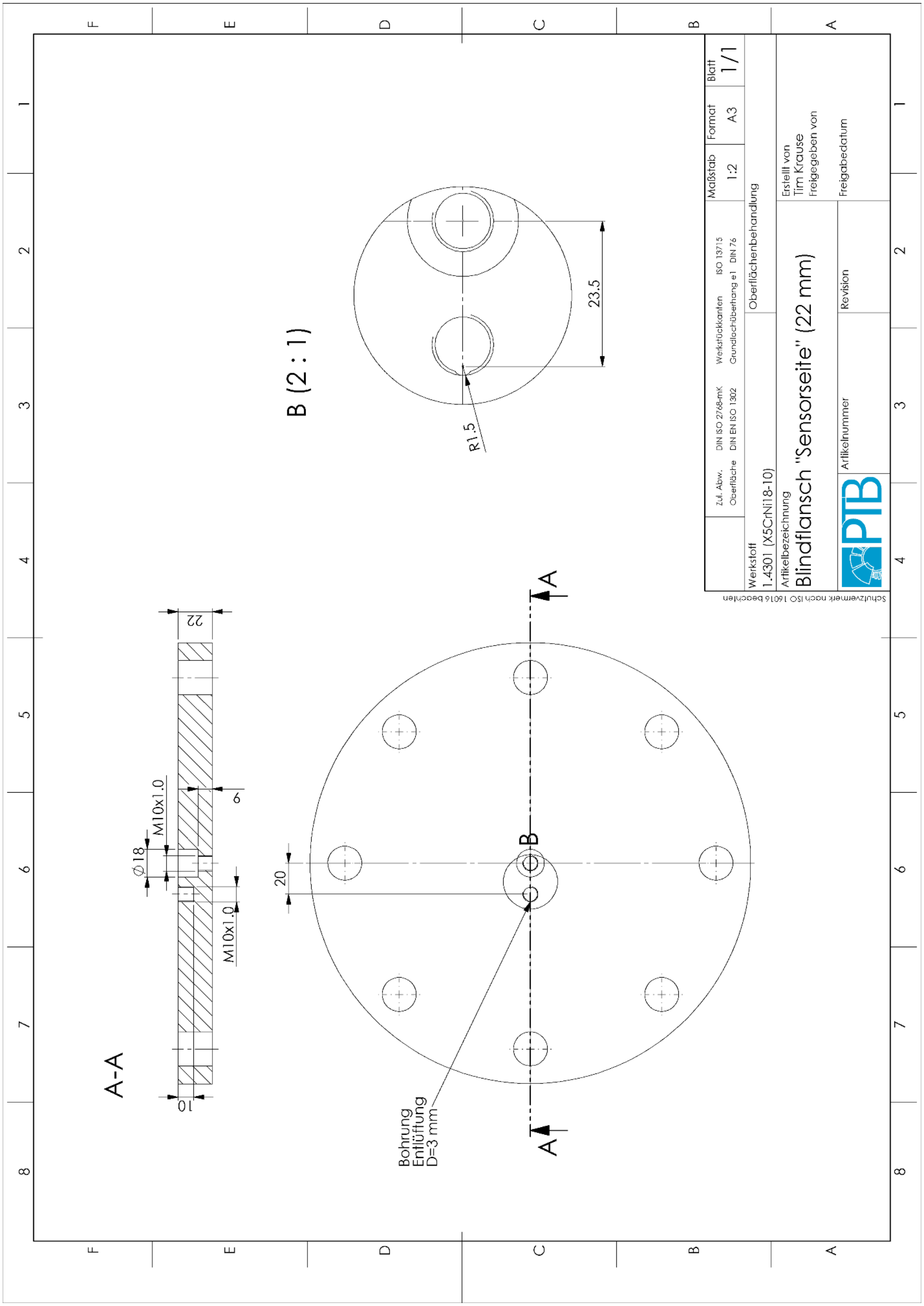

A-A
B (2 : 1)
A
A
B
22
10
6
20
23.5
R1.5
⌀18
M10x1.0
M10x1.0
Bohrung
Entlüftung
D=3 mm
Zul. Abw. DIN ISO 2768-mK
Oberfläche DIN EN ISO 1302
Werkstückkanten ISO 13715
Grundlochüberhang e1 DIN 76
Maßstab 1:2
Format A3
Blatt 1/1
Oberflächenbehandlung
Werkstoff
1.4301 (X5CrNi18-10)
Artikelbezeichnung
Blindflansch "Sensorseite" (22 mm)
Erstellt von
Tim Krause
Freigegeben von
Freigabedatum
Revision
Artikelnummer
Schutzvermerk nach ISO 16016 beachten

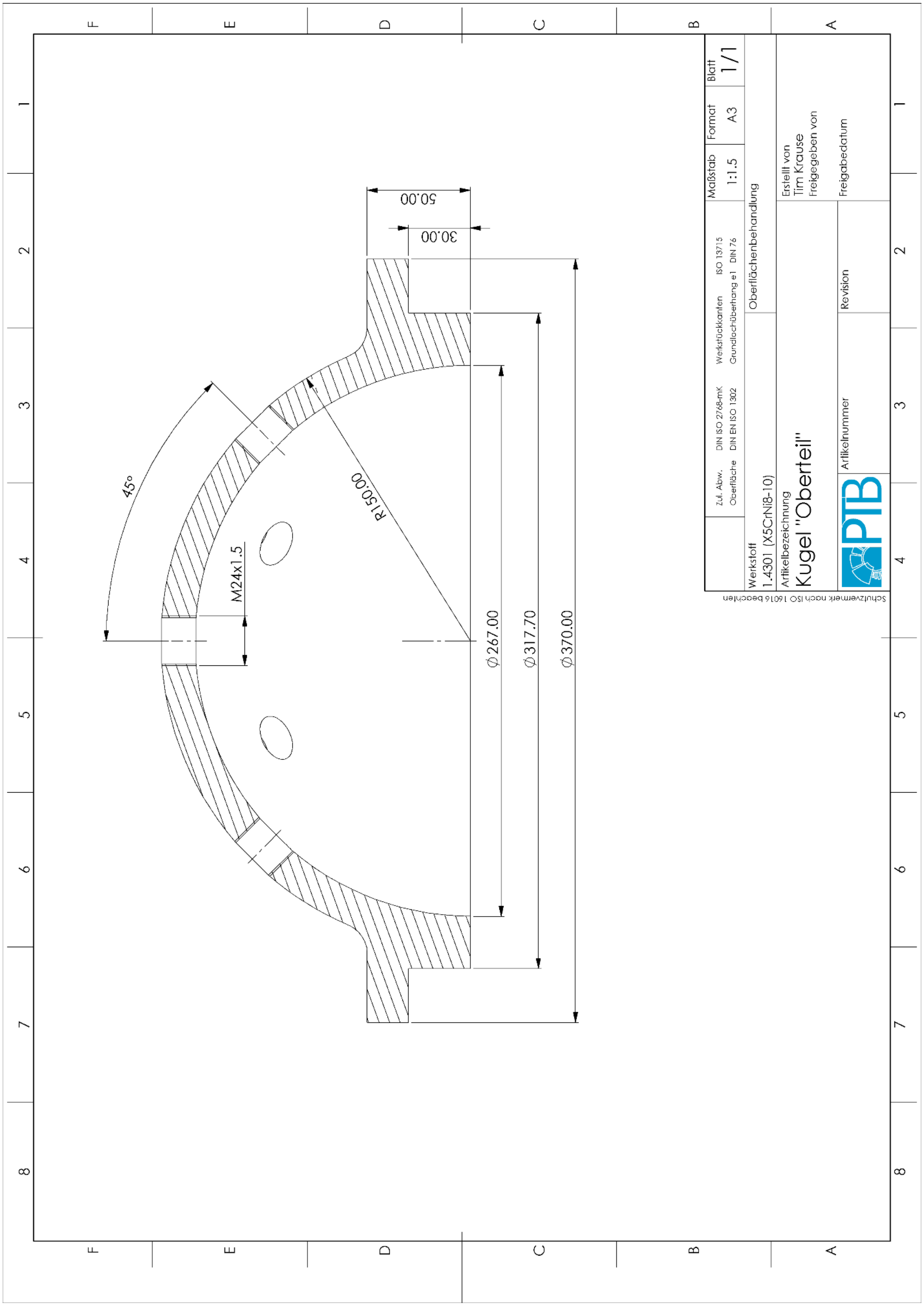

50.00
30.00
45°
R150.00
M24x1.5
∅267.00
∅317.70
∅370.00
Zul. Abw. DIN ISO 2768-mK
Oberfläche DIN EN ISO 1302
Werkstückkanten ISO 13715
Grundlochüberhang e1 DIN 76
Maßstab 1:1.5
Format A3
Blatt 1/1
Oberflächenbehandlung
Werkstoff
1.4301 (X5CrNi8-10)
Artikelbezeichnung
Kugel "Oberteil"
Erstellt von
Tim Krause
Freigegeben von
Freigabedatum
Revision
Artikelnummer
PTB
Schutzvermerk nach ISO 16016 beachten

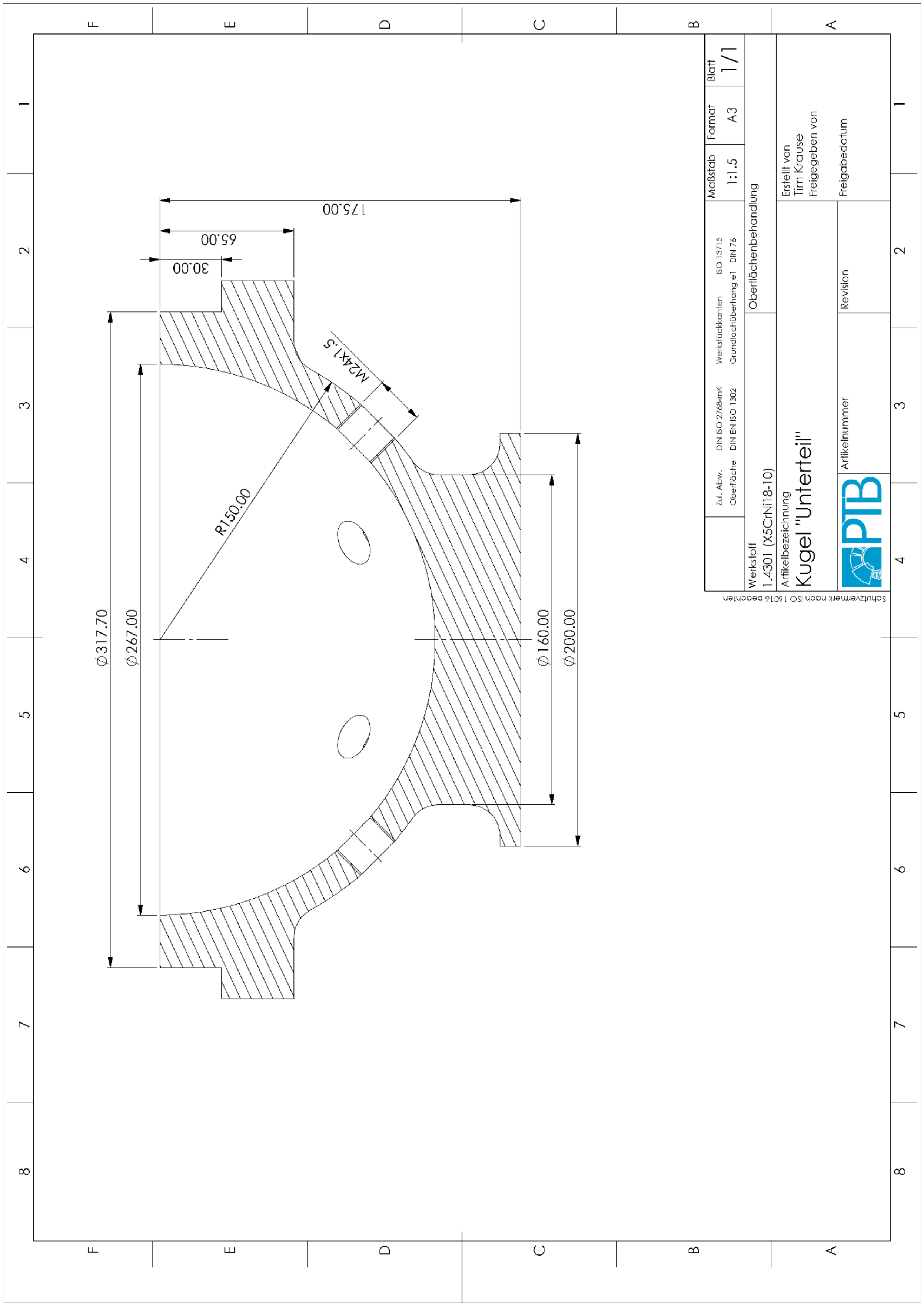
175.00
65.00
30.00
M24x1.5
R150.00
⌀317.70
⌀267.00
⌀160.00
⌀200.00
Werkstoff
1.4301 (X5CrNi18-10)
Zul. Abw. DIN ISO 2768-mK
Oberfläche DIN EN ISO 1302
Werkstückkanten ISO 13715
Grundlochüberhang e1 DIN 76
Oberflächenbehandlung
Maßstab 1:1.5
Format A3
Blatt 1/1
Artikelbezeichnung
Kugel "Unterteil"
Erstellt von
Tim Krause
Freigegeben von
Freigabedatum
Revision
Artikelnummer
Schutzvermerk nach ISO 16016 beachten

APPENDIX 4 – EXPERIMENTAL RESULTS

The following pages consist of the captured data from the repeated tests that were further used for data analysis in order to compare the results consistencies of the pressure sensors.

1. Spherical Enclosure Test – 10.06.2024

Ort:	PTB
Datum:	10.06.2024 - 13:20 - 16:00
Prüfer:	Mona Uunona

Flowrate: 40 l/min und 50 l/min

Measurement	Nominal Pressure (mbar)	H2-Air mixture Temperature (in °C)	Room Temperature (in °C)	O2 content in Gas-Air mixture (in Vol-%)	H2 volume concentration (in Vol-%)	Humidity of H2-Air mixture (in %rH)	P1_Sensor1 (601CAA, SN 5675657) Explosion Pressure (in bar)	P2_Sensor2 (601CAA, SN 5712432) Explosion Pressure (in bar)	P3_Sensor3 (601CAA, SN 5712433) Explosion Pressure (in bar)	P4_Sensor4 (601CAA, SN 6123567) Explosion Pressure (in bar)
1	998.00	21.40	22.00	14.54	31.10	0.04	7.15	7.22	7.21	7.42
2	998.00	23.40	22.00	14.54	31.10	0.04	7.09	7.21	7.22	7.36
3	998.00	23.50	22.00	14.54	31.10	0.04	7.05	7.19	7.15	7.26
4	997.90	23.00	22.00	14.54	31.10	0.04	7.10	7.21	7.24	7.35
5	997.80	23.00	22.00	14.54	31.10	0.04	7.12	7.21	7.18	7.37
6	997.90	23.00	22.00	14.54	31.10	0.04	7.07	7.16	7.16	7.31
7	997.90	23.00	22.00	14.54	31.10	0.04	7.02	7.16	7.19	7.29
8	997.90	23.00	22.00	14.54	31.10	0.04	6.99	7.13	7.15	7.25
9	997.80	23.00	22.00	14.54	31.10	0.04	7.01	7.15	7.12	7.26
10	997.90	23.00	22.10	14.54	31.10	0.04	6.99	7.10	7.13	7.27
Average	**997.91**	**22.93**	**22.01**	**14.54**	**31.10**	**0.04**				

	P1_Sensor1	P2_Sensor2	P3_Sensor3	P4_Sensor4
Average	**7.06**	**7.17**	**7.18**	**7.31**
Std. Deviation	**0.06**	**0.04**	**0.04**	**0.06**
Minimum:	**6.99**	**7.10**	**7.12**	**7.25**
Maximum:	**7.15**	**7.22**	**7.24**	**7.42**
Range	**0.16**	**0.12**	**0.12**	**0.17**

All measurements were performed with 5 kHz TP-Filter (Butterworth, 2nd order)

All measurements were performed with 1 mm RTV silicone membrane on pressure sensor

Devices used:
- Oxygen Analyzer (SERVOMEX 2210)
- Oscilloscope (Yokogawa DL850)
- 8-Channel Charge Amplifier (Kistler LabAmp Type 5167A)
- Piezoresistive Amplifier (Kistler Type 4603)
- Humidity and Temperature sensor (Kistler ExTL-1 61032 Amplifier 4624A)

Oscilloscope settings:
1.0 V/div
2 bar/V
AcqMode: Normal
10 MS/s
1 ms/div

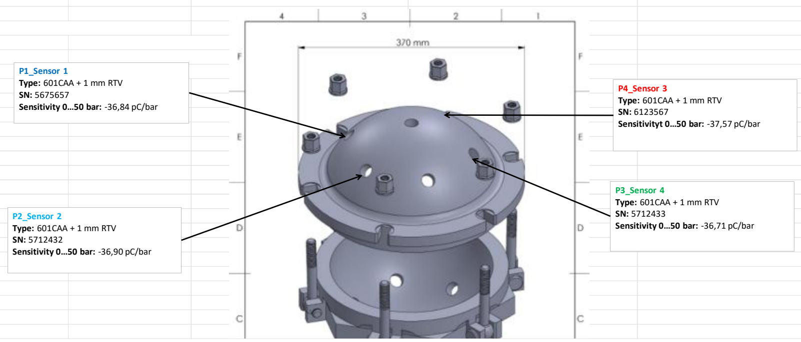

2. Large tube enclosure – 09.07.2024

Ort:	PTB
Datum:	25.06.2024 - 10:30 - 11:20
Prüfer:	Mona Uunona

Flowrate: 40 l/min und 50 l/min

Measurement	Nominal Pressure (mbar)	H2-Air mixture Temperature (in °C)	Room Temperature (in °C)	O2 content in Gas-Air mixture (in Vol-%)	H2 volume concentration (in Vol-%)	Humidity of H2-Air mixture (in %rH)	P1_Sensor1 (601CAA, SN 5675657) Explosion Pressure (in bar)	P2_Sensor2 (601CAA, SN 5712432) Explosion Pressure (in bar)
1	1009.80	24.00	23.40	14.54	31.10	0.10		
2	1009.80	24.00	23.40	14.54	31.10	0.10	6.49	6.68
3	1009.80	25.00	23.50	14.54	31.10	0.40	6.47	6.65
4	1009.70	25.00	23.50	14.54	31.10	0.60	6.40	6.61
5	1009.60	25.00	23.50	14.54	31.10	0.10	6.46	6.65
Average:	1009.74	24.60	23.46	14.54	31.10	0.26		

	P1	P2
Mittelwert:	6.46	6.65
Standardabw:	0.04	0.03
Minimum:	6.40	6.61
Maximum:	6.49	6.68
Spannweite:	0.09	0.07

All measurements were performed with 5 kHz TP-Filter (Butterworth, 2nd order)

All measurements were performed with 1 mm RTV silicone membrane on pressure sensor

Devices used:
- Oxygen Analyzer (SERVOMEX 2210)
- Oscilloscope (Yokogawa DL850)
- 8-Channel Charge Amplifier (Kistler LabAmp Type 5167A)
- Piezoresistive Amplifier (Kistler Type 4603)
- Humidity and Temperature sensor (Kistler ExTL-1 61032 Amplifier 4624A)

Oscilloscope settings:
1.0 V/div
2 bar/V
AcqMode: Normal
10 MS/s
1 ms/div

P1_Sensor 1 (Eingang)
Type: 601CAA + 1 mm RTV
SN: 5675657
Sensitivity 0…50 bar: -36,84 pC/bar

P2_Sensor 2 (Ausgang)
Type: 601CAA + 1 mm RTV
SN: 5712432
Sensitivity 0…50 bar: -36,90 pC/bar

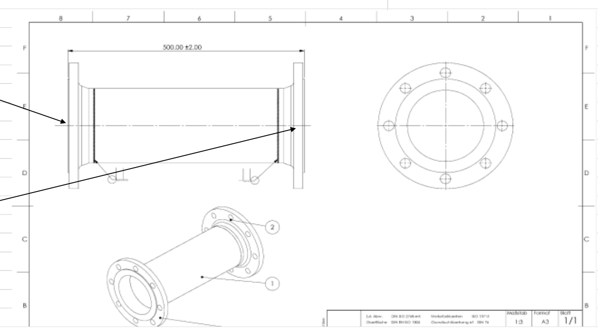

3. Large tube enclosure – 25.06.2024

Ort:	PTB
Datum:	09/07/2024 14:00 - 16:00
Prüfer:	Mona Uunona

Flowrate: 40 l/min und 50 l/min

Measurement	Nominal Pressure (mbar)	H2-Air mixture Temperature (in °C)	Room Temperature (in °C)	O2 content in Gas-Air mixture (in Vol-%)	H2 volume concentration (in Vol-%)	Humidity of H2-Air mixture (in %rH)	P1_Sensor1 (601CAA, SN 5675657) Explosion Pressure (in bar)	P2_Sensor2 (601CAA, SN 5712432) Explosion Pressure (in bar)
1	1007.50	26.00	24.70	14.54	31.10	0.00	6.67	6.78
2	1007.40	26.00	24.70	14.55	31.00	0.00	6.65	6.77
3	1007.40	27.00	24.70	14.54	31.10	0.00	6.61	6.71
4	1007.40	27.00	24.80	14.55	31.00	0.00	6.69	6.83
5	1007.40	27.00	24.80	14.54	31.00	0.00	6.59	6.71
6	1007.30	27.00	24.80	14.54	31.00	0.00	6.58	6.73
7	1007.10	27.00	24.80	14.54	31.00	0.00	6.58	6.72
8	1007.00	28.00	24.80	14.54	31.00	0.00	6.57	6.71
9	1007.00	28.00	24.90	14.54	31.00	0.00	6.56	6.72
10	1006.80	28.00	24.90	14.54	31.00	0.00	6.62	6.75
Mittelwert:	**1007.23**	**27.10**	**24.79**	**14.54**	**31.02**	**0.00**		

	P1_Sensor1	P2_Sensor2
Mittelwert:	**6.61**	**6.74**
Standardabw:	**0.04**	**0.04**
Minimum:	**6.56**	**6.71**
Maximum:	**6.69**	**6.83**
Spannweite:	**0.13**	**0.12**

All measurements were performed with 5 kHz TP-Filter (Butterworth, 2nd order)

All measurements were performed with 1 mm RTV silicone membrane on pressure sensor

Devices used:
- Oxygen Analyzer (SERVOMEX 2210)
- Oscilloscope (Yokogawa DL850)
- 8-Channel Charge Amplifier (Kistler LabAmp Type 5167A)
- Piezoresistive Amplifier (Kistler Type 4603)
- Humidity and Temperature sensor (Kistler ExTL-1 61032 Amplifier 4624A)

Oscilloscope settings:
1.0 V/div
2 bar/V
AcqMode: Normal
10 MS/s
1 ms/div

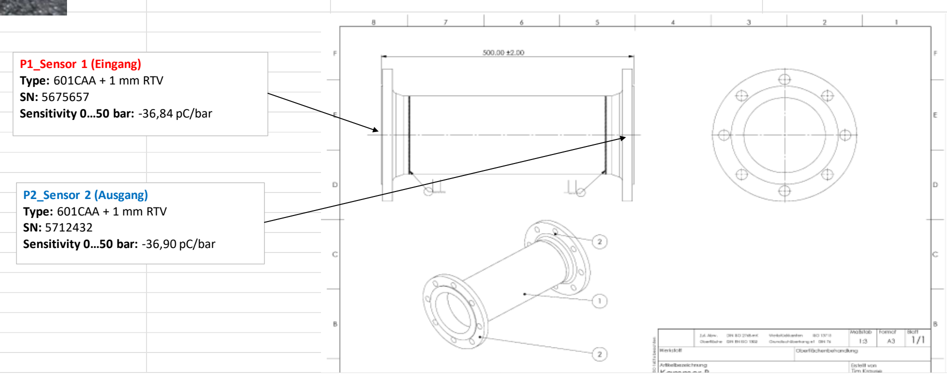

4. Combined tube enclosure (with 15 mm orifice) – 26.06.2024

Location:	PTB, Div 3.54
Date:	26.06.2024 - 14:20 - 16:30
Tester:	Mona Uunona

Flowrate: 80 l/min - 15mm Diameter

Measurement	Nominal Pressure (mbar)	H2-Air mixture Temperature (in °C)	Room Temperature (in °C)	O2 content in Gas-Air mixture (in Vol-%)	H2 volume concentration (in Vol-%)	Humidity of H2-Air mixture (in %rH)	P1_Sensor1 (601CAA, SN 5675657) Explosion Pressure (in bar)	P2_Sensor2 (601CAA, SN 5712432) Explosion Pressure (in bar)
1	1003.40	25.00	24.50	14.54	31.10	0.00	6.15	14.38
2	1003.20	25.00	24.70	14.54	31.00	0.00	6.10	14.81
3	1003.20	26.00	24.80	14.54	31.10	0.00	6.07	14.41
4	1002.90	26.00	24.80	14.54	31.00	0.01	6.06	14.59
5	1002.70	26.00	24.80	14.54	31.00	0.00	5.96	12.64
6	1002.50	27.00	24.90	14.54	31.00	0.00	6.02	13.87
7	1002.30	27.00	24.90	14.54	31.00	0.00	6.12	14.02
8	1002.20	27.00	24.90	14.54	31.00	0.00	5.87	14.86
9	1001.90	27.00	24.80	14.54	31.00	0.00	5.85	14.49
10	1001.70	27.00	24.80	14.54	31.00	0.00	6.05	13.81
Mittelwert:	1002.60	26.30	24.79	14.54	31.02	0.00		

	P1_Sensor1	P2_Sensor2
Average	6.03	14.19
Std deviation	0.10	0.65
Minimum:	5.85	12.64
Maximum:	6.15	14.86
Range	0.30	2.22

All measurements were performed with 5 kHz TP-Filter (Butterworth, 2nd order)

All measurements were performed with 1 mm RTV silicone membrane on pressure sensor

Devices used:
- Oxygen Analyzer (SERVOMEX 2210)
- Oscilloscope (Yokogawa DL850)
- 8-Channel Charge Amplifier (Kistler LabAmp Type 5167A)
- Piezoresistive Amplifier (Kistler Type 4603)
- Humidity and Temperature sensor (Kistler ExTL-1 61032 Amplifier 4624A)

Oscilloscope settings:
1.0 V/div
2 bar/V
AcqMode: Normal
10 MS/s
1 ms/div

P1_Sensor 1
Type: 601CAA + 1 mm RTV
SN: 5675657
Sensitivity 0…50 bar: -36,84 pC/bar

P2_Sensor 2
Type: 601CAA + 1 mm RTV
SN: 5712432
Sensitivity 0…50 bar: -36,90 pC/bar

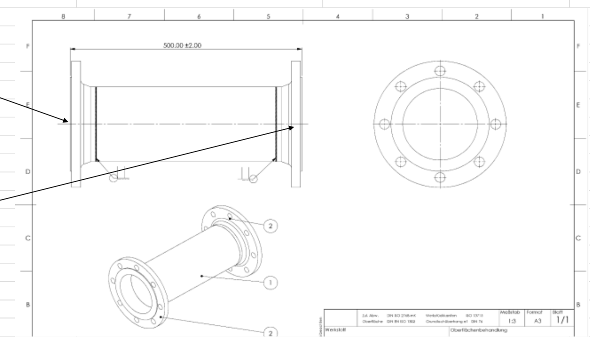

5. Combined tube enclosure (with 58 mm orifice) – 26.06.2024

Location:	PTB, Div 3.54
Date:	26.06.2024 - 14:20 - 16:30
Tester:	Mona Uunona

Flowrate: 80 l/min - 15mm Diameter

Measurement	Nominal Pressure (mbar)	H2-Air mixture Temperature (in °C)	Room Temperature (in °C)	O2 content in Gas-Air mixture (in Vol-%)	H2 volume concentration (in Vol-%)	Humidity of H2-Air mixture (in %rH)	P1_Sensor1 (601CAA, SN 5675657) Explosion Pressure (in bar)	P2_Sensor2 (601CAA, SN 5712432) Explosion Pressure (in bar)
1	1003.40	25.00	24.50	14.54	31.10	0.00	6.15	14.38
2	1003.20	25.00	24.70	14.54	31.00	0.00	6.10	14.81
3	1003.20	26.00	24.80	14.54	31.10	0.00	6.07	14.41
4	1002.90	26.00	24.80	14.54	31.00	0.01	6.06	14.59
5	1002.70	26.00	24.80	14.54	31.00	0.00	5.96	12.64
6	1002.50	27.00	24.90	14.54	31.00	0.00	6.02	13.87
7	1002.30	27.00	24.90	14.54	31.00	0.00	6.12	14.02
8	1002.20	27.00	24.90	14.54	31.00	0.00	5.87	14.86
9	1001.90	27.00	24.80	14.54	31.00	0.00	5.85	14.49
10	1001.70	27.00	24.80	14.54	31.00	0.00	6.05	13.81
Mittelwert:	1002.60	26.30	24.79	14.54	31.02	0.00		

	P1_Sensor1	P2_Sensor2
Average	6.03	14.19
Std deviation	0.10	0.65
Minimum:	5.85	12.64
Maximum:	6.15	14.86
Range	0.30	2.22

All measurements were performed with 5 kHz TP-Filter (Butterworth, 2nd order)

All measurements were performed with 1 mm RTV silicone membrane on pressure sensor

Devices used:
- Oxygen Analyzer (SERVOMEX 2210)
- Oscilloscope (Yokogawa DL850)
- 8-Channel Charge Amplifier (Kistler LabAmp Type 5167A)
- Piezoresistive Amplifier (Kistler Type 4603)
- Humidity and Temperature sensor (Kistler ExTL-1 61032 Amplifier 4624A)

Oscilloscope settings:
1.0 V/div
2 bar/V
AcqMode: Normal
10 MS/s
1 ms/div

P1_Sensor 1
Type: 601CAA + 1 mm RTV
SN: 5675657
Sensitivity 0…50 bar: -36,84 pC/bar

P2_Sensor 2
Type: 601CAA + 1 mm RTV
SN: 5712432
Sensitivity 0…50 bar: -36,90 pC/bar

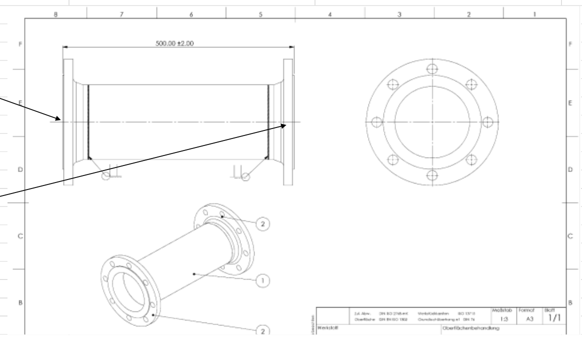

6. Combined tube enclosure (with 90 mm orifice) – 28.06.2024

Location:	PTB, Div 3.54
Date:	28.06.2024 - 09:30 - 12:00
Tester:	Mona Uunona

Flowrate: 80 l/min - 60 l/min 90mm Diameter

Measurement	Nominal Pressure (mbar)	H2-Air mixture Temperature (in °C)	Room Temperature (in °C)	O2 content in Gas-Air mixture (in Vol-%)	H2 volume concentration (in Vol-%)	Humidity of H2-Air mixture (in %rH)	P1_Sensor1 (601CAA, SN 5675657) Explosion Pressure (in bar)	P2_Sensor2 (601CAA, SN 5712432) Explosion Pressure (in bar)
1	1003.70	26.00	24.80	14.54	31.10	0.40	10.31	11.21
2	1003.90	26.00	24.90	14.54	31.10	1.40	9.83	9.75
3	1004.20	27.00	25.00	14.54	31.10	1.40	10.35	10.37
4	1004.40	27.00	25.00	14.54	31.10	0.60	10.09	10.77
5	1004.60	27.00	25.00	14.54	31.10	0.80	10.40	10.99
6	1004.70	27.00	25.00	14.54	31.10	0.00	10.49	11.79
7	1004.80	28.00	25.10	14.54	31.10	0.40	9.83	10.29
8	1004.90	28.00	25.10	14.54	31.10	0.40	9.45	9.57
9	1005.10	28.00	25.10	14.54	31.10	0.10	9.23	9.93
10	1005.30	28.00	25.10	14.54	31.10	0.00	10.16	10.91
Mittelwert:	1004.56	27.20	25.01	14.54	31.10	0.55		

	P1_Sensor1	P2_Sensor2
Average	10.01	10.56
Std deviation	0.42	0.70
Minimum:	9.23	9.57
Maximum:	10.49	11.79
Range	1.26	2.22

All measurements were performed with 5 kHz TP-Filter (Butterworth, 2nd order)

All measurements were performed with 1 mm RTV silicone membrane on pressure sensor

Devices used:
- Oxygen Analyzer (SERVOMEX 2210)
- Oscilloscope (Yokogawa DL850)
- 8-Channel Charge Amplifier (Kistler LabAmp Type 5167A)
- Piezoresistive Amplifier (Kistler Type 4603)
- Humidity and Temperature sensor (Kistler ExTL-1 61032 Amplifier 4624A)

Oscilloscope settings:
1.0 V/div
2 bar/V
AcqMode: Normal
10 MS/s
1 ms/div

P1_Sensor 1
Type: 601CAA + 1 mm RTV
SN: 5675657
Sensitivity 0...50 bar: -36,84 pC/bar

P2_Sensor 2
Type: 601CAA + 1 mm RTV
SN: 5712432
Sensitivity 0...50 bar: -36,90 pC/bar

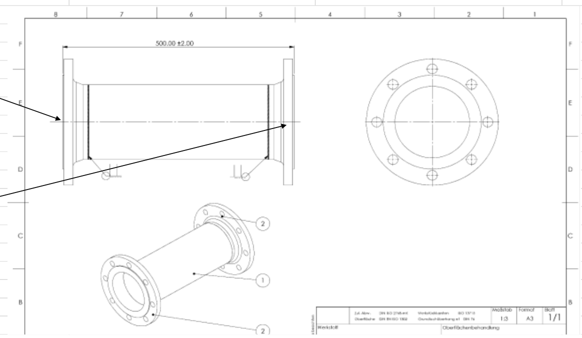

7. Multi-chamber enclosure (empty) – 26.08.2024

Ort:	PTB
Datum:	26.08.2024 10:00:00 - 12:00
Prüfer:	Mona Uunona

Flowrate: 40 l/min und 50 l/min

Measurement	Nominal Pressure (mbar)	H2-Air mixture Temperature (in °C)	Room Temperature (in °C)	O2 content in Gas-Air mixture (in Vol-%)	H2 volume concentration (in Vol-%)	Humidity of H2-Air mixture (in %rH)	P1_Sensor1 (601CAA, SN 5675657) Explosion Pressure (in bar)	P2_Sensor2 (601CAA, SN 5712432) Explosion Pressure (in bar)	P3_Sensor3 (601CAA, SN 5712433) Explosion Pressure (in bar)	P4_Sensor4 (601CAA, SN 6123567) Explosion Pressure (in bar)	P5_Sensor5 (601CAA, SN 5712434) Explosion Pressure (in bar)	P6_Sensor6 (601CAA, SN 5712434) Explosion Pressure (in bar)
1	1014.70	25.00	23.50	14.54	31.10	1.10	6.34	6.73	6.80	6.51	6.79	6.64
2	1014.70	26.00	23.70	14.54	31.10	1.40	6.41	6.75	6.82	6.56	6.83	6.69
3	1014.70	26.00	23.90	14.54	31.10	1.20	6.40	6.66	6.81	6.56	6.77	6.64
4	1014.80	26.00	24.00	14.54	31.10	1.00	6.45	6.73	6.79	6.56	6.77	6.65
5	1014.70	26.00	24.10	14.54	31.10	1.00	6.25	6.69	6.67	6.42	6.69	6.54
6	1014.70	26.00	24.20	14.54	31.10	1.00	6.37	6.75	6.76	6.57	6.81	6.61
7	1014.60	27.00	24.20	14.54	31.10	0.90	6.27	6.65	6.69	6.45	6.67	6.55
8	1014.70	27.00	24.30	14.54	31.10	0.80	6.24	6.63	6.69	6.47	6.70	6.51
9	1014.60	27.00	24.40	14.54	31.10	0.70	6.34	6.63	6.70	6.49	6.71	6.54
10	1014.60	27.00	24.40	14.54	31.10	0.80	6.27	6.65	6.72	6.42	6.74	6.56
Average	**1014.68**	**26.30**	**24.07**	**14.54**	**31.10**	**0.99**						

	P1_Sensor1	P2_Sensor2	P3_Sensor3	P4_Sensor4	P5_Sensor5	P6_Sensor6
Average	**6.33**	**6.69**	**6.75**	**6.50**	**6.75**	**6.59**
Std. Deviation	**0.07**	**0.05**	**0.06**	**0.06**	**0.05**	**0.06**
Minimum:	**6.24**	**6.63**	**6.67**	**6.42**	**6.67**	**6.51**
Maximum:	**6.45**	**6.75**	**6.82**	**6.57**	**6.83**	**6.69**
Range	**0.21**	**0.12**	**0.15**	**0.15**	**0.16**	**0.18**

All measurements were performed with 5 kHz TP-Filter (Butterworth, 2nd order)

All measurements were performed with 1 mm RTV silicone membrane on pressure sensor tip

Devices used:
- Oxygen Analyzer (SERVOMEX 2210)
- Oscilloscope (Yokogawa DL850)
- 8-Channel Charge Amplifier (Kistler LabAmp Type 5167A)
- Piezoresistive Amplifier (Kistler Type 4603)
- Humidity and Temperature sensor (Kistler ExTL-1 61032 Amplifier 4624A)

Oscilloscope settings:
1.0 V/div
2 bar/V
AcqMode: Normal
10 MS/s
5 ms/div

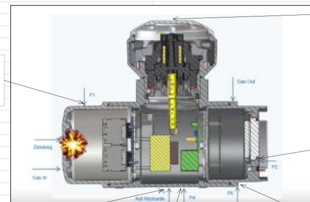

P1_Sensor 5
Type: 601CAA + 1 mm RTV
SN: 5712433
Sensitivity 0...50 bar: -36,71 pC/bar

P1_Sensor 1
Type: 601CAA + 1 mm RTV
SN: 6123567
Sensitivity 0...50 bar: -37.57 pC/bar

P2_Sensor 2
Type: 601CAA + 1 mm RTV
SN: 5675656
Sensitivity 0...50 bar: -36,70 pC/bar

P4_Sensor 3
Type: 601CAA + 1 mm RTV
SN: 5675658
Sensitivityt 0...50 bar: -36.71 pC/bar

P3_Sensor 4
Type: 601CAA + 1 mm RTV
SN: 5712434
Sensitivity 0...50 bar: -36.86 pC/bar

P1_Sensor 6
Type: 601CAA + 1 mm RTV
SN: 5712432
Sensitivity 0...50 bar: -36.90 pC/bar

8. Multi-chamber enclosure (with internal installations) – 27.08.2024

Ort:	PTB
Datum:	27/08/2024
Prüfer:	Mona Uunona

Flowrate: 40 l/min und 50 l/min

Measurement	Nominal Pressure (mbar)	H2-Air mixture Temperature (in ℃)	Room Temperature (in ℃)	O2 content in Gas-Air mixture (in Vol-%)	H2 volume concentration (in Vol-%)	Humidity of H2-Air mixture (in %rH)	P1_Sensor1 (601CAA, SN 5675657) Explosion Pressure (in bar)	P2_Sensor2 (601CAA, SN 5712432) Explosion Pressure (in bar)	P3_Sensor3 (601CAA, SN 5712433) Explosion Pressure (in bar)	P4_Sensor4 (601CAA, SN 6123567) Explosion Pressure (in bar)	P5_Sensor5 (601CAA, SN 5712434) Explosion Pressure (in bar)	P6_Sensor6 (601CAA, SN 5712434) Explosion Pressure (in bar)
1	1016.00	26.00	23.60	14.54	31.00	1.40	6.93	14.12	7.60	7.41	7.31	11.81
2	1015.90	26.00	23.70	14.54	31.00	1.10	6.96	13.71	7.48	7.16	6.87	12.57
3	1015.90	26.00	23.80	14.54	31.00	1.10	7.08	12.03	7.13	7.21	7.16	11.69
4	1015.80	26.00	23.90	14.54	31.00	0.80	6.99	13.15	7.57	7.83	7.33	11.23
5	1015.70	26.00	24.00	14.54	31.00	0.90	6.84	14.32	7.69	7.29	7.01	11.71
Average	**1015.86**	**26.00**	**23.80**	**14.54**	**31.00**	**1.06**						

	P1_Sensor1	P2_Sensor2	P3_Sensor3	P4_Sensor4	P5_Sensor5	P6_Sensor6
Average	**6.96**	**13.47**	**7.49**	**7.38**	**7.14**	**11.80**
Std. Deviation	**0.09**	**0.92**	**0.22**	**0.27**	**0.20**	**0.48**
Minimum:	**6.84**	**12.03**	**7.13**	**7.16**	**6.87**	**11.23**
Maximum:	**7.08**	**14.32**	**7.69**	**7.83**	**7.33**	**12.57**
Range	**0.24**	**2.29**	**0.56**	**0.67**	**0.46**	**1.34**

All measurements were performed with 5 kHz TP-Filter (Butterworth, 2nd order)

All measurements were performed with 1 mm RTV silicone membrane on pressure sensor tip

Devices used:
- Oxygen Analyzer (SERVOMEX 2210)
- Oscilloscope (Yokogawa DL850)
- 8-Channel Charge Amplifier (Kistler LabAmp Type 5167A)
- Piezoresistive Amplifier (Kistler Type 4603)
- Humidity and Temperature sensor (Kistler ExTL-1 61032 Amplifier 4624A)

Oscilloscope settings:
1.0 V/div
2 bar/V
AcqMode: Normal
10 MS/s
5 ms/div

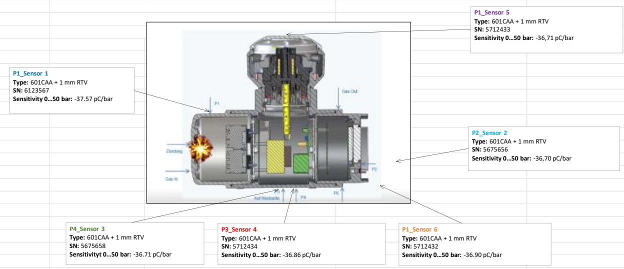

APPENDIX 5 – PYTHON PROGRAMMING SCRIPT

The following python script was used for data analysis and visualization purposes across all tests and enclosure configurations. The graphical plots of the results in this thesis were generated with the help of this python script.

While the script presented here demonstrates its application for one specific enclosure, similar scripts were employed for data analysis for all other enclosures.

```
---
import datetime
# Read file
file_name = 'Complex vessel 2.CSV'  # Filename
file_handler = open(file_name, 'r')  # r for read-only
content = file_handler.read()
table = []  # Read table data
rows = content.split('\n')
for i in range(len(rows)):
    columns = rows[i].split(',')  # Delimiter
    table.append(columns)

# Create data lists
time = []
P1 = []
P2 = []
P3 = []
P4 = []
P5 = []
P6 = []
```

```
table_data = table[16:]  # Remove header

z = table[8][1]  # Increment for time axis
print(z)

for i in range(0, len(table_data) - 1):  # Convert data to numbers

    time.append(table_data[i][0])
    time[i] = i * float(z) * 1000
    P1.append(table_data[i][1])
    P1[i] = float(P1[i])
    P2.append(table_data[i][2])
    P2[i] = float(P2[i])
    P3.append(table_data[i][3])
    P3[i] = float(P3[i])
    P4.append(table_data[i][4])
    P4[i] = float(P4[i])
    P5.append(table_data[i][5])
    P5[i] = float(P5[i])
    P6.append(table_data[i][6])
    P6[i] = float(P6[i])

# Calculate maximum values
max1 = max(P1)
max2 = max(P2)
max3 = max(P3)
max4 = max(P4)
max5 = max(P5)
max6 = max(P6)
```

```
# Calculate minimum values


# Plot

import matplotlib.pyplot as plt


ax1 = plt.figure(num=None, figsize=(16,9), dpi=100, facecolor='w', edgecolor='k').add_subplot(111)


line1 = ax1.plot(time, P1, color='cyan', label="$P1-Sensor1_{max}$: " + str(round(max1, 2)) + " bar", linewidth=1.0)

line2 = ax1.plot(time, P2, color='green', label="$P2-Sensor2_{max}$: " + str(round(max2, 2)) + " bar", linewidth=1.0)

line3 = ax1.plot(time, P3, color='salmon', label="$P3-Sensor3_{max}$: " + str(round(max3, 2)) + " bar", linewidth=1.0)

line4 = ax1.plot(time, P4, color='blue', label="$P4-Sensor4_{max}$: " + str(round(max4, 2)) + " bar", linewidth=1.0)

line5 = ax1.plot(time, P5, color='gray', label="$P5-Sensor5_{max}$: " + str(round(max4, 2)) + " bar", linewidth=1.0)

line6 = ax1.plot(time, P6, color='maroon', label="$P6-Sensor6_{max}$: " + str(round(max6, 2)) + " bar", linewidth=1.0)

ax1.axis([0, 20, 0, 15])


ax1.set_xlabel('Time in ms', fontsize=25)

ax1.set_ylabel('Pressure in bar', fontsize=25)

ax1.tick_params(labelsize=18)


# Plot with updated legend

ax1.legend(loc='upper right', bbox_to_anchor=(0.98, 0.98), borderaxespad=0, title="Legends", fontsize=14, ncol=1)


plt.grid(True, which='both')

plt.minorticks_on()
```

```
plt.title('Multi-chamber enclosure pressure piling effect', fontsize=25)
plt.savefig('Multi-chamber pressure piling.png', format='png')  # Save file
plt.show()  # Show plot
plt.close()
```